INFORMATION TO USERS

The most advanced technology has been used to photograph and reproduce this manuscript from the microfilm master. UMI films the text directly from the original or copy submitted. Thus, some thesis and dissertation copies are in typewriter face, while others may be from any type of computer printer.

The quality of this reproduction is dependent upon the quality of the copy submitted. Broken or indistinct print, colored or poor quality illustrations and photographs, print bleedthrough, substandard margins, and improper alignment can adversely affect reproduction.

In the unlikely event that the author did not send UMI a complete manuscript and there are missing pages, these will be noted. Also, if unauthorized copyright material had to be removed, a note will indicate the deletion.

Oversize materials (e.g., maps, drawings, charts) are reproduced by sectioning the original, beginning at the upper left-hand corner and continuing from left to right in equal sections with small overlaps. Each original is also photographed in one exposure and is included in reduced form at the back of the book.

Photographs included in the original manuscript have been reproduced xerographically in this copy. Higher quality 6" x 9" black and white photographic prints are available for any photographs or illustrations appearing in this copy for an additional charge. Contact UMI directly to order.

U·M·I

University Microfilms International
A Bell & Howell Information Company
300 North Zeeb Road, Ann Arbor, MI 48106-1346 USA
313/761-4700 800/521-0600

Order Number 9103015

Estimation of sensible heat flux from remotely sensed surface temperatures

Cooper, Daniel Ira, Ph.D.

The University of Arizona, 1990

U·M·I
300 N. Zeeb Rd.
Ann Arbor, MI 48106

ESTIMATION OF SENSIBLE HEAT FLUX FROM REMOTELY SENSED SURFACE TEMPERATURES

by

Daniel Ira Cooper

A Dissertation Submitted to the Faculty of the
SCHOOL OF RENEWABLE NATURAL RESOURCES
in Partial Fulfillment of the Requirements
For the Degree of
DOCTOR OF PHILOSOPHY
WITH A MAJOR IN WATERSHED MANAGEMENT
in the Graduate College
THE UNIVERSITY OF ARIZONA

1 9 9 0

THE UNIVERSITY OF ARIZONA
GRADUATE COLLEGE

As members of the Final Examination Committee, we certify that we have read the dissertation prepared by Daniel Ira Cooper

entitled ESTIMATION OF SENSIBLE HEAT FLUX FROM REMOTELY SENSED SURFACE TEMPERATURES

and recommend that it be accepted as fulfilling the dissertation requirement for the Degree of Doctor of Philosophy.

Lloyd W. Gay	6/1/90 Date
Richard H. Hawkins	6/1/90 Date
Zbigniew O. Osmolski	6/1/90 Date
Allen D. Matthias	6/1/90 Date
James R. Simpson	6/1/90 Date

Final approval and acceptance of this dissertation is contingent upon the candidate's submission of the final copy of the dissertation to the Graduate College.

I hereby certify that I have read this dissertation prepared under my direction and recommend that it be accepted as fulfilling the dissertation requirement.

Dissertation Director Lloyd W. Gay	6/1/90 Date

STATEMENT BY AUTHOR

This dissertation has been submitted in partial fulfillment of requirements for an advanced degree at The University of Arizona and is deposited in the University Library to be made available to borrowers under the rules of the Library.

Brief quotations from this dissertation are allowable without special permission, provided that accurate acknowledgment of source is made. Requests for permission for extended quotation from or reproduction of this manuscript in whole or in part may be granted by the head of the major department or the Dean of the Graduate College when in his or her judgment the proposed use of the material is in the interests of scholarship. In all other instances, however, permission must be obtained from the author.

SIGNED: 

ACKNOWLEDGMENTS

I would like to thank Erica Cooper for providing her editorial skills and time in editing this dissertation.

I also want to thank Lawrence Cohen for his helpful suggestions on writing style.

Finally, I wish to express my appreciation to Dr. L.W. Gay for his continuing support and encouragement while I was developing the theory and writing of this dissertation.

This dissertation research was supported in part by the Arizona Agricultural Experiment Station Hatch Project, "Remote Sensing of Sensible Heat flux."

CONTENTS

CONTENTS--continued

CONTENTS--continued

LIST OF ILLUSTRATIONS

Figure

LIST OF ILLUSTRATIONS--continued

LIST OF TABLES

Table

ABSTRACT

A series of energy-balance experiments were performed over a winter wheat field in Southern Arizona. A Bowen ratio energy-balance system (BREB), anemometer, and thermal infrared thermometer (IRT) were placed in the center of the field on day 15 of 1988 shortly after germination. The BREB system generated 12-minute averages of net radiation, soil heat flux, latent energy, and sensible heat flux (H) throughout the season, terminating on day 152, just before harvest. On day 134, an eddy-correlation system was placed adjacent to the BREB system, where it collected H-data concurrently for 17 successive days. The data from the BREB and eddy-correlation systems were regressed against each other to quantify their field performance. The regression standard error (SE) between the two systems was ± 40 W/m^2. BREB H-data was used as a "standard" to evaluate three different sensible heat flux models that are suitable for remote sensing applications. The three models require thermal canopy temperature, air temperature, and wind speed as input. Two of the three models use aerodynamic resistance theory, one of which is stability corrected, and the third remote-sensing model employs Monin-Obukhov turbulent transfer theory. The regression analysis between the BREB H-values and the three remote-sensing models shows that the stability corrected aerodynamic resistance model and the Monin-Obukhov model are capable of estimating H-values over a wide range of surface and atmospheric conditions.

INTRODUCTION

If investigators studying water resources and global climate problems are to describe and predict environmental changes at local, regional, and synoptic scales, they need information on the spatial distribution of water use. Water can be considered as either a mass or as an equivalent amount of latent energy that would be consumed by vaporization. Researchers attempting to acquire data on water use must understand surface-atmosphere interactions and be able to apply the principles of surface energy balance. The surface energy balance equates available energy (the sum of net radiation Q and soil heat flux G) going into and out of a natural surface to the turbulent fluxes (sensible heat H and latent energy LE). Latent energy is readily converted into an equivalent depth of water that is vaporized in evapotranspiration, ET. With knowledge of the magnitude, direction and distribution of LE, resource managers can determine water use for a given region.

However, unlike available energy, which can be measured easily with radiometers and heat flux plates, turbulent fluxes must be estimated with more complex instrument systems. Sensible and latent energy fluxes at vegetated surfaces can be measured at a point above an evaporating surface by four methods:

1. Bowen ratio energy balance (BREB),
2. eddy correlation,

3. profile or aerodynamic approach, and

4. mass balance or lysimetry.

Spatial estimates of the energy balance with these methods require that a number of instrument systems be operated simultaneously. Unfortunately, these instrument systems are difficult and expensive to operate at any scale.

Remote-sensing techniques offer an alternative approach for developing spatial LE estimates. Although remote-sensing technology cannot measure LE directly, it can measure spatial averages of variables—such as surface temperature—that are closely related to LE. Surface temperature measurements (T_r) from thermal remote sensors are potentially useful for estimating both Q and H, provided the remotely sensed surface temperatures are accurate.

Surface temperature also can be combined with supplementary estimates of solar and atmospheric radiation to provide estimates of Q and combined with air temperature and wind speed to provide estimates of H. The value of G can be estimated as a function of Q and T_r, and measurements or estimates of Q and G can be combined with the remotely sensed H-values to provide estimates of LE as a residual in the surface energy balance. Thus, H becomes an important term in the surface energy balance: it can be measured by both surface and remote-sensing instruments and it can lead to an estimate of LE. It is now becoming

feasible to develop local–, regional–, and synoptic–scale estimates of H from remotely sensed data by means of recent advances in high-speed computers, remote sensor technology, and modeling techniques.

Since H can be estimated by instruments that are positioned remotely as well as those that are positioned at the surface, models based on remotely sensed data can be validated. If remote-sensing techniques can yield reasonable estimates of H at a point, then this new technology can likely generate spatial averages. However, before remotely sensed data can be used with confidence, appropriate models must first be evaluated and the accuracy of the sensible heat flux estimates must be defined.

The Problem

All models require validation with a "truth-set" before they can be accepted as a research tool. Energy–balance models using remotely sensed data can be validated with widely accepted BREB instrumentation. However, difficulty and expense have limited validation experiments comparing remote-sensing models and direct measurements of the surface energy balance. An experiment to perform this task was designed by the National Aeronautical and Space Administration (NASA) as part of the International Satellite Land Surface Climatology Project (ISLSCP). The ISLSCP field comparisons were made at a site in Kansas (Sellers et al. 1988) during the summers of 1986, 1987, and 1988, but the results have

not yet been widely published.

Experiments to validate energy-balance instruments at other locations have generally been limited to short periods over a limited range of environmental conditions. Thorough evaluations are needed over times long enough to include a wide range of atmospheric and surface conditions.

The Objectives

This study addresses the problems associated with estimating H-values from remotely sensed data. The primary objective is to develop and validate models for estimating H from a combination of data measured remotely and at the surface. I tested the Monin-Obukhov (1954) and the Penman-Monteith aerodynamic resistance models (Monteith 1964) against direct measurements from the BREB system. I also verified the performance of the BREB system by comparing it with an eddy-correlation system.

The experiments were conducted at an irrigated winter wheat site at the Maricopa Agricultural Center in southern Arizona. The continuous measurements extended for 135 days, covering most of an entire growing season. The Monin-Obukhov and aerodynamic resistance models used infrared thermometer canopy temperatures along with wind speed and air

temperature to estimate H-values. The results were compared with Bowen ratio estimates to determine which model best conformed to the "ground-truth" measurements. Unlike previous studies, the instrument comparisons reported here were long enough to include a wide range of the surface and atmospheric conditions that occur in semiarid regions.

1. OVERVIEW OF ENERGY-BALANCE MEASUREMENTS

Disciplines such as agriculture, forestry, and watershed management use evapotranspiration (ET) estimates for the analysis of water use. Evapotranspiration is difficult to measure directly, but it can be estimated with techniques that use the surface energy balance. The surface energy balance—the sum of the radiant and turbulent fluxes going into and out of the surface—is given by

$$Q + G + LE + H = 0 \ , \qquad (1.1)$$

where Q is the net radiation, G is the soil heat flux, and H and LE are the sensible and latent heat fluxes, respectively.

Sensible heat flux is the convective heat transfer between moving parcels of air. Natural convection is caused by changes in the density of heated parcels of air, whereas forced convection is generated by external (shear) forces acting on the parcels. Latent heat is the energy released when matter changes phase from solid to liquid or from liquid to gas without changing its kinetic energy or temperature. Units for flux densities are watts per square meter. Fluxes toward the surface are positive; those away from the surface are negative. The values of Q and G can be measured directly with commercial sensors, but LE and H must be measured by other means, such as the Bowen ratio energy-balance (BREB) technique. By applying the surface energy-balance and BREB techniques, one can measure ET from LE (1 mm = 2.45 MJ/m^2).

The Bowen ratio Method

The BREB method partitions available energy (Q and G) into turbulent heat fluxes (H and LE). The values of LE and H are calculated from gradients of potential air temperature ($\Delta\theta/\Delta z$) and vapor pressure ($\Delta e/\Delta z$) above the surface by means of the model developed by Bowen (1926). In practice, the temperature and vapor pressure gradients are approximated by the difference between the potential temperature ($\Delta\theta$) and vapor pressure (Δe) measured by psychrometers at two heights above the top of the canopy.

Bowen's ratio ß is the ratio of H to LE:

$$ß = \frac{H}{LE} = \frac{-\rho C_p K_h (\Delta\theta/\Delta z)}{-(\rho L \epsilon K_e/P)(\Delta e/\Delta z)} , \qquad (1.2)$$

where
ρ is air density [kg/m^3],
C_p is the specific heat of air [J/kgK],
L is the latent heat of vaporization [kg/m^{3}K],
ϵ is the ratio of molecular weight of water to dry air [kg/kg],
P is atmospheric pressure [mb],
K_h is the eddy diffusivity for heat [m/s],
K_e is the eddy diffusivity for vapor [m/s],
$\Delta\theta/\Delta z$ is the potential temperature gradient with respect to height [K/m], and
$\Delta e/\Delta z$ is the vapor pressure gradient with respect with height [mb/m].

Bowen's model assumes that the eddy diffusivities for heat and vapor are similar. Thus, equation (1.2) reduces to

$$ß = \frac{C_p P}{\epsilon L}\left[\frac{\Delta\theta}{\Delta e}\right] . \qquad (1.3)$$

The psychrometric constant γ is equal to $C_p P/\epsilon L$, so equation (1.3)

becomes $ß = \gamma(\Delta\theta/\Delta e)$. We partition LE and H from the energy balance by algebraically rearranging equation (1.1) for LE and incorporating ß to yield

$$LE = \frac{-(Q + G)}{(1 + ß)} , \qquad (1.4)$$

and

$$H = ß\ LE . \qquad (1.5)$$

Because Bowen's ratio assumes similarity between K_h and K_e, diabatic corrections for stable and unstable air masses are not required. As an illustration of these effects, consider a parcel of air vertically displaced. In a stable atmosphere, the parcel will tend to return to its original position. In a neutral atmosphere, the parcel tends to remain at the new position. In an unstable atmosphere the parcel will continue to rise until the parcel is in equilibrium with its environment. Diabatic corrections account for wind profile changes due to the retarded or enhanced buoyancy of the air. In a stable atmosphere the wind will be greater than that of a neutral atmosphere, and under unstable conditions, the wind will be less than a neutral atmosphere.

Bowen ratio systems are commonly used for ET experiments even though they are mechanically complex and often difficult to operate. Tanner (1960) applied Bowen's (1926) energy-balance method to measuring ET in agriculture, and subsequent developments have improved on Tanner's psychrometers, data acquisition system, and field procedures. The most striking improvement has come with the acceptance of the need to

interchange psychrometers between measurements. If psychrometers measure temperatures over a small distance, systematic errors in the sensors can be about the same size as the gradient. Interchanging the psychrometers removes the effects of systematic bias on the small gradients (Sargent and Tanner 1967).

Analysis of Sensor Errors

The Bowen ratio psychrometer temperature sensors have definable levels of precision that are used to estimate the accuracy and precision of psychrometric measurements. Measurement errors combined with estimated errors in various components of a Bowen ratio system can yield estimates of possible errors in the sensible and latent heat fluxes.

Fuchs and Tanner (1970) estimated the maximum absolute error in LE and H by propagating the maximum range of wet- and dry-bulb temperature errors through the Bowen ratio equations. Using low-precision temperature sensors and data-acquisition systems in their calculations, they estimated the maximum error for sensible heat to be as much as 31% for bare soil surfaces. They noted that the size of the errors in the H and LE fluxes depend on the magnitude of the temperature gradient: large gradients have relatively small errors and small gradients have large errors. However, interchanging the psychrometers should remove the systematic errors.

Holbo (1973) calculated probable errors by using average temperature errors instead of maximum errors. He calculated the effect of average temperature errors on the H and LE equations, finding that the errors in calculating H over a dry pumice surface were between 3% and 15%. Sinclair et al. (1974) used expected error values for the psychrometers to estimate the probable errors in Bowen ratio LE. Because the probable errors in LE were between 5% and 10%, they concluded that "most of the error can be traced to the 5% error in net radiation." The work by Holbo and by Sinclair et al. indicated that for dry surfaces, when the gradients should be large and the atmosphere unstable, the error in H will be small, and a portion of it might be associated with radiation measurements rather than psychrometric measurements.

Spittlehouse and Black (1980) used high-precision psychrometers on a exchange mast in a forest environment to estimate the probable error in LE derived from the Bowen ratio. Although the temperature gradients above a forest can be small, the average error in LE was ±15%. The errors became significantly larger when ß was greater than 4 and the vapor pressure gradients were small. Philip (1987) calculated the theoretical upper bound for the Bowen ratios with air and surface temperatures above 0°C, concluding that the maximum value of ß would not exceed 3.85. Thus, large errors in LE associated with ß's greater than 4 should not be a problem.

Experimental Verification of Flux Measurement Systems

The Bowen ratio method often has been compared with mass-balance lysimeters and eddy-correlation instruments, but these experiments have generally been short. The errors and uncertainties associated with Bowen ratio measurements have been examined both theoretically and experimentally. In this section, earlier work in the field will be reviewed before the enhanced experiments of this study are described.

Intercomparisons

Osmolski and Gay (1983) and Gay and Greenberg (1985) evaluated the variability among Bowen ratio systems. In these studies, LE fluxes were measured for 4 and 6 days, respectively, with side-by-side Bowen ratio systems at uniform, irrigated alfalfa sites. Net and soil heat fluxes were averaged from two sets of sensors so that the available energy was the same for both Bowen ratio systems. They found, for a wide variety of environments and a wide range of fluxes, that the variability in daily totals between the two systems was as little as ±2.4%. Gay (1988) reported the results of a study conducted during a 24-h period in late spring in Arizona. He calculated that 30-min average values of LE from the Bowen ratio, the eddy correlation, and the average of three lysimeters agreed within ±10%. The peak LE reached 750 ±75 W/m^2. For this smooth, uniform, irrigated surface (stable diabatic conditions)

—similar to the site used in the current study—the Bowen ratio measured the turbulent fluxes with very consistent results.

Comparisons With Lysimetry

Blad and Rosenberg (1974), comparing soybean LE using the Bowen ratio and lysimeters, reported deviations that ranged from 10% to 20%. Since they did not interchange psychrometers, fixed errors in the temperature sensors may have biased the Bowen ratio values and thus increased the error in LE. In contrast, Denmead and McIlroy (1969) measured LE fluxes from nonirrigated wheat using a Bowen ratio system with interchangeable psychrometers. The Bowen ratio LE results were within about ±10% of those from a lysimeter.

Brownridge (1985) examined daily totals and 30-min averages of H and LE from irrigated winter wheat at Phoenix, Arizona, for 10 days scattered throughout the growing season. The results from the Bowen ratio systems were similar to results from three lysimeters. She reported that Bowen ratio estimates of daily totals for the daylight hours were within ±15% of the measured values. The lysimeters overestimated LE relative to the Bowen ratio LE in the late afternoon. Brownridge also showed that the variability among the three lysimeters was substantially higher than either the variability between two Bowen ratios or the variability between the mean lysimeter measurements and the mean Bowen ratio method

results. Thus, variability reduces the confidence in the lysimetric measurements. She suggested that a possible cause for the discrepancies might be the effects of advection on the lysimeters because the lysimeter variability was highest under advective conditions.

Comparison with Eddy-correlation

For measuring H, the eddy-correlation method has become fairly popular because of recent technological advances in simplifying the sensors associated with such systems (Campbell and Unsworth 1979). Most comparisons between eddy-correlation and BREB techniques have been made over rough forest canopies (McNeil and Shuttleworth 1975; Spittlehouse and Black 1979, 1980; Shuttleworth et al. 1984; Denmead and Bradley 1985) with agreement of H-estimates generally being about ±15%. McNeil and Shuttleworth (1975) compared hourly averaged H-fluxes over a rough-canopy pine forest. They derived their data from eddy correlation using a Gill anemometer, a fine-wire thermocouple system, and a Bowen ratio system in which the psychrometers were interchanged. The measurement uncertainty (the standard error at 95% confidence) between the two systems was ±20 W/m^2 with H-fluxes ranging from -20 to 400 W/m^2. Spittlehouse and Black (1980) concluded that if the temperature and vapor pressure gradients were large and ß's were negative, eddy-correlation and Bowen ratio LE values would agree within ±20%.

Massman et al. (1990) compared the LE results from an eddy-correlation system based on a sonic anemometer and platinum resistance thermometer with results from a weighing lysimeter over a natural grass surface in Colorado. They evaluated the LE from both systems with 30-min averages. The difference between LEs from the two systems was not much greater than ±60 W/m^2, and the lysimeter overestimated the eddy-correlation LE values regardless of the moisture condition of the surface.

Development of Practical Sensible Heat Flux Models

Over the past three decades, many researchers have focused on developing models to estimate sensible heat flux from thermal radiometer (remote-sensing) data. With the invention of thermal radiometers in the mid-1960s, the concept of estimating H from remote sensing has shown potential for use in the field of agrometeorology. The basic approach uses remotely sensed surface temperature and local measurements of wind and air temperatures to estimate sensible heat exchange between the surface and the air. Jackson et al. (1977) suggested the use of linear models to convert the difference between the canopy temperature and air temperature into sensible heat flux. Carlson et al. (1981) used the surface thermal inertia (the difference between the day and night surface temperatures) to estimate the turbulent fluxes. An approach that has gained wide acceptance is the use of aerodynamic resistance models to

estimate the resistance of heat transfer from the surface to the atmosphere. These models are used in conjunction with canopy temperature, air temperature, and wind speed data to estimate H. However, before any of these models can be used on a routine basis, they must be evaluated with ground-truth.

The following sections briefly outline the history and development of models suitable for remote sensing of H at the surface. Since the 18th century, scientists have recognized that differences between the canopy surface temperature and air temperature should be directly related to H (Brutsaert 1982). However, until the early 1970s, no models existed that would convert remotely sensed temperatures to H-values. The focus of many early studies was on finding exchange coefficients or scaling terms (usually a slope term from a linear model) that could relate the canopy-air temperature gradient to sensible heat flux.

Empirical Linear Models

Jackson et al. (1977) proposed a simple linear model that used empirical wind speed functions as an exchange coefficient to transform the canopy-air temperature gradient into H. To test the validity of their hypothesis, they compared H-values measured with a wheat-covered lysimeter with estimates of H modeled from concurrent meteorological and infrared thermometer (IRT) data. They concluded that H was a linear

function of the canopy–air temperature differences but that wind speed did not significantly affect the H-values. Because the variability between the measured and modeled data was large, the model needed refinement. To address the inconsistencies in the linear model, Seguin and Itier (1983) developed an analytical approach that incorporated simple stability corrections for diabatic near-surface atmospheric conditions. They concluded that separate equations for stable and unstable atmospheres must be used if H is to be modeled properly because the simple linear model assumed an atmosphere of neutral stability, which is not the prevalent condition above a canopy.

Thermal Inertia Considerations

An alternative approach, proposed by Price (1980) and Carlson et al. (1981), estimates soil moisture from paired, day–night satellite thermal images. Soil moisture provides the basis for an empirical assessment of H or LE without the need for local meteorological data. However, the surface temperature variability associated with soil moisture variability can be as much as 15°C in the daytime and as little as 3°C at night. The temperature differences between day and night can be the same as or smaller than the variability in daytime surface temperature, thus reducing the sensitivity of these types of models. These models have not been adopted by many researchers, and most of the advances in remote-sensing models for H result from improvements in the canopy-air

temperature approach advocated by Jackson et al. (1977).

Aerodynamic Resistance Models

In the 1970s, empirical regression coefficients were replaced by aerodynamic resistance (r_a) models. Monteith's (1964) aerodynamic resistance model used wind speed to determine the resistance to H moving between the canopy and the atmosphere. He assumed that the surface is a single, uniform, transpiring leaf, where the resistance to H-transport is approximated by u/U* where U* is friction velocity and u is the wind speed. The friction velocity is calculated from the log-linear wind profile above the canopy. Campbell (1977) improved on Monteith's work by expanding u/U_*, to u/U_*^2, which incorporates both the friction velocity for momentum transport and heat. He also recognized that the exchange height for momentum and heat (the locations in the canopy that are the source and sink of the momentum and heat flux) must be added to the model so that it can be used in many environments. Mahrt and Ek (1984) used Monteith's approach for their conductance model, which incorporated empirical stability corrections. More recently, Hatfield (1985) used an aerodynamic resistance model similar to Monteith's to evaluate H-values calculated from remotely sensed canopy temperatures (IRT) and air temperatures. He recognized that r_a and crop phenology are related by canopy geometry. Because the exchange height is directly proportional to the plant height, the aerodynamic properties of a field must be taken

into account before the parameters of the model can be determined.

Aerodynamic Resistance Comparison

Huband and Monteith (1986b) compared Bowen ratio H-values over wheat with those from an r_a model (Hr_a) that used IRT temperatures. Their r_a model was very simple: $r_a = u/U_*^2$ [s/m], where U* was calculated from the log-linear profile of wind speed. However, their modeled H results did not correlate closely with the Bowen ratio (HBr). Their best statistical model was $Hr_a = 0.88$ HBr + 38 W/m^2 ($r^2 = 0.88$). Because they used winter wheat in their study, the results can be used directly in this dissertation. They had a wind profile system (not available at the Maricopa site) for measuring aerodynamic parameters such as displacement height and roughness length.

Jackson et al. (1987) used airborne and surface IRT values as input into a stability-corrected r_a model developed by Mahrt and Ek (1984) to estimate H and LE (LE by residual of the energy balance). They compared their remote-sensing H-fluxes with Bowen ratio measurements made at the same time. Interestingly, the model was not sensitive to wind speed changes. This finding is important because in southern Arizona, H is highly affected by advection (Brownridge 1985). Kustas et al. (1989) compared Bowen ratio data with an improved r_a model that incorporated Monin-Obukhov stability corrections. Their model worked well under

stable conditions at an irrigated field, but it was insensitive to bare surfaces under unstable atmospheres.

Summary

Energy-balance measurements made by a BREB system are useful as ground-truth for evaluating remote-sensing models of H-values. The H-values measured by the BREB system have acceptable errors, 10% to 15% when the gradients are not small. Over irrigated surfaces, the BREB system is both consistent and as accurate as any other method available, including lysimetry or eddy correlation. Until recently, the most successful approaches for estimating H from remotely sensed data used aerodynamic resistance models. However, these models as currently formulated are not applicable to all environments—for example, dry surfaces—or in unstable diabatic atmospheres (Kustas et al., 1989).

2. METHODS AND MATERIALS

This chapter describes the methods, the instruments, the data-processing techniques, and the study site used for this investigation.

Bowen ratio Instrumentation

The Bowen ratio energy-balance (BREB) instrumentation used to gather data for this study was developed at the University of Arizona and has been in use for several years (Gay 1988). The BREB system includes two ceramic-wick, fan-aspirated psychrometers mounted on a vertical exchange mast. The exchange mast is used to interchange the psychrometers over a vertical distance that can be set from 0.5 m to 1.0 m. Periodically interchanging the psychrometers on the mast can eliminate systematic biases from averaged measurements of the small atmospheric gradients of wet- and dry-bulb temperatures. For example, the temperature gradient measured by subtracting the temperatures from two sensors at two levels might include a bias in one sensor. When the gradient is calculated by subtracting the upper temperature from the lower temperature, the bias is added to the gradient. When the sensors are interchanged and the gradient calculated from two sets of observations, the bias is eliminated by subtraction since it appears at both measurement levels.

Highly stable voltmeters are used to minimize random errors from the

BREB system. The voltmeters integrate the voltages over time to reduce the effects of random voltage variations. In addition, shielded cables block radio frequency noise, further reducing random errors.

The BREB system was started on day 15, 1988 (about 20 days after seeding) and operated until day 152 (harvest). The BREB psychrometers were sampled continuously for 3 minutes (at 2 samples per second), interchanged, allowed to come into equilibrium for 3 minutes, and then the 6 minute cycle of sampling, interchange and rest was begun again. Each 6 minute cycle thus contained 3 minutes of continuous sampling and 3 minutes of equilibration time with sampling suspended. Two such 6-minute cycles were combined to yield 12-minute means of the surface fluxes and associated microclimate data.

The temperature difference $\Delta\theta$ was calculated from the dry-bulb temperatures sampled at two heights above the canopy. The vapor pressure difference Δe was calculated from the wet-bulb temperature measured concurrently with the dry bulb in each psychrometer, using the standard psychrometric formula. I converted the vapor pressure e from each set of psychrometer readings using Murray's (1967) exponential relationship between temperature and vapor pressure, and calculated the Bowen ratio ß from equation 1.3. The value of the psychrometric constant γ can be analytically computed as $0.66\ P/P_0$, where P is the ambient atmospheric pressure and P_o is atmospheric pressure at sea level (1013 mb). The

ratio P/P_0 was calculated from the expression $(288-0.0065\ z)/288^{5.56}$, where z is the elevation above sea level (Gay and Greenberg 1985). The value of Q was measured with a single-dome, Fritschen-type net radiometer, and the value of G was taken as the soil heat flux measured by a pair of soil heat-flux disks connected in parallel and installed just below the soil surface.

Equations (1.4) and (1.5) were used to partition the available energy (Q and G) into LE and H from the gradients of temperature and vapor pressure. Ancillary meteorological data included wind speed, incoming solar radiation, and thermal emitted surface temperature; they were measured with an R.M. Young anemometer, a Kipp pyranometer and an Everest IRT, respectively. The measurements made with the psychrometers, radiation sensors, and ancillary instruments were sampled with a Hewlett Packard HP3421A A/D logger controlled by an HP71B hand-held microcomputer using Arizona Evapotranspiration (AZET) software developed by Gay and Greenberg (1985). The HP71B and AZET software stored raw data for each 6-min period, either in RAM or on a 3.5-in. floppy disk. The energy balance could be computed every 12 min and the computed values either displayed or printed.

Data Handling and Processing

The data from the Bowen ratio and eddy-correlation systems were

converted from field storage (tapes and diskettes) into scaled outputs (fluxes, temperatures, etc.), and then transferred into an IBM-AT computer. Large ASCII files, typically containing 7 days of field BREB data, were entered into an analytical software package (RS/1) that has numerical and statistical routines for both batch and real-time programs. A series of RS/1 programs organized and stored the data as 24-hour tables, each containing two hundred and forty 6-min values of Bowen ratio and associated microclimate measurements.

Filtering

I checked the Bowen ratio data for internal consistency using Ohmura's (1982) criteria which identifies periods when the Bowen ratio data must be filtered. There are two conditions when the Bowen ratio data require filtering: (1) when ß equals -1.0 or (2) when the polarities of H and LE do not match the polarities of $\Delta\theta$ and Δe. The value of ß is -1 when H and LE have the same size but opposite polarity. When ß equals -1, equation 1.4 is undefined, and Q and G cannot be properly partitioned into H and LE.

Since there are uncertainties in the calibration of the net radiometer, soil heat flux plates, and the psychrometer wet- and dry-bulb sensors, the BREB system requires a rejection region when ß approaches -1 (Gay 1986). At night or early morning when Q and G are of opposite

polarity but approach equality in absolute value, measurement errors can give an incorrect polarity to the available energy, and the direction of the fluxes will be opposite of the properly measured gradients. Since the measurement errors in the fluxes and gradients are size dependent, a rejection region is required for filtering the BREB data. The rejection region for the BREB system I used is ß = -1 ±0.25. The size of the rejection region was determined from observations of system performance. According to the rationale used by Gay (1986), the RS/1 filter program tests to see if ß–values are between -0.75 and -1.25; when this condition occurs the program sets LE = 0 and H = -(Q + G). The filter program then tests for polarity agreement between H and LE and between $\Delta\theta$ and Δe, respectively. If the polarities of the fluxes and gradients are not in agreement, then the filter program sets LE = -(Q + G) and H = 0. The polarities are then retested, and if still not in agreement, then the filter program sets LE = 0 and H = -(Q + G). The periods when ß approaches -1 and/or polarity errors occur usually occur at night when the fluxes of Q and G are small. Consequently, H and LE are small, and the error introduced by the filtering process must also be small.

Interpolation

Several problems with the Bowen ratio instrumentation arose during the 1988 measurement campaign. Loss of data resulted from three types

of problems: (1) failure of the microcomputer or data logger (complete data loss), (2) failure of the mast exchange mechanism (loss of temperature and vapor gradient data), and (3) premature exhaustion of water in the wet-bulb psychrometer reservoir (loss of vapor gradient data). I interpolated missing data by comparing data collected before and after the failure or by referencing to concurrent data collected with other sensors. Specific interpolations are identified below.

All data for days 36 and 68 were inexplicably lost during transfer and handling. Complete data loss therefore occurred on only 2 of 137 days attempted. Mean daily flux values for the two missing days were interpolated from pyranometer data with the assumption that on a daily basis (1) Q is directly proportional to incoming solar radiation (Kd), and (2) LE is directly proportional to Kd. The percentage change in solar radiation between days 36 and 37 and between days 68 and 69 was 5% and 3%, respectively. Since these changes were very small, the missing flux values for days 36 and 68 were approximated by the measured values from days 37 and 69.

Temperature and vapor gradient data were lost for short periods on several days when the BREB system mast failed to exchange the psychrometers. This problem usually occurred just before dawn, when the main storage batteries were at their lowest charge. Normal operation always resumed when the solar cells began recharging the storage

batteries after sunrise. This exchange failure affected the gradients in about 130 12-minute periods out of 16,200. The affected periods were on days 51–54, 59, 72–75, 110, 129, and 138–140. I interpolated the gradients linearly between missing periods. Since the available energy was always quite small during the predawn failures, errors associated with interpolation were of little consequence in the daily energy balance.

The Bowen ratio equipment was serviced weekly. Occasionally, one of the water supply reservoirs ran dry, and vapor pressure could not be calculated. These failures, usually for only a few hours duration, occurred on days 18, 26, 31, 35, 46, 123, 137, and 144. A total of 64 hours were affected out of 3240 hours recorded. The Bowen ratios for those affected periods were replaced by ß–values for the same time periods on similar, recent days, and the values of H and LE recalculated with the substitute ß–values and the measured Q– and G–values. This substitution introduced little error because the problem usually occurred during the night and early morning, just before the BREB system was inspected and the reservoirs refilled.

Sensor Calibration and Evaluation

The optimal operation of the BREB system and ancillary sensors requires adequate calibration and evaluation of the instruments. This

maintenance was performed with the use of standard statistical procedures and side-by-side intersensor comparisons. The following section describes the calibration of the BREB psychrometers, net radiometer, and infrared thermometer (IRT) used in this study.

Temperature Sensor Calibration

The ceramic-wick psychrometers use resistance temperature detectors (RTDs) as wet- and dry-bulb sensors. To ensure precise temperature measurements, I calibrated the RTDs in the laboratory using an incremental-temperature water bath technique described by Osmolski (1985). In this technique, a precision platinum resistance thermometer (PRT) and the RTDs are immersed in a recirculating water bath filled with crushed ice and water. As ice water is heated to 50°C in successive 5°C increments, the voltage of the RTDs and PRT sensors are measured with a high-precision voltmeter. The RTD voltage output is regressed against the PRT temperature, and the resulting curve is fitted with a third-order polynomial that gives the RTDs precision that is typically ±0.009°C, with correlation coefficient (r^2) of 0.9999, and mean square errors of 0.008°C at 95% confidence (Osmolski 1985).

Psychrometer Evaluation

The RTD sensor precision does not define the behavior of the

psychrometer, so a standard must be used. Although standards—such as the Assman psychrometer—exist, their precision is lower than that of the RTDs. Instead, I evaluated the psychrometer variability to approximate the precision. The psychrometer variability could be determined by interinstrument comparison of the RTDs. During the comparison I minimized the environmental influences on the RTDs by operating the psychrometers in the laboratory, side by side without interchange, so that the two sets of wet and dry bulbs could be compared directly under the same temperature and humidity conditions. I assumed that the air being measured by the two psychrometers was the same. In theory, perfectly matched psychrometers should exhibit no variation between sensors, and the difference between the mean temperatures measured by the sensors should be zero. However, since some variation between sensors always exits, the temperature differences between individual wet and dry bulbs exposed to the same environment is an index of their precision.

The analysis of 22 records, each a 4-min mean, showed that average differences between the two wet bulbs, was 0.037°C with a standard deviation (SD) of ±0.004°C and a range from 0.01°C to 0.06°C. The differences between the two dry-bulb RTD's averaged 0.012°C with a SD of ±0.002°C and a range from 0.00°C to 0.03°C. Although the RTD sensors used for the wet and dry bulbs have near-uniform precision in the water bath calibration, the wet-bulb RTDs in the psychrometer are incased in ceramic wicks that may vary in thickness, conductivity, and wetting.

Thus, each wet bulb is in a unique environment, and responses may differ from one wet bulb to another, increasing the sensor–to–sensor temperature variability compared with the dry bulbs.

The instantaneous errors in LE and H computed by propagating the wet– and dry–bulb uncertainties of 0.05°C and 0.01°C, respectively, into the Bowen ratio equations (1.4) and (1.5) are within the range of errors calculated in previous studies, such as by Holbo (1973). For instance, at the Maricopa site on day 132 at 1200 hours, Q, G, and the average temperatures of the upper and lower wet bulbs and dry bulbs are 746 W/m^2, -62 W/m^2, 19.69°C, 18.55°C, 33.44°C, and 34.26°C, respectively. Applying equations (1.3)–(1.5) to the radiation and temperature data gives an LE of -836 W/m^2, an H of 153 W/m^2 and a ß of -0.18. To calculate the extreme range of instantaneous systematic errors for these values at this time, the biases of 0.05°C and 0.01°C for the wet and dry bulbs, respectively are added to the upper temperatures and subtracted from the lower temperatures. In this case, LE is -822 W/m^2, H is 138 W/m^2, and ß is -0.17. The percentage errors for LE and H are about ±2% and ±12%, respectively, for these selected values. However, the psychrometer exchange procedure would remove these systematic errors from the fluxes.

Net Radiometer Calibration

The calibration of the net radiometer should be verified from time

to time. I checked the agreement of two net radiometers by side-by-side comparisons in the field. I compared two net radiometers since the instruments to measure the individual short- and long-wave radiation components were not available. From this comparison, the variability could be determined from statistical analysis.

For 11 days, from day 124 to day 135 of 1988, two similar net radiometers made by the same manufacturer were exposed side by side over the winter wheat. They operated under both cloudy and clear skies, ideal conditions for evaluating the instruments. The radiation values from the two net radiometers (X102 and Q176) were regressed against each other and plotted in Figure 1. Note that the values from the morning and afternoon underestimated and overestimated, respectively, the 1:1 line.

The scatter in Figure 1 is probably due to differences in the net radiometer leveling. The regression standard error, used as the interinstrument net radiometer uncertainty, was ±12 W/m^2 at 95% confidence. Other regression coefficients for the comparison were as follows: r^2 was 0.99, the slope was 1.04, and the intercept was 6.9 W/m^2. The difference between an ideal comparison (r^2 and slope of 1, intercept and SE of 0) and the measured regression coefficients was relatively small compared with the average daylight net radiation values, which were about 400 W/m^2. Figure 2A and 2B compare the fluxes from Q176 and X102 for a clear and cloudy day. The agreement between the two radiometers

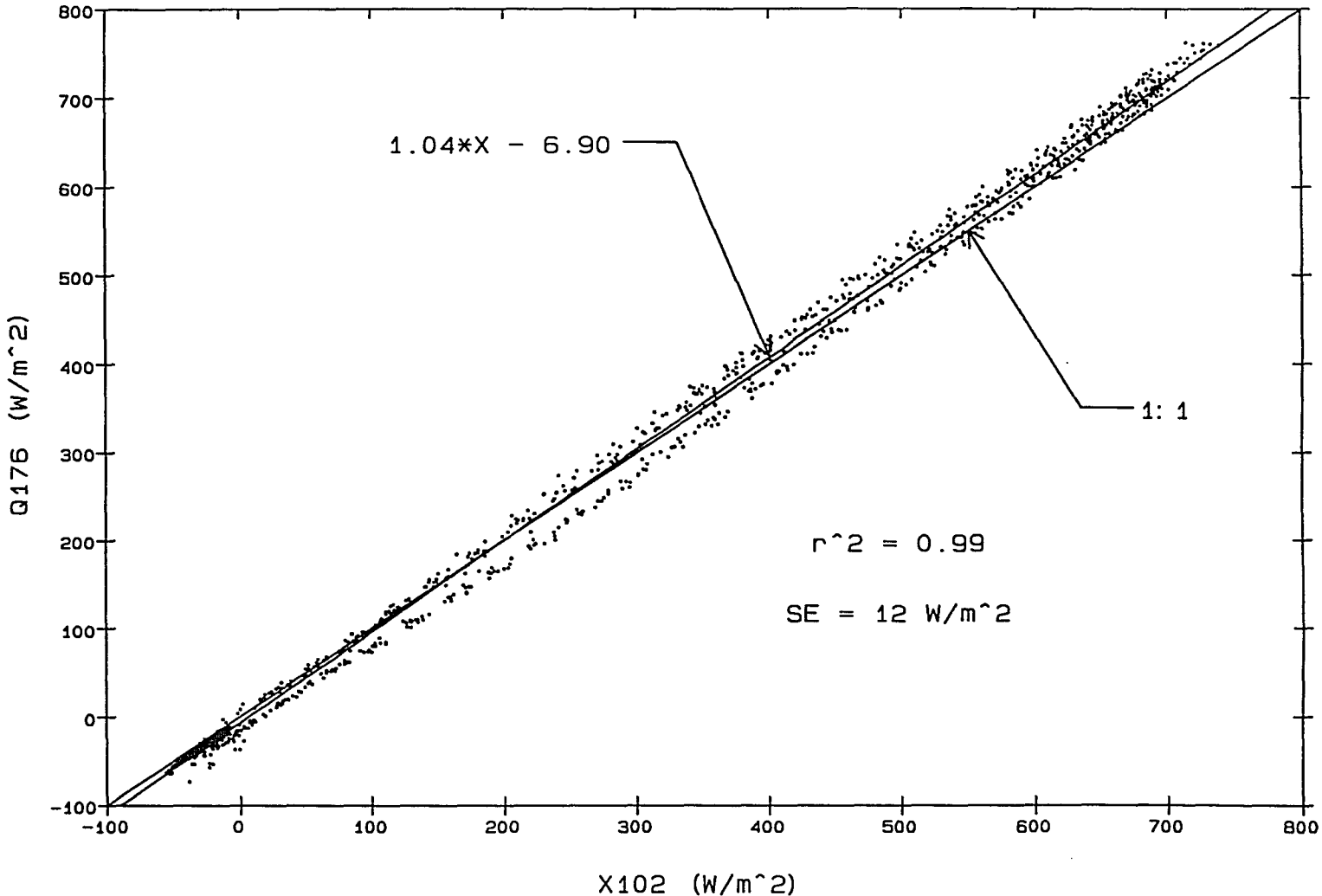

Figure 1. Comparison of two net radiometers set side by side over winter wheat.

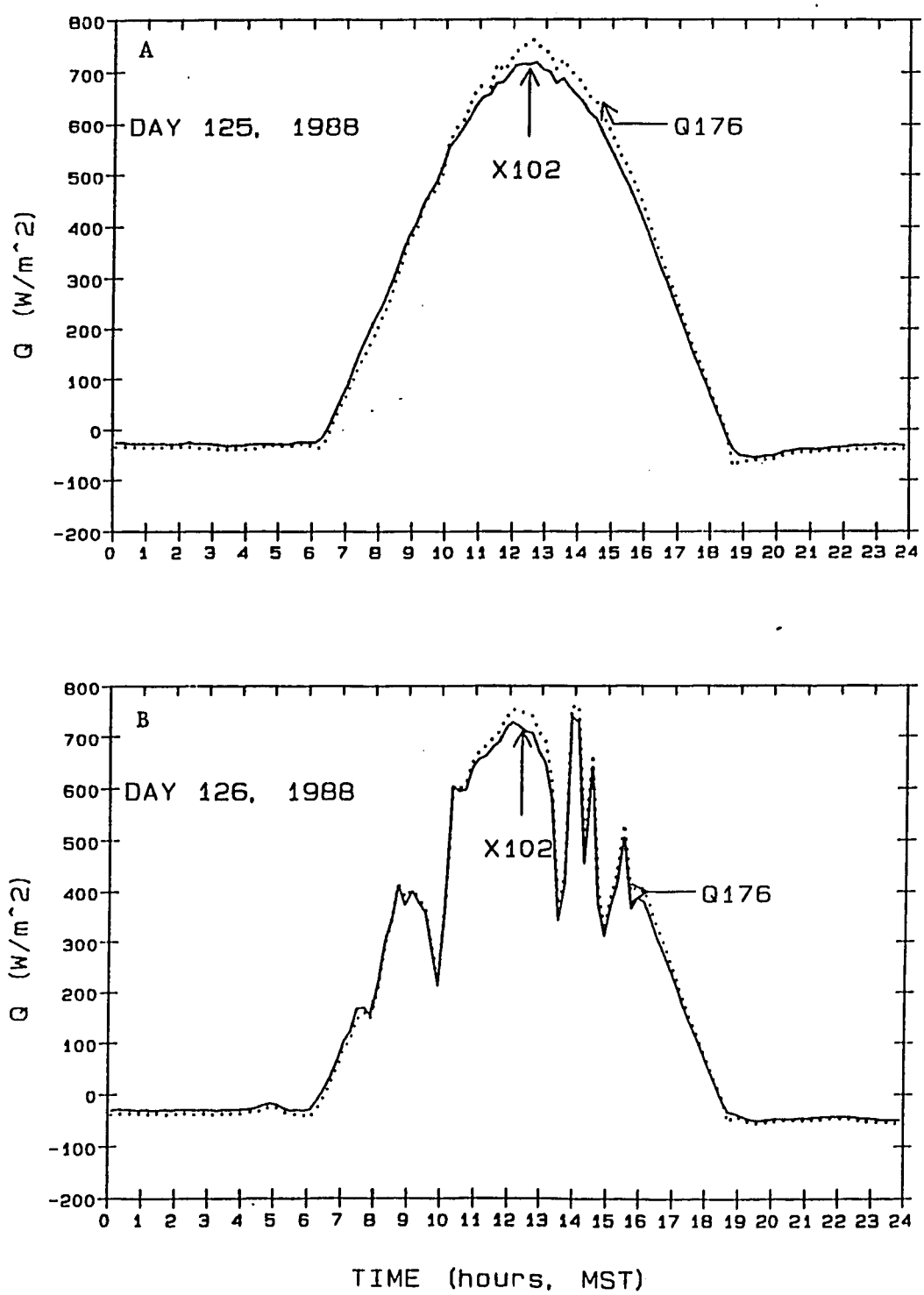

Figure 2. Comparison of two net radiometers over the diurnal period
A. Clear skies, day 125, 1988.
B. Partly cloudy skies, day 126, 1988.

over a wide range of environmental conditions is within the ±5% agreement that is thought to be reasonable for net radiation (Fritschen 1965).

Infrared Radiometer Calibration

The IRT was calibrated by the manufacturer and again at the U.S. Water Conservation Laboratory in Phoenix, Arizona. Under ideal conditions, the IRT has an accuracy and precision of 0.1°C. It was mounted in the field with a dual-wall shield (an outer wall of galvanized sheet metal and a inner wall of PVC pipe separated by a 50-mm air space) to reduce solar heating of the instrument housing. However, long-term diurnal heating and cooling cycles associated with field operation could cause drift in the absolute temperature values generated by the IRT, so every 6 weeks the IRT calibration was checked with an Everest blackbody calibration target. The target was placed in front of the optical cavity of the IRT, and the target and IRT read simultaneously. The IRT underestimated the blackbody temperature by an average of +0.275°C. The offsets ranged from +0.25°C to +0.3°C, with ambient temperatures varying between 10°C and 35°C over the length of the field season.

The Experimental Site at the Maricopa Agricultural Center

An ideal site for experiments to evaluate micrometeorological

instruments and models must have certain features to ensure high- quality results. These attributes are related to the climate, surface geometry, and vegetation of the study site. Atmospheric variability should cover a wide spectrum of conditions (warm-cold, moist-dry, clear and cloudy skies, etc.). Unlike the atmosphere, the surface should be as regular and uniform as possible: the topography should be flat with large fetch, and the soil water status should be uniform. The vegetation should have several qualities: the crop density should be uniform, the crop height should be uniformly short, and canopy closure should occur quickly after emergence. The winter wheat site at the University of Arizona's Maricopa Agricultural Center (MAC) meets these requirements.

MAC is located 7.6 km east of Maricopa, in Pinal County, about 100 km northwest of a Tucson. The farm is a 1.3- by 1.5-km^2 rectangle covering 770 hectares at a mean elevation of 358 m above sea level. All the fields have been precision-leveled with a laser theodolite to minimize topographic variability and to facilitate irrigation. The soil is a sandy clay loam from the Casa Grande and Trix soil associations. These reclaimed saline and sodic soils are composed of over 50% sand to a depth of 1 m. The instrument systems that collected data during the 1988 field campaign were situated over winter wheat in field 15 (Figure 3). Field 15 measures about 350 m in the east-west direction and about 850 m in the north-south direction.

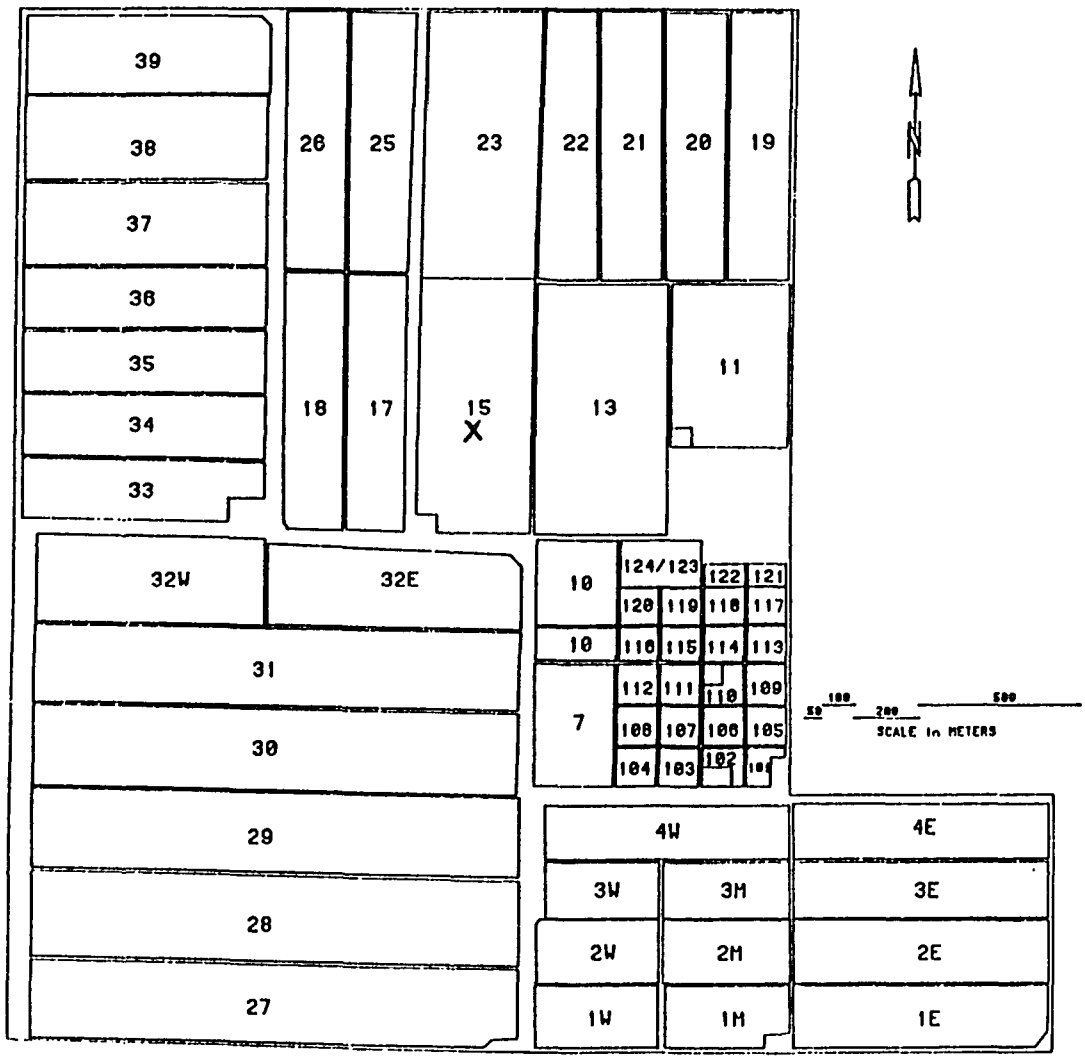

Figure 3. Site map of the Maricopa Agricultural Center.

Climate

Maricopa has a semiarid climate, typical of the desert southwest (Sellers and Hill 1974). The average yearly precipitation is approximately 280 mm. Precipitation follows a bimodal monsoon-type distribution with most of the rainfall occurring in the summer. During the summer (typically August), convective heating of the desert floor causes widely scattered showers in the late afternoons; these storms are usually associated with high wind speeds and moving dust. The moisture in the larger storms originates in weak tropical disturbances that move northward into the continent from the Gulf of California. Only in August do the average monthly precipitation events exceed 25 mm at Maricopa. The summer average monthly rainfall is usually less than 10 mm. In winter (December and January), eastward-moving air masses containing small amounts of moisture from the Pacific Ocean deliver short, light, sporadic showers. Summer air temperatures are warm, averaging about 30°C from July to August. Temperatures are typically about 20°C in the morning, rising to 35°C in the afternoon. In the winter, the temperatures are more pleasant, averaging about 25°C in the afternoon and sometimes dropping below freezing in the early morning. The temperature regime for the 1988 winter wheat season was typical for Maricopa. Twenty-four hour average temperatures at the start of the measurements in January were about 10°C. By midseason, in March, they reached 15°C, and by late May (day 147) they climbed to 30.3°C.

Rain at the MAC farm was measured by a tipping bucket rain-gauge operated as part of the AZMET meteorological network (Brown 1988). Precipitation events (dates and amounts) for 1988 are recorded in Figure 4. Of the 15 precipitation events that occurred during the growing season, the largest delivered less than 14 mm, while most delivered between 2 and 3 mm. Crop water requirements were satisfied by locally pumped ground water. During the study period, field 15 was flood irrigated on day 351 of 1987 and on days 21, 53, 75, 98, 116 and 143 of 1988. About 0.15 m of water was applied to the fields during each irrigation application.

Winter Wheat Characteristics

The experimental field was seeded with winter wheat (Triticum aestivium L., Aldente), on day 361, December 27, 1987, with emergence occurring around the 1st of January 1988. The wheat was sown by drilling in 0.22 m wide rows running north–south with a seed density of about 295 kg/hectare. Within 50 days of planting, canopy closure was complete.

Location of Instrumentation

Instrumentation in field 15 consisted of a Bowen ratio system (exchange mast, psychrometers, net radiometer, soil heat–flux plates, and a 12–V battery charged by a solar-cell, an IRT mounted on a heavy tripod,

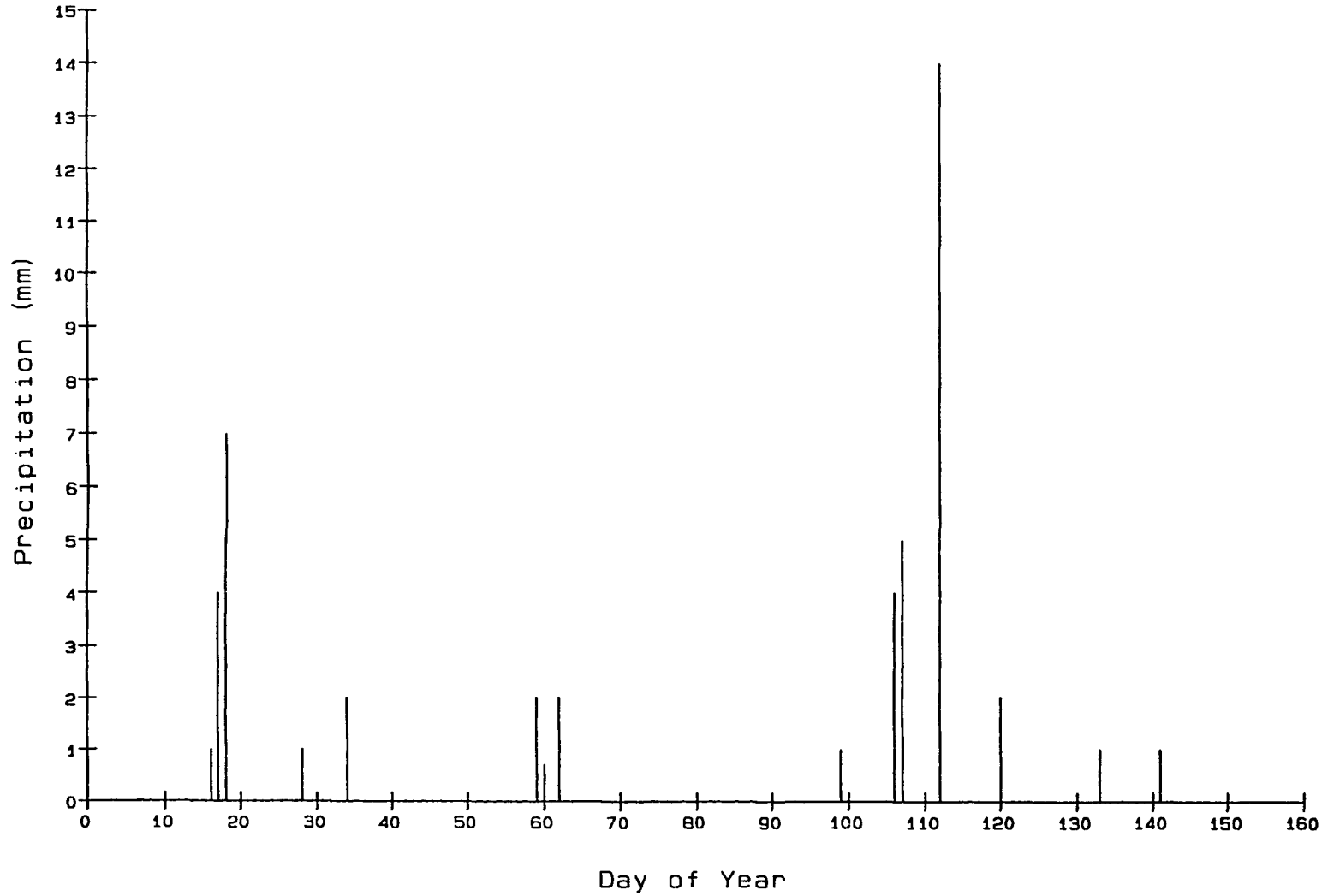

Figure 4. Precipitation during the 1988 winter wheat growing season.

an anemometer. The Bowen ratio mast was situated near the center of the field with the data logger located in a mobile laboratory 40 m northeast of the instruments. An eddy-correlation system was installed in the field for several weeks near the end of the experiment.

According to standard practice for operating the BREB system over a crop, the psychrometers were mounted on an exchange mast of length 1 m with the lower psychrometer 0.2 m above the top of the wheat canopy. In addition, an anemometer was positioned approximately 2 m above the canopy. As the wheat grew, the psychrometers and anemometer were raised to maintain their relative positions above the canopy, as shown in Figure 5. The net radiometers were set 1.7 m above the canopy, and the soil heat-flux plates were buried at a depth of -0.01 m. The sonic anemometer and fine-wire thermocouple sensors on the eddy-correlation system were positioned 1 m above the canopy. The fetch-to-height ratio in 1988 was about 175 in 1988 for the predominant wind direction (northwest).

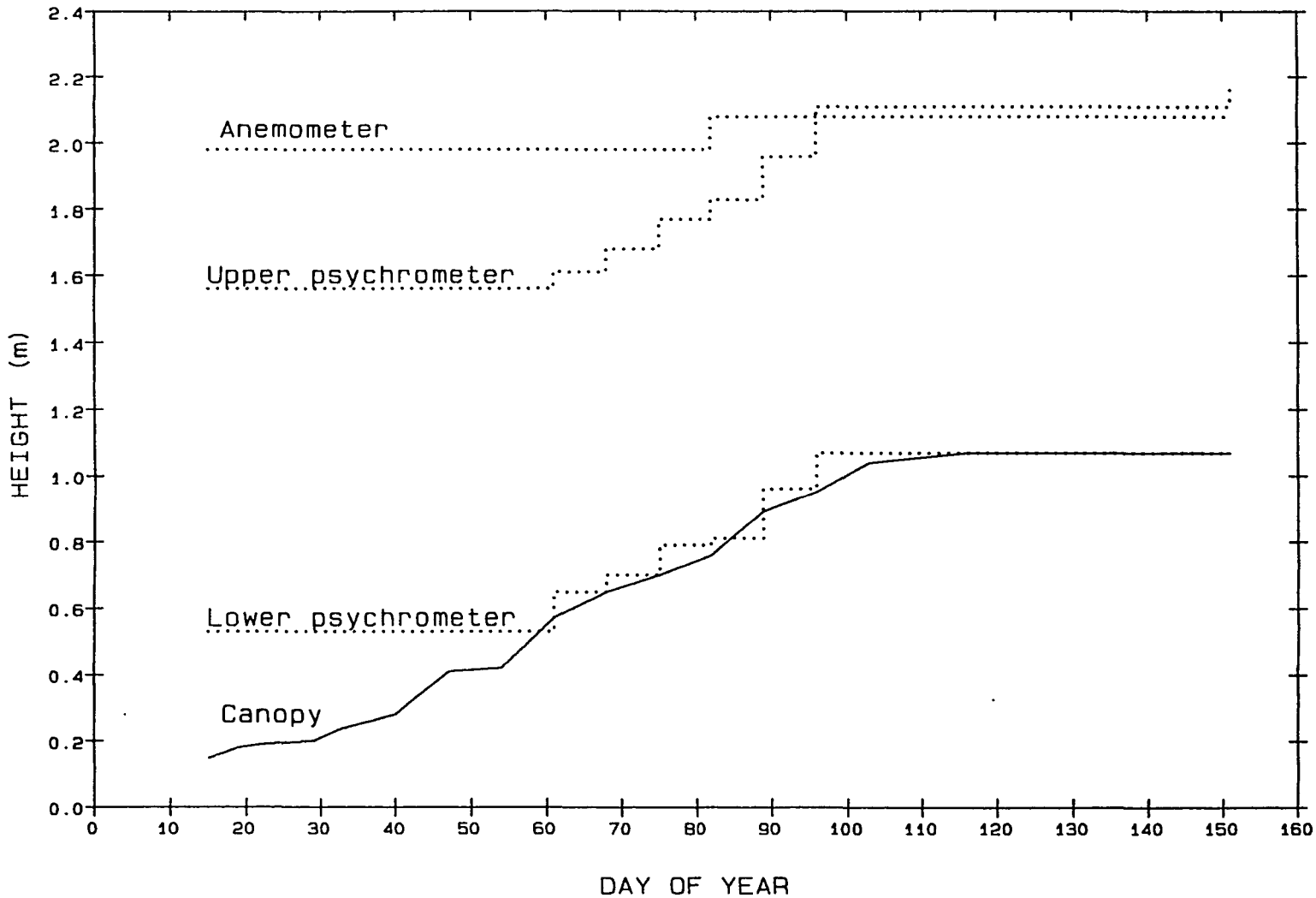

Figure 5. Canopy and instrument heights during the 1988 winter wheat growing season.

3. ENERGY–BALANCE RESULTS

This chapter describes the Bowen ratio energy–balance measurements made over winter wheat. The BREB measurements were made at 12-min intervals for 137 days in 1988, from day 15 to day 151. Energy–balance data were analyzed within discrete blocks of time based on individual 24–hour diurnal cycles and as a data set representing the entire season.

The seasonal analysis describes the effects of climate, surface, and soil moisture characteristics on the energy balance. The growing season and the post senescence period are considered separately.

The physiological status of the irrigated wheat (transpiring or senesced) controlled the partition of available energy into either sensible heat or latent energy, which in turn controlled the stability of the atmosphere just above the crop. During active growth and high transpiration, the canopy was markedly cooler than the air and stable (inversion) conditions prevailed ($H > 0$). After the wheat senesced and latent energy decreased, the canopy became warmer than the air, and unstable (lapse) conditions prevailed ($H < 0$). Because sensible heat is advective when $H > 0$ and convective when $H < 0$, the comparisons of the two methods for measuring sensible heat flux covered a wide range of flux magnitudes and directions.

Diurnal Energy Balance

The BREB measurements were processed into one hundred and thirty-seven 24-hour diurnal data sets, each containing one hundred and twenty 12-min averages of Q-, G-, H- and LE-fluxes measured in watts per square meter. Daily energy totals, in MJ/m^2, were obtained by integration of the 12-min flux values from the beginning to the end of the day. Latent energy totals can also be expressed as an equivalent depth of water, ET, in units of millimeters according to the relation 2.45 MJ/m^2 = 1.00 mm at 20°C. Although fluxes leaving the surface are considered negative, ET equivalent depths are always shown as positive in this study.

Because of the large numbers of plots and the consistency of the data, I selected representative days for description. Four days were sufficient to illustrate the differences between the energy balances of actively growing wheat and senesced wheat: early (day 37), late (day 130), and overcast (day 62) days within the growing period and a day within the senesced period (day 142). Table 1 contains a summary of the 24-hour totals of Q, G, H, LE and ET for days 37, 62, 130, and 142. Plots of the energy balance are shown in Figures 6A to 6D.

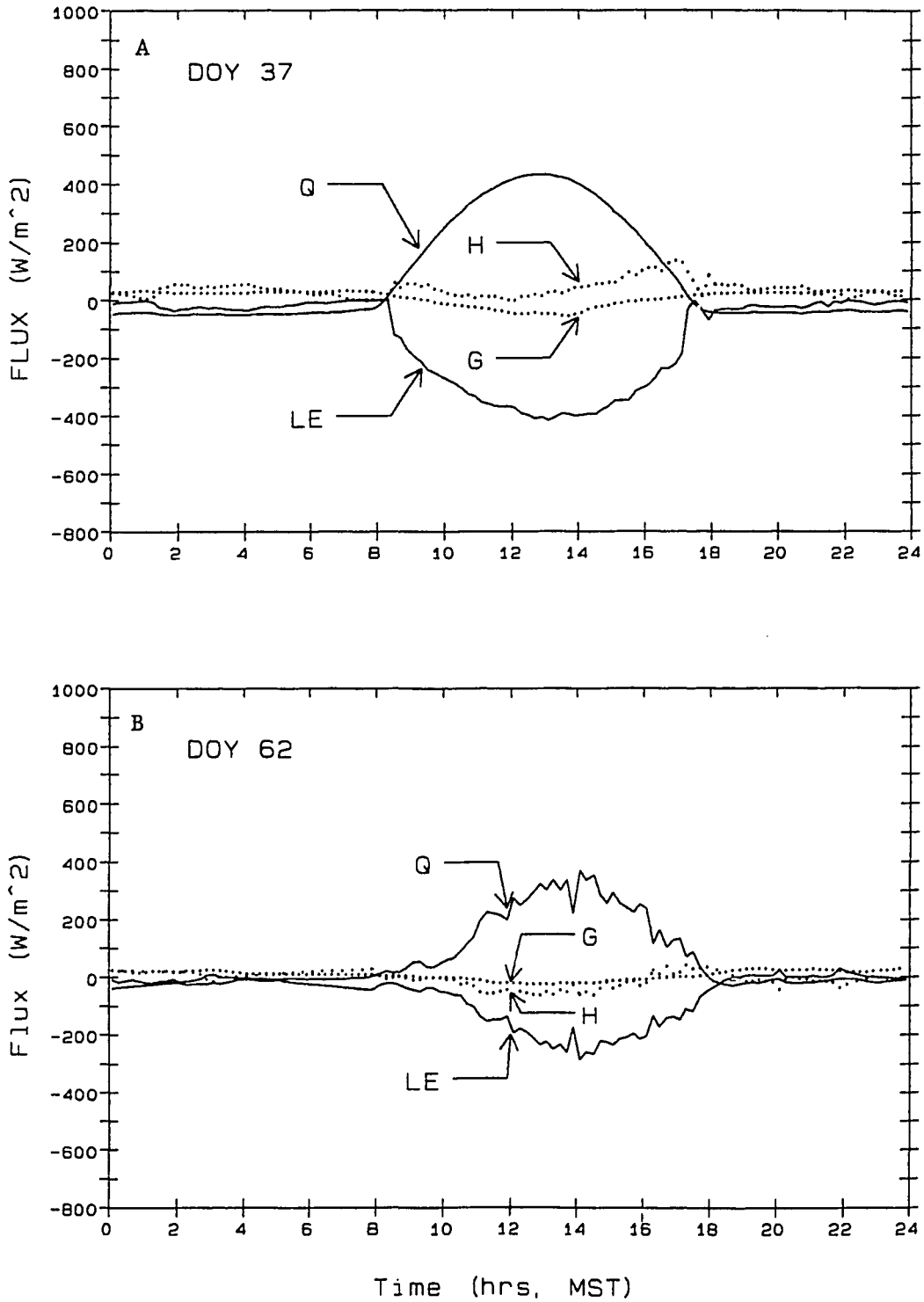

Figure 6. 12-minute energy fluxes from BREB of winter wheat
A. Early season clear sky, day 37, 1988.
B. Mid-season cloudy sky, day 62, 1988.

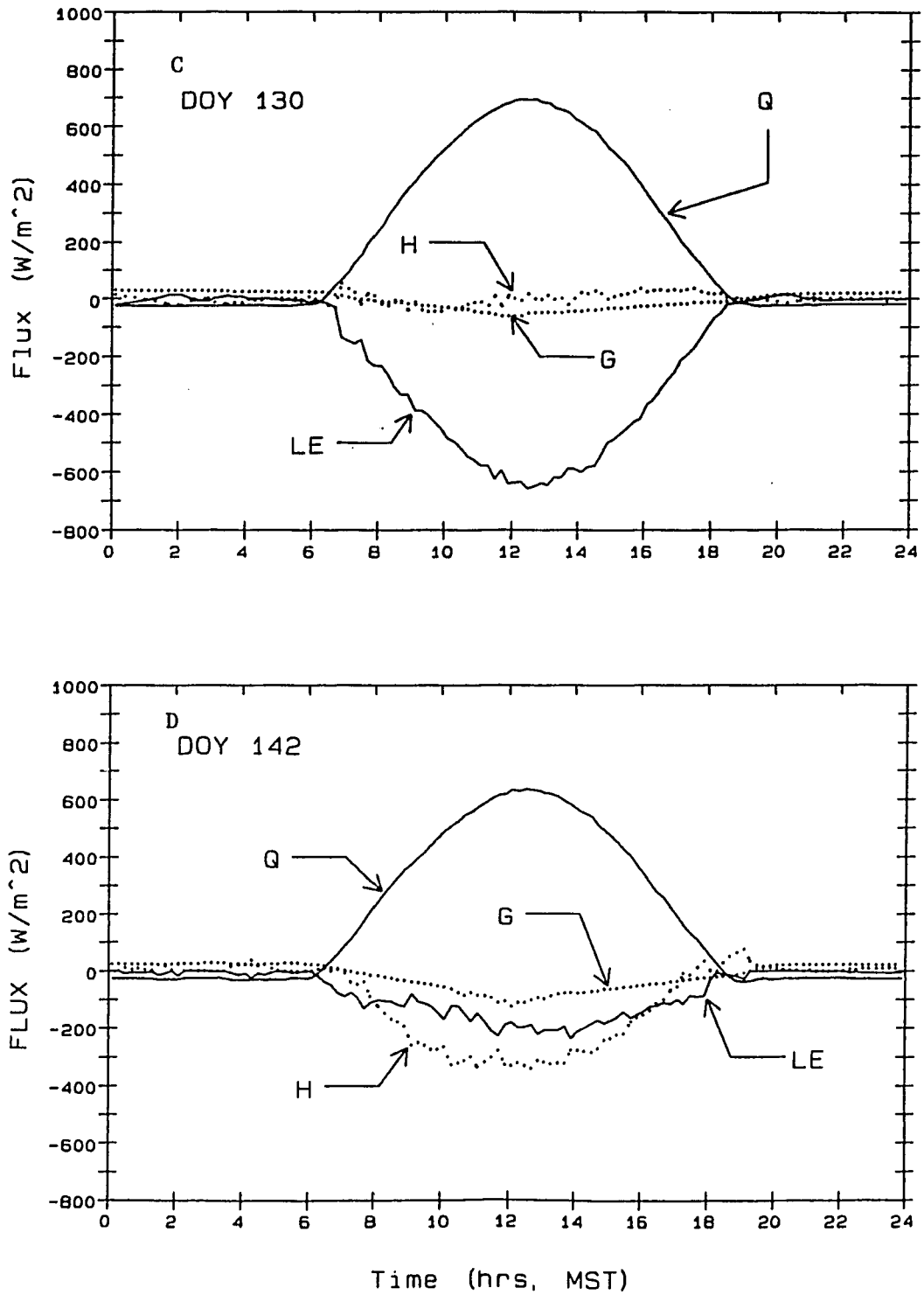

Figure 6. 12-minute energy fluxes from BREB of winter wheat
C. Late season clear sky, day 130, 1988.
D. Late season clear sky, day 142, 1988.

Table 1. Daily mean energy balance for four selected days

DOY[1]	Date	Q MJ/m²	G MJ/m²	H MJ/m²	LE MJ/m²	ET mm	Comments
37	6 Feb 88	6.91	0.88	3.38	-11.16	4.6	Clear, growing
62	3 Mar 88	5.57	0.62	-1.25	-4.94	2.0	Cloudy, growing
130	10 May 88	17.39	-0.19	0.19	-17.39	7.1	Clear, growing
142	22 May 88	15.53	-1.39	-10.97	-3.30	1.3	Clear, senesced

The smooth Q- and G-flux curves in Figures 6A, C, and D are a common feature of the clear-day energy balance (the prevalent condition at Maricopa). Solar and net radiation rise and fall symmetrically throughout a day with clear skies. In contrast, the example of an overcast day (day 62 in Table 1, Figure 6B) shows reduced and variable fluxes of net radiation, associated with higher variability in G, H, and LE relative to days with clear skies. In the absence of solar radiation at night, net radiation consists of incoming and outgoing long-wave fluxes that are almost in equilibrium, so Q is close to 0. With net radiation small, the G, H, and LE fluxes are also close to 0.

The size and shape of the LE diurnal curve is closely related to the size and shape of the Q-curve; in Figures 6A-D, the relative symmetry between the LE and Q-curves is evident. However, LE is affected by the surface conditions that control the partitioning of available energy into turbulent fluxes. For irrigated crops in semiarid areas, sensible heat energy is often advected to the canopy from the surrounding desert (H >

[1]Day of year.

0). Under clear skies, the growing wheat energy balance (Figures 6A and C) shows clearly that LE exceeds Q when H is large and positive. The opposite extreme is reached after the wheat has senesced (Figure 6D, day 142), when available energy was partitioned mostly into H (H < 0) so that LE is much smaller than Q.

Evapotranspiration totals for these four selected days range from 1.3 to 7.1 mm, as shown in column 7 of Table 1. The ET amounts follow the available energy when the wheat is growing: ET was moderate early in the growing season (day 37), low on the overcast day (day 62), and largest late in the season (day 130). The value of ET was smallest late in the season, when the wheat was dry (as on day 142), even though available energy was large.

Actively Growing Wheat

The wheat was planted on day 361 of 1987 (December 27), and emerged around day 1 of 1988 in a moist, cool environment. As the wheat grew, the canopy gradually increased in density until it closed around day 50 (February 27) and reached its maximum height on day 115 (March 25). The seed heads were full by day 130 (May 8).

The green, moist, transpiring wheat transforms available energy (Q and G) into latent energy as liquid water is converted into water vapor. The daily totals in Table 1 illustrate seasonal effects on the surface

energy balance. The largest portion of the available energy is Q, and total daily Q for the growing wheat increased about 250% between day 37 and day 130. Daily total G, however, remained small throughout the growing period because most of the energy absorbed by the soil during the day was given up at night. Horizontal energy and mass transfer played a major role in driving the ET process on day 37. Nearly 30% of the latent energy used to convert liquid water to vapor came from advected H. Only a small amount of advected sensible heat contributed to latent energy near the end of the growing season on day 130. The amount of energy advected to vegetation, however, depends on environmental factors such as wind as well as on the physiological status of the vegetation. The measurement of the sensible heat term is the major focus of this dissertation.

Senesced Wheat

The senesced wheat retained the same crop geometry as the growing, maturing wheat. However, the process of senescence shuts down plant transpiration, so the wheat is dry and less resilient than when growing. This change in plant water status markedly affects the surface energy balance.

After the wheat senesced on day 137, the net radiation decreased somewhat. The value of G became more negative as more energy was transferred into the soil each day, further decreasing available energy. Available energy (Q + G) on day 142 was about 82% of that on day 130, but

LE was only 19% as large. With the wheat dry and not transpiring, little water was available to be converted to vapor, the canopy became warmer than the air, and the available energy was partitioned into sensible heat rather than latent energy.

Seasonal Energy Balance

The mean daily Q–, G–, H– and LE–fluxes measured by the Bowen ratio from day 15 to day 151 provide the basis for a seasonal energy balance of the winter wheat. The effects of climate and the changing surface characteristics can be seen in the behavior of the seasonal energy balance throughout the season. The daily averages of the seasonal energy balance is recorded in Figure 7. Precipitation events greater than 1 mm and the dates of irrigation are also shown in the figure. Each irrigation application averaged about 150 mm, about an order of magnitude greater than the largest precipitation event. As a matter of interest, neither the irrigation nor the precipitation appeared to increase the ET rates that followed, suggesting that water was not limiting during the 1988 growing season.

Effects of Climate

The characteristics of the study site make it possible to distinguish climatic effects on ET from surface effects. The discussion of climatic effects is restricted to the growing season up to senescence on day 137,

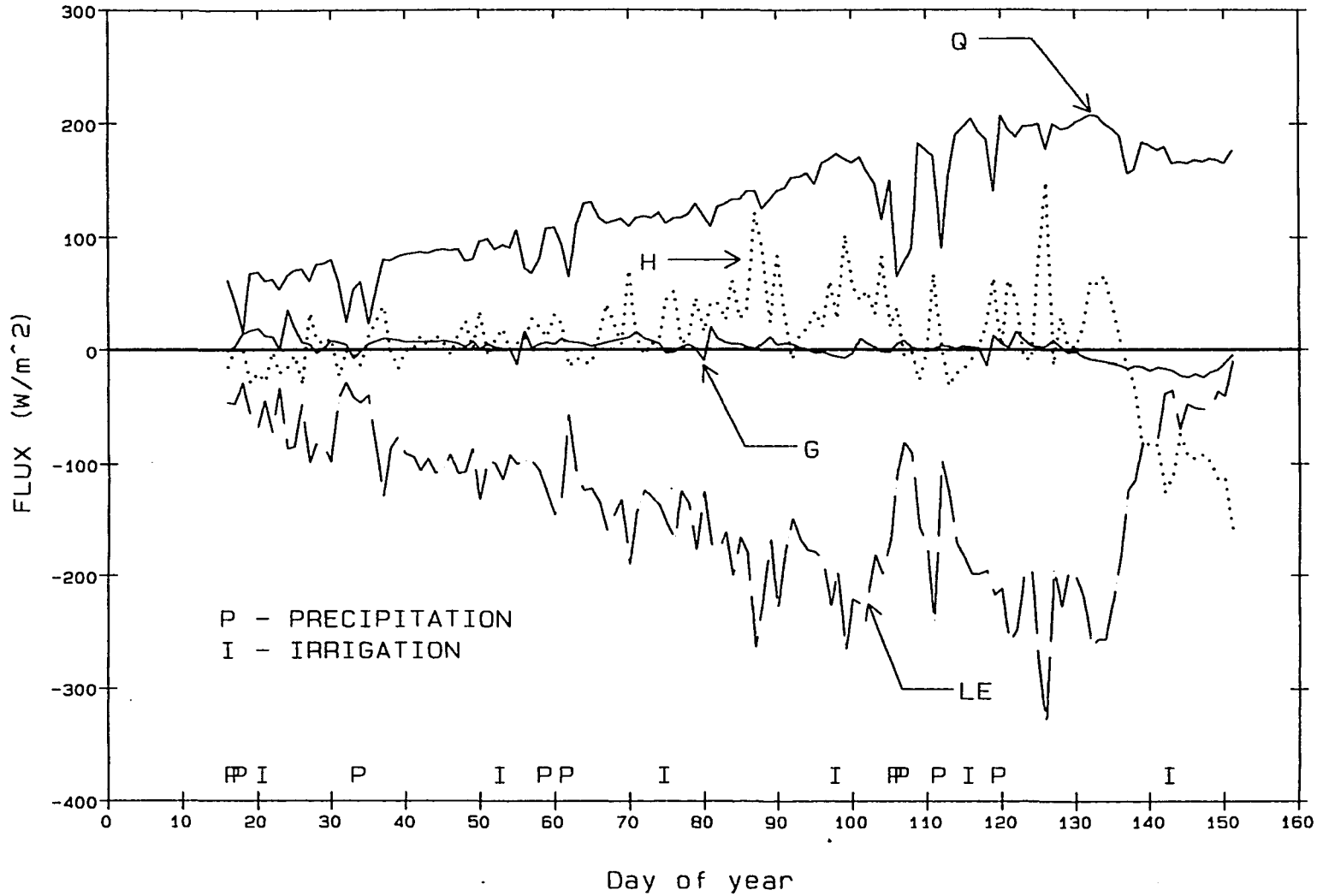

Figure 7. Mean daily energy fluxes for winter wheat in 1988.

during the period that the wheat was actively transpiring.

The net radiation portion of the energy balance makes up most of the available energy, with the soil heat flux being rather small. For the 1988 season, the 24-h average daily Q was always positive and increased as the growing season progressed from winter into spring. Large drops in Q are synonymous with the precipitation events and cloudiness, as can be seen in Figure 7 for days 18, 33, 57, 62, 106, and 112.

The value of G remained small throughout the growing season because the soil was covered by vegetation. The amount of energy absorbed by the soil over a 24-hour period is about equal to the amount released, so the average daily G remained close to zero. The mean daily flux consistently went negative in the late spring (after day 129), indicating that the soil had begun warming.

The size of LE increased (became more negative) throughout the spring as the wheat developed and insolation increased. Average daily LE increased from about -50 W/m^2 for clear days at the beginning of the season, when the wheat and available energy were small, to a maximum of -330 W/m^2 on day 126, when winds were high. The major variability in the daily LE trend is due to the effects of clouds on net radiation; as radiation drops, available energy decreases, but when the skies clear, LE returns to its previous level. Wind plays a secondary role in the variability of LE during the growing season. When warm winds blow over

the cool canopy, H is extracted from the air and LE increases. Examples are days 87 and 126. For a given amount of available energy during the growing season, H is more positive and LE is more negative on windy days.

Effects of Surface Characteristics

The maturation and senescence of the wheat crop on day 137 significantly altered the surface energy balance. The value of Q leveled off and decreased slightly, then G became more negative, significantly reducing the available energy. As the wheat ripened and dried, the plants changed color from green to brown, increasing the canopy reflectivity and canopy temperature relative to the air. The physiological process of ripening reduced the absorption of solar radiation and increased the emission of outgoing long-wave radiation, thus reducing the amount of net radiation absorbed by the canopy.

The drying of the canopy following senescence markedly affected the partition of available energy into sensible and latent heat. The sensible heat flux reached maximum daily means of about 150 W/m^2 on windy days during the growing season. The flux increased (became more negative) after senescence, reaching a maximum value of -162 W/m^2. The magnitude of the daily mean LE on days when the evaporative demand was high during the growing season (day 126) was -330 W/m^2, and this decreased to only -10 W/m^2 following senescence.

Seasonal Totals

The daily mean energy-balance terms were totaled for each day in the season, in units of MJ/m^2. Flux totals were estimated by extrapolation for the 15-day period between the time of emergence and the start of Bowen ratio measurements. All flux totals were converted to equivalent depths of ET (2.45 MJ/m^2 = 1.0 mm) and tabulated in Table 2. The tabulation divides the total into three periods: the extrapolated period (days 1-15), the growing period (days 16-136), and the postsenescence period (days 137-151) The average ET for the growing season (days 1-134) was 4.61 mm/day. The measured range in LE values for days 16 to 134 were 11.9 mm on day 126 and 1.3 mm on day 32. Measured LE dropped to 0.4 mm in the postsenescence period, while H climbed to an equivalent depth of 5.6 mm.

Table 2. Energy balance of winter wheat over the 1988 season.

Q	G	H	LE	ET_{TOT}	ET_{AVG}	#Days	Comments
	MJ/m^2			mm			
63	0	-18	-45	18.3	1.2	15	Extrapolated 1 to 15
1227	43	190	-1460	594.9	5.0	118	Growing 16 to 134
253	-24	-115	-114	46.5	2.7	17	Senesced 135 to 151
1543	19	57	-1619	658.8	4.4	151	Total or Average

A simple water balance for the winter wheat can now be calculated. If we assume that soil water storage is approximately equal at the beginning and end of the study period, then ET = irrigation +

precipitation - drainage. Pre-emergence irrigation plus six more irrigations during the growing season introduced about 1050 mm to the wheat crop. Up to harvest, ET consumed about 650 mm, and precipitation added an additional 48 mm. Drainage is thus estimated as approximately 1050 - 650 - 48 = 352 mm. This estimate leads to the conclusion that the 1988 winter wheat at MAC received about 2.3 irrigation cycles in excess of its ET needs. The removal of accumulated salts requires water in excess of the wheat ET needs to flush the soil, which accounts for the irrigation application just before harvest (day 143).

The next chapter compares sensible heat flux derived by the Bowen-ratio and eddy-correlation systems.

4. EXPERIMENTAL VALIDATION OF THE BOWEN RATIO

Bowen ratio sensible heat flux values are used as a "truth-set" for model evaluation. If the Bowen ratio H-values are to be used with confidence, the data should be validated by a set of independent H measurements, such as those obtained from an eddy-correlation system through the covariance of vertical wind and air temperature fluctuations. Eddy-correlation measurements of sensible heat flux were acquired over a wide range of surface and atmospheric conditions to validate Bowen-ratio sensible heat flux data.

Eddy-Correlation Method

The one-dimensional eddy-correlation method determines H by measuring fluctuations of vertical wind speed (W'), air temperature (T'), and the covariance ($\overline{W'T'}$) (Swinbank 1951, Brutsaert 1982). Eddy-correlation H is computed from

$$H = -\rho C_p \overline{W'T'} \quad , \tag{4.1}$$

where ρ and C_p are air density and specific heat, respectively, and the overbar denotes a time average of the product of W' and T'. Equation (4.1) is valid when the mean vertical wind (W) is zero. The wind and air temperature sensor data were preprocessed in a Campbell Scientific Incorporated (CSI) 21X Micrologger and stored on cassette tape to yield the covariance $\overline{W'T'}$ and its associated statistical parameters. During

the experiment, values of W′ and T′ were sampled at 0.2–s intervals and averaged over the same 12-min period used by the Bowen ratio. The value of W′ was measured with a CSI Model CA27 continuous, switched-wave, sonic anemometer; the value of T′ was measured with a CSI 13–μm, type–E (chromel-constantan), fine-wire thermocouple attached to the CA27 and placed 0.03 m from the sonic path. Calibration of the sonic anemometer is not required although a drift adjustment can be made when the mean vertical wind speed deviates from zero. A laboratory test of the sonic anemometer in a closed container showed that its output was zero when the mean vertical wind was zero.

Comparison Experiment

The eddy–correlation system was placed in the winter wheat field 10 m away from the BREB system on day 134. It collected 12-min mean H–values simultaneously with the BREB until day 152, when both systems were removed shortly before the wheat was harvested. The field performance of the two systems was evaluated by linear regression analysis of the 12–min fluxes from the Bowen ratio and eddy–correlation systems. The analysis included the computation of slopes, intercepts, their associated standard errors, r^2–values, and the standard error of the regression line. The standard error of the regression was used as an estimate of the measurement uncertainty for the two instruments under growing and senesced field conditions.

Diurnal H Fluxes

In Figure 8, sensible heat flux values from Bowen ratio (HBr) and eddy-correlation (Hec) systems are plotted against time of day for days 135 and 149 using 12-min means. The close relationship between HBr and Hec throughout each day illustrates that the two systems are in excellent agreement. The agreement between the two independent measurements of sensible heat is maintained under both stable (day 135) and unstable (day 149) conditions. Figure 8 also illustrates how the physiological state of the canopy affects partitioning of available energy into sensible heat at the surface, with a resulting effect on the surface energy balance. The canopy of actively growing wheat on day 135 was transpiring heavily and the transpiration rate was enhanced by extraction of sensible heat from the atmosphere. The positive H-flux reached about 100 W/m^2 during the late afternoon. However, by day 149 the wheat had senesced and physiological changes halted transpiration. As transpiration decreased, the canopy transferred an ever-increasing portion of the available energy (Q + G) by convection into the atmosphere. The relatively large H from the dry canopy on day 149 was directed away from the canopy and reached values as large as -400 W/m^2 at midday.

Statistical Processing

Since the magnitude of H was close to 0 W/m^2 at night, analysis was

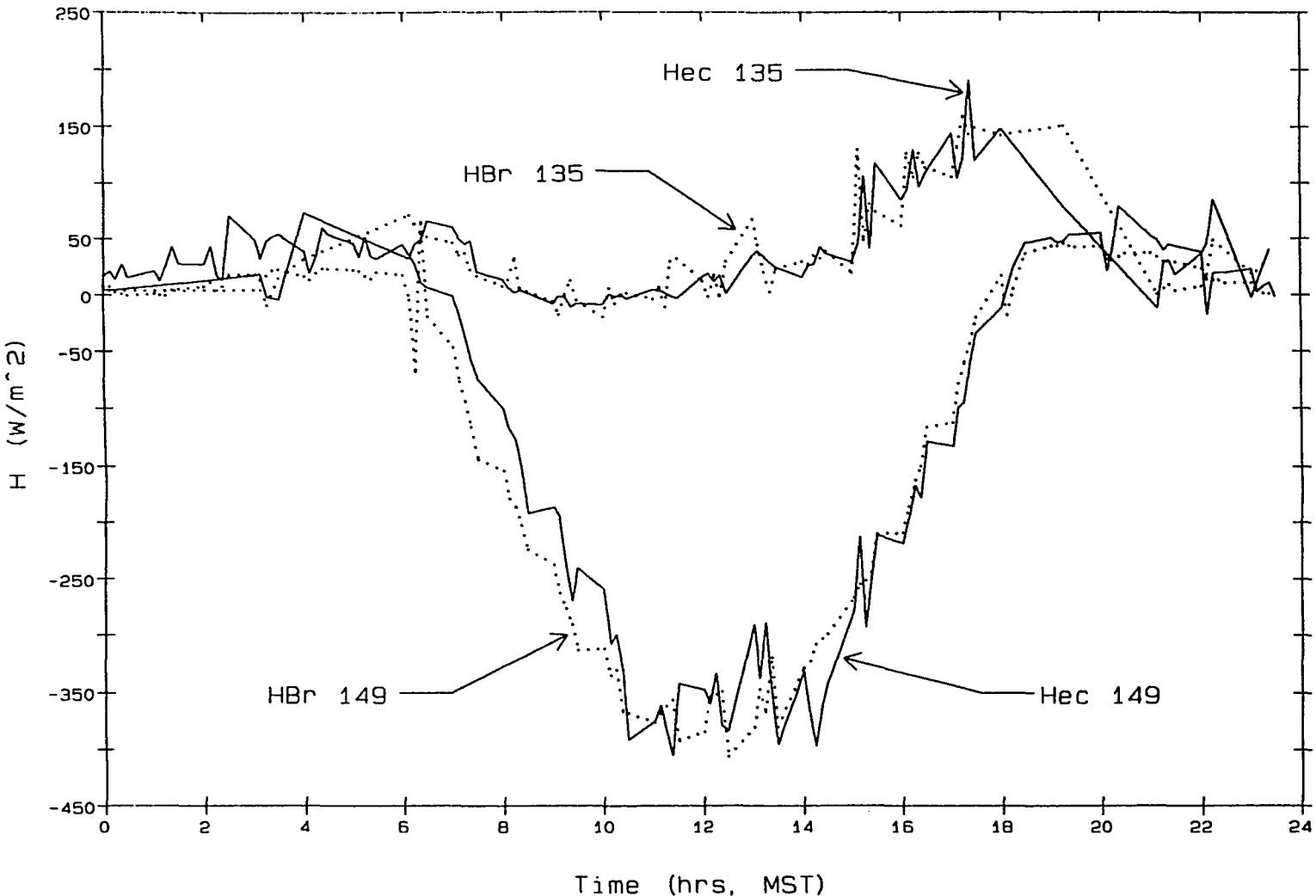

Figure 8. Comparison of sensible heat fluxes for days 135 and 149 of 1988, as measured by Bowen ratio and eddy correlation systems.

restricted to the daylight hours between 0630 and 1730 to minimize statistical bias caused by artificially increasing the population of small fluxes relative to larger, daytime ones. The daylight data were statistically analyzed using regression and analysis of variance routines in RS/1. HBr and Hec fluxes were regressed for each of the 17 days that data were collected. Slopes, intercepts, standard errors (SE), r^2–values, and normalized percent differences (NPDs) between means are tabulated in Table 3.

As an example, mean 12-min daylight H–fluxes from both systems were plotted in Figure 9 for days 135 and 149 of 1988. The mean H–value on day 135 was small and positive (37 W/m^2, stable) and the regression equation was Hec = (0.84 HBr + 4.3) with SE = 24 W/m^2, an r^2 = 0.84, and an NPD = 4% (Table 3). As the canopy senesced and dried, the H–fluxes changed from stable to unstable, the daylight mean H–values increased in size, the r^2–values and slopes increased, and the NPDs decreased. By day 149, the H–values were large and negative (-226 W/m^2, unstable), and the regression equation was Hec = (1.02 HBr + 17.2) with SE = 42 W/m^2, r^2 = 0.91 and NPD = 6% (Table 3).

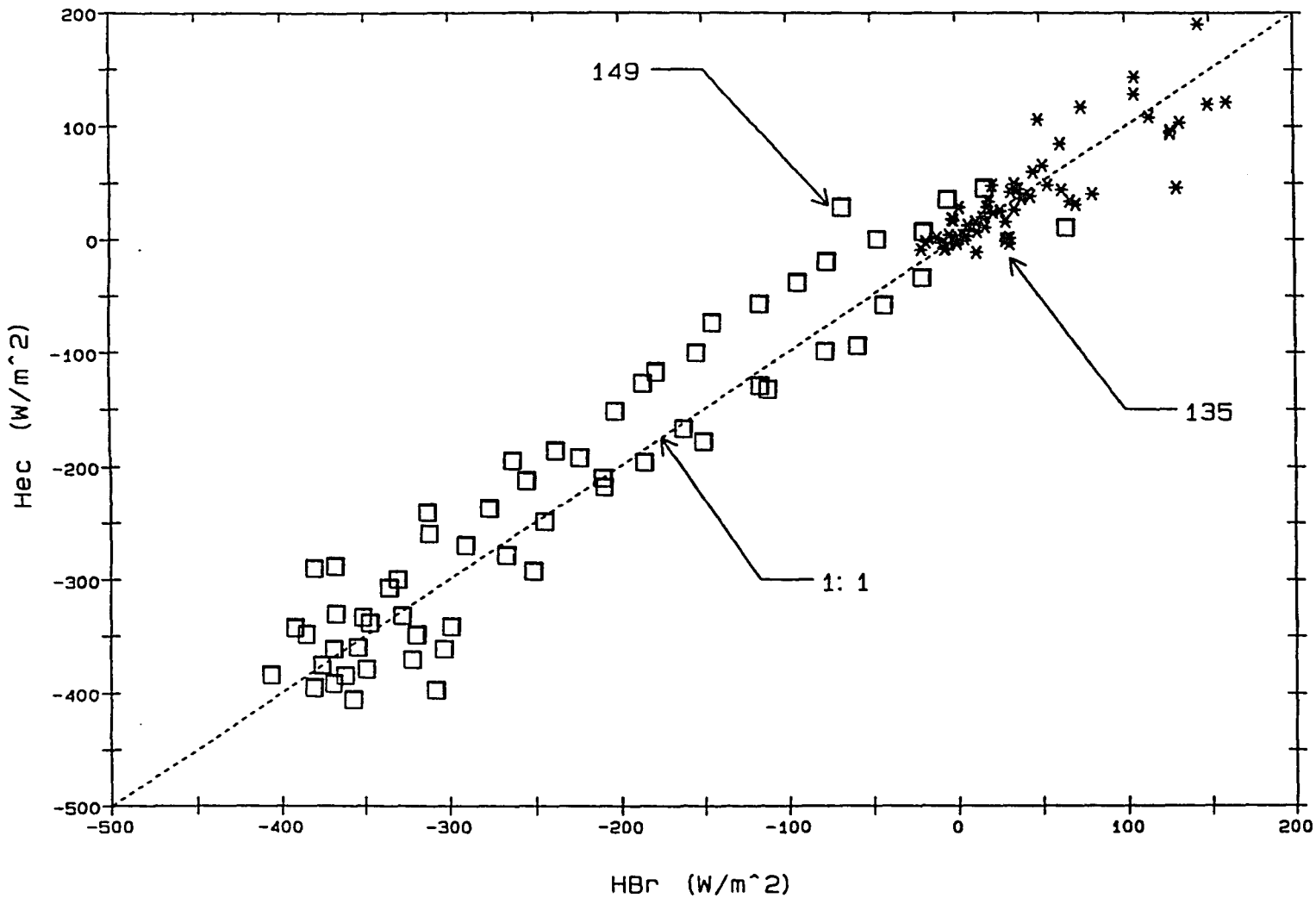

Figure 9. Distribution of 12-minute daylight sensible heat fluxes of HBr vs. Hec for days 135 and 149 of 1988.

Table 3. Regression analysis of HBr vs. Hec for days 135 to 151 during daylight hours.

DATE 1988	r^2	SLOPE	INTCP W/m^2	AVG H±SE	AVG HBr	AVG Hec	%DIFF. (HBr-Hec)/HBr
135	0.74	0.84	4.3	37±24	38	36	4
136	0.66	0.83	0.9	-3±17	-6	-1	83
137	No Bowen ratio data					-22	
138	0.78	0.95	13.0	-54±71	-67	-41	41
139	0.78	0.59	-31.1	-157±46	-179	-134	25
140	0.78	0.80	-3.5	-161±37	-175	-146	16
141	0.85	0.74	0.7	-161±37	-185	-136	26
142	0.84	0.64	-15.2	-167±34	-194	-140	28
143	0.78	0.69	-17.4	-155±47	-173	-136	22
144	No Bowen ratio data					-148	
145	0.82	0.78	-17.0	-191±55	-208	-174	16
146	0.93	1.00	17.0	-205±34	-213	-196	8
147	0.85	0.85	5.7	-189±42	-208	-170	18
148	0.95	1.03	16.7	-208±28	-218	-198	9
149	0.91	1.02	17.2	-226±42	-232	-219	6
150	0.91	1.11	30.1	-253±45	-255	-252	1
151	0.95	0.93	20.3	-276±31	-296	-255	14

The evaluation process is based on standard statistical measures of regression correlation between the two systems. The quality of the linear regression relationships between HBr and Hec is defined by five parameters: r^2, slope, intercept, standard error, and the average NPD between the two instruments. The NPD reduces the bias in differences between the means because H is much smaller for growing wheat then for senesced wheat. Agreement between the Bowen ratio and eddy correlation improves as r^2–values and slopes approach 1, as intercepts approach 0, and as standard errors and differences between means decrease. The agreement between sensors throughout this period is illustrated in Figure 10, which shows the 1988 daily daylight means from each instrument and

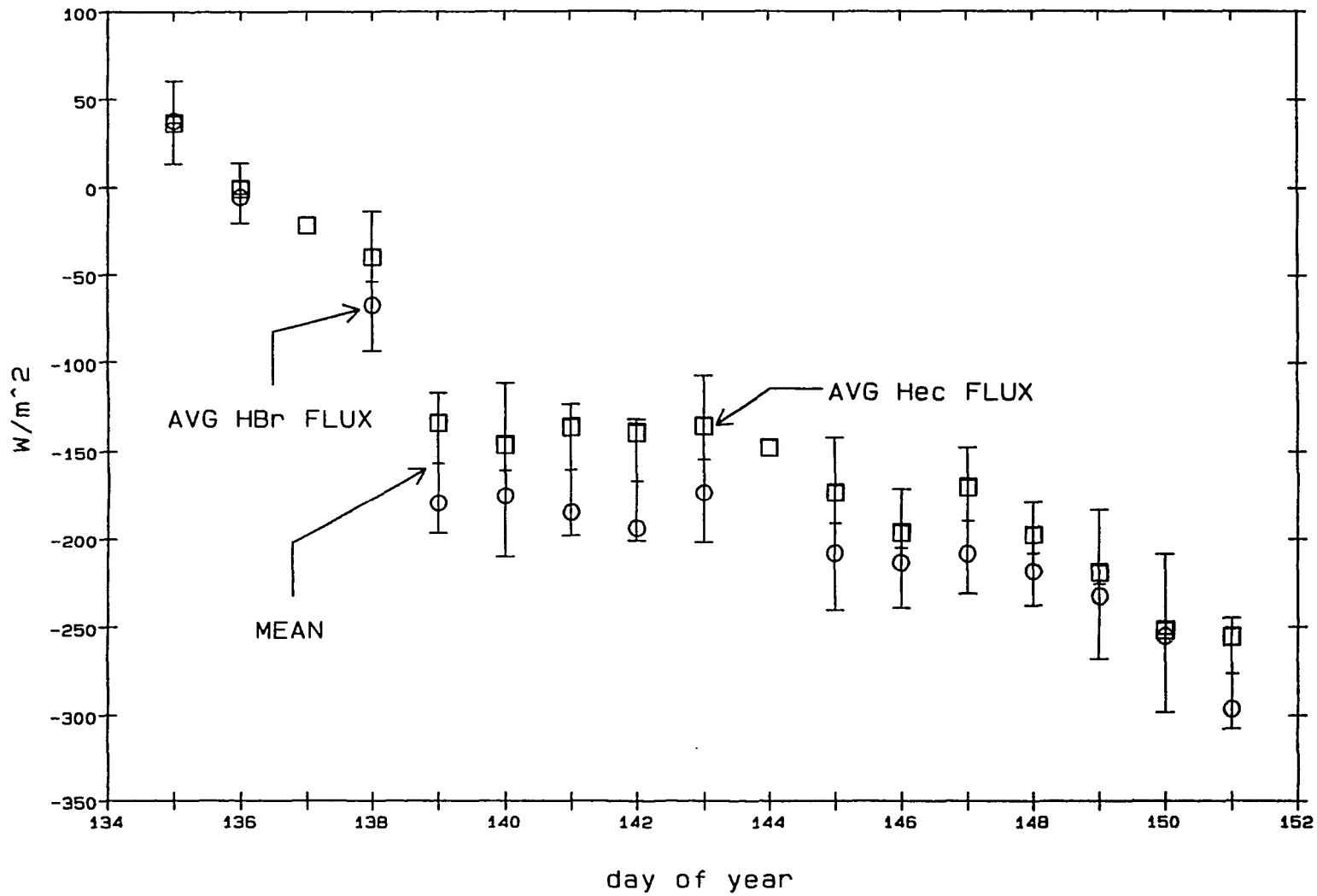

Figure 10. Mean daylight sensible heat fluxes from Bowen ratio and eddy correlation with error bars for days 135 to 151 of 1988.

their associated standard error bars (at 68% confidence). The error bars were calculated with regression SEs from the 12-min daylight values of HBr and Hec on each day.

Comparison Results

The winter wheat was growing when the comparisons began, and sensible heat was advected from the atmosphere to the cool transpiring canopy. The average daytime ß of the transpiring crop on day 135 was -0.09, since $LE < 0$, $H > 0$ and H was almost 10% of LE. As the wheat dried, the average ß–values steadily increased to +5 by day 151, indicating that $H < 0$ and H was now about 5 times greater than LE. In absolute terms, the average daylight sensible heat fluxes during the comparisons changed from about +40 W/m^2 toward the surface to about -275 W/m^2 away from the surface.

The 12-min daylight data were pooled into a 15–day data set containing 867 data pairs. Data pooling removes the effect of daily climatic and environmental variables. Furthermore, small statistical distortions associated with temporal correlation were minimized when the individual days were pooled into a single population. Overall HBr–to–Hec relationships were developed from the regression analysis of the pooled data set. The model derived from linear regression is $Hec = 5 + 0.88\ HBr$, with $r^2 = 0.89$ and SE = 44 W/m^2. The regression intercepts of +5 W/m^2 are very

close to zero, and the slope of 0.88 confirms that Hec is smaller (less negative) than HBr. The data values, linear model, 95% prediction bands, and 1:1 line are shown in Figure 11. From the regression and analysis of variance (AOV), this comparison shows that near the mean, 12-min Hec is estimated with 95% confidence at about -148 ±85 Wm^2.

Comparison Uncertainties

If the Bowen ratio and eddy-correlation systems were perfect, and if all fluxes were accounted for, then any divergence between them would be due entirely to differences in the instruments. However, radiation measurements (Q and G) associated with the BREB system also have uncertainties that might prevent energy-balance closure and induce errors independent of the Bowen ratio. Figure 11 shows that the HBr estimates are consistently larger (more negative) than the corresponding Hec values. Calibration, leveling or position errors in net radiometers and soil heat flux disks affect available energy estimates. Any errors in the available energy (Q + G) will proportionately affect the error in HBr, whereas Hec is estimated independently of available energy. Also, the Bowen ratio system measured just the soil heat flux (G) at -0.01 m; changes in thermal storage in vegetation and the uppermost 1 cm of soil were not estimated. Unmeasured gains in thermal storage in the morning would cause an overestimation of available energy and a proportionate overestimation of HBr with respect to Hec. Over the entire day, the loss

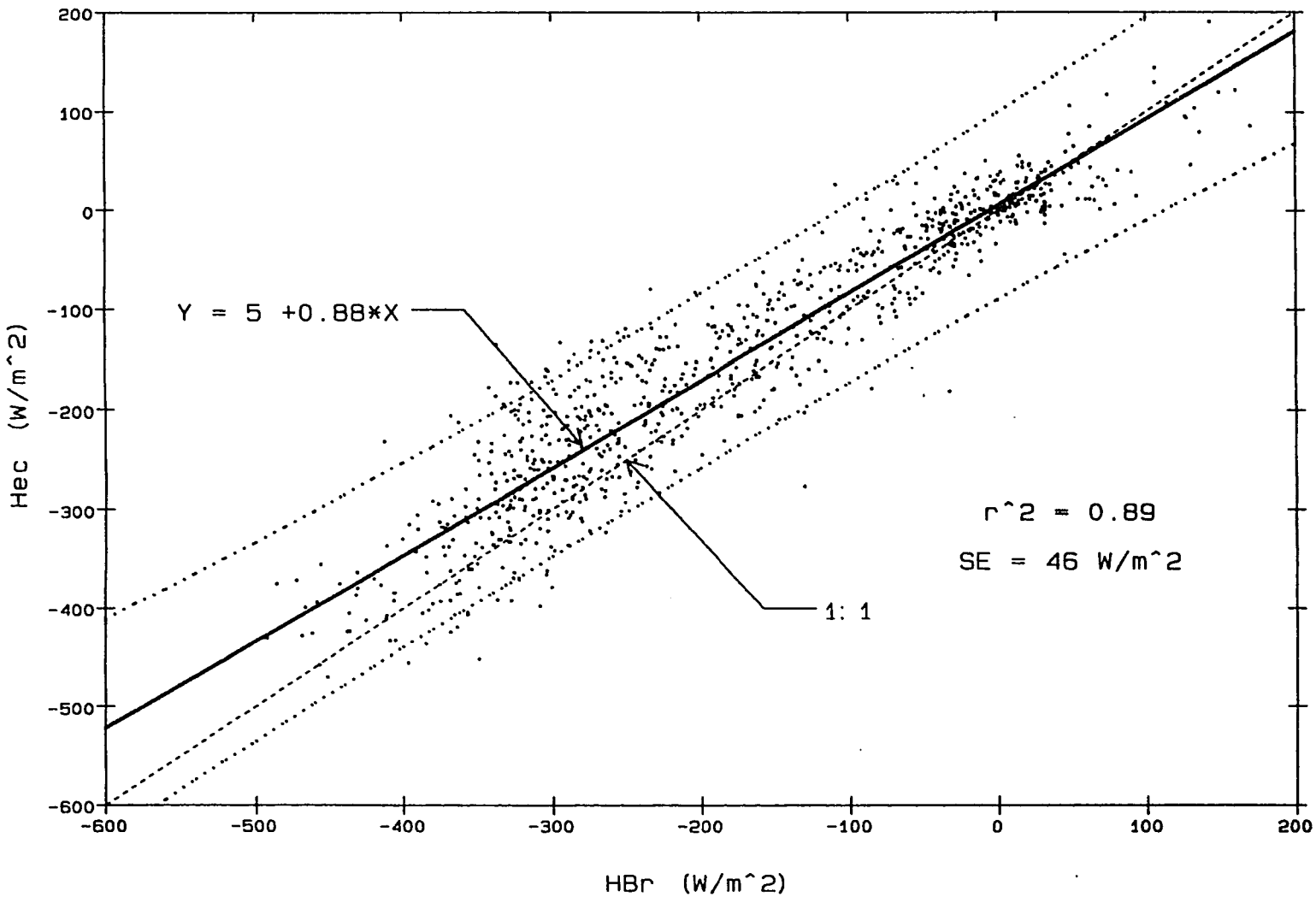

Figure 11. Comparison of Bowen ratio and eddy correlation 12-minute daylight values for 17 days in 1988.

of energy from storage in the late afternoon and at night balances the morning overestimate. However, as mentioned earlier, this analysis covers only the daylight hours.

If data on plant density and specific heat were available for this wheat site, changes in canopy thermal storage could be estimated as a function of the change in canopy temperature with time. Brownridge (1985) calculated the thermal storage of winter wheat as a function of time at a site about 50 km north of MAC, finding that the values ranged from 5 to 14 W/m^2, with the larger values occurring around sunrise and sunset. Her analysis indicates that changes in thermal storage amount to only a few percent of the available radiation, and the difference between closure for a 24-h period is even smaller. The thermal storage changes in the vegetation are not likely to be a significant part of the difference between the measurement systems.

Discussion of System Comparisons

Bowen ratio and eddy-correlation estimates of H were reasonably related over a wide range of values and conditions (+180 W/m^2 to -450 W/m^2), with an r^2-value of 0.89 for the pooled populations. On individual days when the plant-soil environment was relatively dry and H was large, the r^2-values were about 0.90, slopes approached 1.0, the intercepts were small (about 10% of the average H-flux), and the standard

errors ranged between 10% and 20% of the average fluxes. In a moist environment (days 135 to 138), the absolute differences between the two systems were small, but the percentage errors were large, with NPD between the two systems reaching a maximum of 83%. The r^2-values were also lower for the moist period, ranging from 0.66 to 0.78.

During the 17-day study, the Bowen ratio and eddy-correlation systems operated over growing and senesced plant canopies associated with stable and unstable atmospheric conditions, respectively. With this wide range of environments, the regression analysis showed that the sensible heat measurements from both systems were in general agreement. However, differences between Bowen ratio and eddy- correlation H-values appear to be systematic at diurnal intervals and for the pooled data set. HBr values were consistently greater than Hec values on all 17 days, whether the data were computed as mean daylight values or in the pooled population. These difference might be explained by one of the following: (1) The net radiation values in the BREB were overestimated. (2) The eddy-correlation system did not acquire the complete eddy spectrum of sensible heat flux because it was too close to the surface or the frequency response was inappropriate for the crop surface. (3) A combination of problems from both the Bowen ratio and eddy-correlation systems contributed to the differences.

5. DEVELOPMENT OF SENSIBLE HEAT FLUX MODELS

Development of the Monin-Obukhov and aerodynamic resistance models will be discussed in this chapter. These models yield estimates of turbulent exchange coefficients for sensible heat flux. The exchange coefficients can then be used to calculate the sensible heat flux from temperature and wind speed data for comparison with the Bowen ratio estimates.

Historical Development

According to Brutsaert (1982), the Monin-Obukhov theory was first formulated in 1946 (Monin and Obukhov 1954) and was translated from Russian into English by Monin and Yaglom in 1971. Monin-Obukhov turbulent transfer theory was an attempt to model the energy exchange process from fundamental physical principles, as opposed to empirical relationships. Turbulent exchange of sensible heat was modeled as a non-linear function of two scaling parameters for velocity and eddy length, called friction velocity (U_*) and length (L), (Panofsky and Dutton 1984). Numerical solutions for the Monin-Obukhov surface turbulence terms, such as U_* and L, were generated by Paulson (1970) and verified by Businger et al. (1971) and Brutsaert (1982). However, numerical solutions for the nonlinear Monin-Obukhov terms are computationally intensive, requiring extensive use of computer

technology. The computational requirements and the limited capabilities of computers several decades ago may have served as one of the stimuli for development of more simplified models.

The linear aerodynamic resistance model derived by Monteith (1964) is an alternative approach to estimating turbulent fluxes at the surface. The early aerodynamic resistance (r_a) models were simple and valid only for neutral atmospheric conditions. Monteith modeled the transfer of turbulent fluxes from a canopy as a resistance derived from an analysis of the momentum flux, based on the log-profile of wind speed. This resistance could be applied to the transfer of sensible heat and latent energy as well, if the surface behaved as a uniform two dimensional plane (the "big leaf" assumption). Monteith (1964) used friction velocity (U_*) and wind speed (u) to estimate the movement of momentum and heat from a reference surface into the atmosphere under neutral conditions as $r_a = U_*^2/u$. It became apparent that neutral conditions are not prevalent in most environments and that corrections should be applied for non-neutral atmospheres. Furthermore, U_* is difficult to measure directly with instrumentation and is usually estimated from wind profile models. Campbell (1977) expanded Monteith's wind profile model to include separate U_* estimates for both momentum and heat calculated from plant height measurements, but did not consider effects of atmospheric stability upon the turbulent fluxes.

The effect of atmospheric stability on the turbulent exchange at the surface became the focus of studies in the 1970's. Atmospheric stability refers to buoyancy forces associated with temperature and density conditions of the air. In summary, a parcel of air displaced vertically in a neutral atmosphere tends to remain in its new position. A displaced parcel tends to rise in an unstable atmosphere, and sink in a stable atmosphere. Stability can be inferred from the air temperature profile in non-condensing atmospheres near the surface. In neutral conditions, potential temperature declines with height at the dry adiabatic lapse rate (-0.0098°C/m). The potential temperature increases with height in stable conditions and decreases with height in unstable conditions at a rate greater than -0.0098°C/m. Potential temperature is the temperature of a dry parcel of air brought adiabatically to sea level (1013 mb).

Thom and Oliver (1977) published a model that uses Richardson numbers (Ri) for a diabatic stability correction of the aerodynamic resistance. Their model uses empirically derived regression constants to fit[1] the results to selected small data sets. Mahrt and Ek (1984) proposed a refinement that combined Thom and Oliver's stability correction with physical explanations based on Monin-Obukhov theory. The Mahrt–Ek stability corrections use Monin-Obukhov similarity theory to integrate the bulk aerodynamic relationships between two reference levels in the

---

[1]. Many empirical models use fitting techniques developed by Holbo (1971) to impose their own stability corrections on the data.

atmosphere, but employ the Ri approximation instead of Monin-Obukhov's diabatic corrections.

Stability corrections based on Ri are empirical (Brutsaert 1982). The Ri correction requires empirical fitting because Ri does not account for how buoyancy varies with height and how it affects wind and temperature gradients (Louis 1979). The empirical nature of the Mahrt–Ek stability corrections (Mahrt and Ek 1984) is indicated by their observation that the corrections are "based on previous observations and certain asymptotic constraints ...[which] leads to the following dependence for the unstable case (Ri < 0)...." Jackson et al. (1987) used the aerodynamic resistance formulation of the empirical Mahrt and Ek (1984) conductance model for remotely sensed H-estimates. Kustas et al. (1989) expanded the Campbell (1977) canopy-atmosphere resistance model by using Monin-Obukhov theory to include the effects of stability. They used the fundamental Monin-Obukhov stability corrections instead of an empirical Ri-based model.

The fundamental Monin-Obukhov model and two aerodynamic resistance models are examined in detail in the following sections. The Campbell (1977) resistance model is not stability corrected. The Kustas et al. (1989) resistance formulation of the Monin-Obukhov model uses a single stability correction made at the topmost level of wind and temperature measurements. The Monin-Obukhov turbulent transfer model uses stability

corrections at two heights; the top level of measurements, and the lower level of measurements within the canopy.

The Monin-Obukhov Model of Sensible Heat Flux

The model used in this dissertation evolved from the aerodynamic approach developed by several researchers. By following the investigators' assumptions and generalizations, we can see how the Monin-Obukhov parameters were incorporated into a sensible heat flux model. The first portion of this discussion reviews the sensible heat flux equation, discusses surface geometry and diabatic atmospheric conditions, and concludes with a unified, stability-corrected, sensible heat flux model. In the final two sections, the development and practical application of the Monin-Obukhov model and its associated parameters will be explained.

General Development of the Monin-Obukhov Model

The general equation for the gradient form of sensible heat flux (H, W/m^2), is

$$H = -\rho C_p K_h (d\theta/dz), \qquad (5.1)$$

where
ρ is the density [kg/m^3],
C_p is the specific heat [J/kg°C],
K_h is the exchange coefficient [m/s],
$d\theta/dz$ is the potential-temperature gradient with respect to height [°C/m].

Before this equation can be solved, $d\theta/dz$ and K_h must be found. Temperature gradients are routinely measured with several types of instruments such as thermocouples, RTDs and IRTs. Exchange coefficients cannot be measured directly and must be estimated from flux transport processes. The processes that transport sensible heat flux and energy into and out of the surface are dominated by the mean wind speed above the surface. According to Prandtl (1932), the exchange process followed a logarithmic profile of wind with height (within the surface boundary layer). The gradient of the logarithmic wind profile can be approximated for smooth surfaces under neutral conditions by measurements at two levels as

$$u_2 - u_1 = \frac{U_*}{k} \ln \frac{(z_2)}{(z_1)} , \qquad (5.2)$$

where
u is the mean wind speed at height z [m/s],
U_* is the friction velocity [m/s],
k is Von Karman's constant (0.41),
z is the measurement height [m],
and the subscripts refer the level where measurements are made.

The log-profile law appropriate for a rough surface is;

$$u = \frac{U_*}{k} \ln \frac{z}{z_0} , \qquad (5.3)$$

where z_0 is an integration constant called the roughness length. Note that the wind profile is not displaced upward in equation (5.3).

The log-profile over a vegetated surface is displaced upward so that the plane where wind speed is zero is located somewhere within the canopy. The wind profile above the canopy will fit the log-profile

formulation if the measurement heights are referenced to the zero plane. Monteith (1973) defines the measurement height as z-d, where d is the zero-plane displacement, so the wind log profile law becomes

$$u = \frac{U_*}{k} \ln \frac{z-d}{z_0} , \qquad (5.4)$$

where d is the zero plane displacement [m].

According to Monteith (1973) and Campbell (1977), the momentum and heat exchange coefficients are obtained for neutral conditions by taking the derivative of equation 5.4 for momentum ($du/d[\ln(z-d/z_{om})]$ and for heat ($du/d[\ln(z-d/z_{oh})]$)). If $K_m = K_h$ then

$$K_m = kU_*(z-d+z_{om}) , \qquad (5.5)$$

and

$$K_h = kU_*(z-d+z_{oh}) , \qquad (5.6)$$

where
K_m and K_h are exchange coefficients for momentum and heat, respectively [m/s],
z_{om} is the roughness length for momentum [m], and
z_{oh} is the roughness length for sensible heat flux [m].

Substituting equation (5.6) into equation (5.1) and integrating from d to $z-d+z_{oh}$ yields

$$H = -\rho C_p U_* k \frac{d\theta}{\ln[(z-d)/z_{oh}]} . \qquad (5.7)$$

The sensible heat flux equation (5.7) is for "rough" surfaces under neutral atmospheric conditions. According to Brutsaert (1982), Monin and Obukhov (1954) proposed that the variable L define the "stability length" [m]. When $L > 0$, atmospheric conditions are stable; when $L < 0$,

atmospheric conditions are unstable; and when $L = \infty$, atmospheric conditions are neutral. The stability of the atmosphere can be accounted for if L is used in the flux equations. The equation for L is

$$L = \frac{U_*^3 \rho}{kg(H/TC_p)} , \tag{5.8}$$

where
T is the mean temperature between two heights [K] and
g is the acceleration due to gravity [m/s].

If a length measurement, z-d, is included with L, the relative size and direction of eddies moving to and from the surface are represented by the Monin-Obukhov dimensionless variable ζ:

$$\zeta = \frac{z-d}{L} . \tag{5.9}$$

Diabatic stability corrections have been derived from equation (5.9) by Panofsky (1963) and integrated by Paulson (1970) into Ψ-functions. By substituting equation (5.9) into (5.6) and adding the Ψ stability correction, the sensible heat flux gradient equation is now

$$H = -\rho C_p U_* k \frac{d\theta}{\ln(\zeta) - \Psi sh(\zeta)} , \tag{5.10}$$

where Ψsh and Ψsm are the heat and momentum stability corrections, respectively. For practical purposes, $d\theta$ is measured at two levels above the surface, Brutsaert (1982) expands equation (5.10) for two levels as

$$H = -\rho C_p U_* k \frac{(\theta_2-\theta_1)}{\ln(\zeta_2/\zeta_1) - \Psi sh_2 + \Psi sh_1} , \tag{5.11}$$

The Ψ-functions for both stable and unstable atmospheric conditions

are described by Paulson (1970). For unstable atmospheric conditions,

$$\Psi sm = 2\ \ln[(1+X)/2]+\ln[(1+X^2)/2]- 2\ \arctan(X)+\pi/2, \text{ and} \quad (5.12)$$

$$\Psi sh = 2\ \ln[(1+X^2)/2], \quad (5.13)$$

where

$$X = (1+ß\zeta)^n\ . \quad (5.14)$$

The values of both ß and n are empirical fitting terms. For stable and neutral atmospheric conditions,

$$\Psi sm = \Psi sh = -5.2\zeta\ . \quad (5.15)$$

Dyer (1967) found that for momentum and heat flux, the X terms were equivalent. The values of ß and n were empirically defined by Dyer (1967) and Dyer and Hicks (1970) from experimental data collected in Australia. They were independently defined by Paulson (1970) and later verified by Businger (1971) as ß = -16 and n = ¼.

The sensible heat flux equation (5.11) is used in this dissertation as the Monin-Obukhov "model." However, finding values for ζ, and the Ψ– functions requires solving for U_*, H, and L by recursive techniques. The next section will discuss the details and practical considerations involved in solving for U_*, H and L, as well as the use and operation of the Monin-Obukhov model with remotely sensed surface temperatures.

Application of the Monin-Obukhov Sensible Heat Flux Model

Understanding how the Monin-Obukhov flux equations operate requires

that the surface geometry, measurements, and corrections applied to the data be defined by examination of the assumptions and conditions used to delineate the surface boundary layer, gradients of temperature and wind speed, atmospheric stability corrections, and the logic used for computing Monin-Obukhov sensible heat flux.

The canopy geometry defines the elevation of the plant/atmosphere interface. At this point, called the exchange height, most of the momentum and energy exchange take place. The two parameters used to describe the exchange height as a function of plant height are the displacement height d and roughness length (z_{om} for momentum and z_{oh} for heat). Huband and Monteith (1986a) found that for winter wheat, $d = 0.63 \cdot h$, where h is the height of the canopy. Cowan (1968) and Campbell (1977) found that $z_{om} = 0.13$ h and $z_{oh} = 0.2\ z_{om}$. From these parameters, the exchange height elevation for momentum and heat are defined for the Monin-Obukhov model as $d+z_{om}$ and $d+z_{oh}$, respectively.

Modeling Monin-Obukhov sensible heat flux requires gradient measurements of temperature and wind speed. IRT and air temperature measurements provide the required temperature gradient between the surface and the air, and the wind at one level provides an estimate of the wind gradient since u=0 at $d+z_{oh}$. The wind speed gradient is used to estimate the friction velocity, (Brutsaert 1982) as

$$U_* = \frac{(u_2-u_1)k}{\ln(\zeta_2/\zeta_1)} - \Psi sm_2 + \Psi sm_1 \ . \qquad (5.16)$$

Since the wind is assumed to be zero at the exchange height in the canopy ($d+z_{om}$) where most of the mechanical energy is absorbed by the vegetation, the IRT measurement level is also assumed to be at the exchange height.

The functions Ψsm and Ψsh are used to correct U_* and H, respectively, for unstable and stable conditions associated with thermal stratification of the atmosphere within the boundary layer. The diabatic atmospheric stability is evaluated from the magnitude and polarity of the Monin-Obukhov parameter (equation 5.9); this parameter describes the relative size and direction of eddies moving to and from the surface. When ζ approaches 0, the atmosphere approaches neutral conditions, and the air temperature declines with height at the dry adiabatic lapse rate (0.0098°C/m), and no stability correction is required. When $\zeta > 0$ (moist, cool surface; warm air), the atmosphere is stable, and the Ψ–function for stable air is used (equation 5.15). When $\zeta < 0$ (dry, warm surface; cool air) the atmospheric stratification is unstable, and the Ψ–function for unstable air is used (equations 5.12 and 5.13). However, the application of the Monin-Obukhov functions are limited. Under highly stable conditions, when $z/L > 1$, the Ψ–functions are difficult to determine, but there is some evidence to suggest an upper limit of $\zeta = -5.2$ regardless of the size of z/L (Brutsaert 1982). This condition occurs periodically and in this study when $z/L > 1$, ζ is set to -5.2, the limit at which Ψ can be reliably evaluated.

The model parameters U_*, H, and L are asymptotic functions that can be evaluated by recursive methods since U_* and H use measured values of wind speed and temperature. The iterative process used in this study is diagramed in Figure 12. It starts by first calculating d, z_{om}, and z_{oh} as a function of plant height for a given day (d = 0.63 h, and z_{om} = 0.13 h, z_{oh} = 0.2 z_{om}). Next, the Ψ-functions and L are initialized for a neutral atmosphere (L = 1000, and $\Psi sm_1 = \Psi sm_2 = \Psi sh_1 = \Psi sh_2 = 0$). Then the IRT surface temperature, air temperature, and wind speed for a given time on that day are input, and the program calculates an initial ζ and solves for U_* using the measured wind speed data. Then U_* is used along with the IRT and air temperature data to estimate H and to calculate a new L value. With the calculated L value, ζ is recomputed, an appropriate stability function is selected, and the stability functions for momentum and heat flux calculated at levels z_1 and z_2. Convergence of the solution for L is achieved when the difference between the absolute values of L from the previous and present iterations approaches zero. If convergence is not achieved, then U_* is recomputed with the previous ζ and Ψ-functions, and new values of H, L, ζ, and Ψs are computed. This process is repeated until L converges. After convergence is complete (usually within five iterations), the H-flux for that time period is stored and the procedure takes the next set of observations.

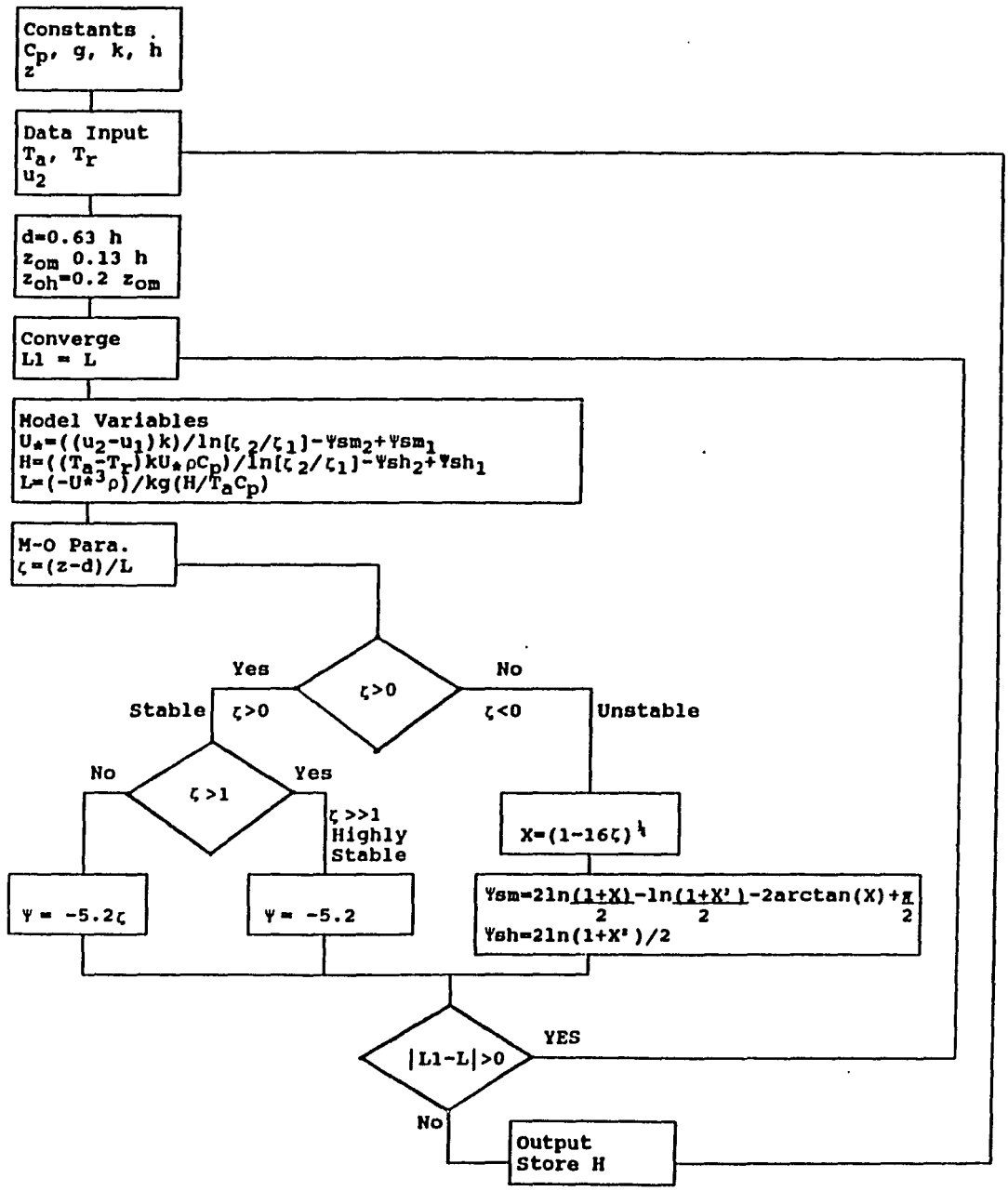

Figure 12. Flow chart for Monin-Obukhov model computations.

The Aerodynamic Resistance Model of Sensible Heat Flux

Aerodynamic resistance models calculate the sensible heat flux by adjusting the temperature difference between the surface and the atmosphere with a resistance function estimated from wind speed measurements made near the surface. The generalized sensible heat flux equation using an aerodynamic resistance function is

$$H = - \frac{\rho C_p \Delta\theta}{r_a} \quad , \qquad (5.17)$$

where
ρ is the density [kg/m^3],
Cp is the specific heat [J/kg°C],
r_a is the aerodynamic resistance [s/m],
$d\theta/dz$ is the potential-temperature gradient with respect to height [°C/m].

Of the many aerodynamic resistance models have been published in the literature, the Campbell (1977) and the Jackson (1987) r_a models were examined for possible testing. They both have a similar response to wind, computing r_a as an exponential decay curve with asymptotes at both low and high wind speeds. The Campbell (1977) formulation was chosen as the resistance model to be compared to the Monin-Obukhov model. The Campbell formulation can be derived from wind profile models, and is relatively simple, being uncorrected for stability. The Kustas model was also chosen for comparison; it is the r_a formulation of the Monin-Obukhov turbulent transfer model, and uses Ψ stability corrections for the upper level (z_2), similar to those described earlier in connection with the Monin-Obukhov model (equations 5.12, 5.13 and 5.14). I view the Kustas

model as the resistance version of the Monin-Obukhov model, corrected for stability at a single level. The development of the aerodynamic resistance concept will be discussed next.

General Development of the Aerodynamic Resistance Model

The Campbell and Kustas r_a models use the Campbell (1977) wind log-profile definition for vegetated surfaces as

$$u = \frac{U_*}{k} \ln \frac{z-d+z_{om}}{z_{om}} , \tag{5.18}$$

where
z is the height of the wind speed measurement [m],
d is the zero plane displacement [m], and
z_{om} is the roughness length for momentum [m],

and the friction velocity is

$$U_* = \frac{ku}{\ln[(z-d+z_{om})/z_{om}]} . \tag{5.19}$$

The sensible heat flux (from Campbell 1977), similar to equation (5.11) for neutral conditions, is

$$H = -\rho C_p k U_* \frac{(\theta_2-\theta_1)}{\ln[(z-d+z_{oh})/z_{oh}]} \tag{5.20}$$

By substituting U_* in equation (5.19) into equation (5.20), we have

$$H = -\rho C_p[(\theta_2-\theta_1)] \frac{k^2 u}{[\ln(z-d+z_{oh})/z_{oh}]\ [\ln(z-d+z_{om})/z_{om}]} . \tag{5.21}$$

From equation (5.21), K_h is now

$$K_h = k^2 u / \left[\ln\left(\frac{z-d+z_{oh}}{z_{oh}}\right) \right] \left[\ln\left(\frac{z-d+z_{om}}{z_{om}}\right) \right] , \tag{5.22}$$

from equation 5.17, $K_h = 1/r_a$. (5.23)

Therefore r_a in the Campbell r_a model is

$$r_a = \left[\ln\left(\frac{z-d+z_{oh}}{z_{oh}}\right) \ln\left(\frac{z-d+z_{om}}{z_{om}}\right) \right] / k^2 u \ . \quad (5.24)$$

Kustas et al. (1989) recently added Ψ stability correction functions for heat flux and momentum to equation (5.24) using Monin-Obukhov theory. Their model development begins with the Wallace et al. (1984) r_a model and Campbell's (1977) surface geometry:

$$r_a = \ln\left(\frac{z-d+z_{oh}}{z_{oh}}\right) / kU_* = \left[\ln\left(\frac{z-d+z_{om}}{z_{om}}\right) + \ln\left(\frac{z_{om}}{z_{oh}}\right) \right] / kU_* \ . \quad (5.25)$$

The U_* in equation (5.25) is replaced by equation (5.19), and

$$r_a = \frac{\left[\ln^2\left(\frac{z-d+z_{om}}{z_{om}}\right) + \ln\left(\frac{z_{om}}{z_{oh}}\right) \right] \left[\ln\frac{z-d+z_{om}}{z_{om}} \right]}{k^2 u} \ . \quad (5.26)$$

Kustas et al. (1989) added Ψ stability corrections [equations (5.12), (5.13), and (5.14)] to equation (5.26), to obtain (using Campbell's surface geometry)

$$r_a = \frac{\left[\ln\frac{z-d+z_{om}}{z_{om}} + \ln\left(\frac{z_{om}}{z_{oh}}\right) - \Psi sh_2 \right] \left[\ln\frac{z-d+z_{om}}{z_{om}} - \Psi sm_2 \right]}{k^2 u} \ . \quad (5.27)$$

Application of the Aerodynamic Resistance Model

Sensible heat flux was calculated with equation (5.17) with r_a computed from either Campbell's equation 5.24, or Kustas equation 5.27. Solving these equations requires surface and air temperatures, wind speed, and crop height. The air temperature was measured above the

canopy with a RTD temperature sensor, and surface temperature was measured remotely by an IRT. Crop height (h) is used to calculate the displacement and roughness lengths following Campbell (1977) as d = 0.63 h, z_{om} = 0.13 h, and z_{oh} = 0.2 z_{om}.

The Kustas resistance model uses stability corrections, while Campbell's resistance model is not corrected for stability. Kustas et al. (1989) compared two methods for computing Ψ stability corrections: one from the Monin-Obukhov method, and the other from the empirical Richardson number (Ri) approach. The use of Ri to compute the stability correction is simpler then the more complex computation required for the Monin-Obukhov Ψ-functions. The results were in good agreement as the difference between the stability corrections computed with the iterative Monin-Obukhov Ψ-functions and with the linear Ri approach was only about 5 percent. In this study, I used the fundamental Monin-Obukhov Ψ stability corrections in the Kustas model, evaluated at the upper level (z_2) elevations.

The computation of H with the aerodynamic resistance models from Campbell (1977) and Kustas et al. (1989) is diagrammed in Figures 13 and 14. The computations are as follows:

1. The displacement height and roughness lengths (d and z_{oh}, z_{om}) are calculated from the plant height data.
2. Upper level stability corrections from Monin-Obukhov (equations 5.12

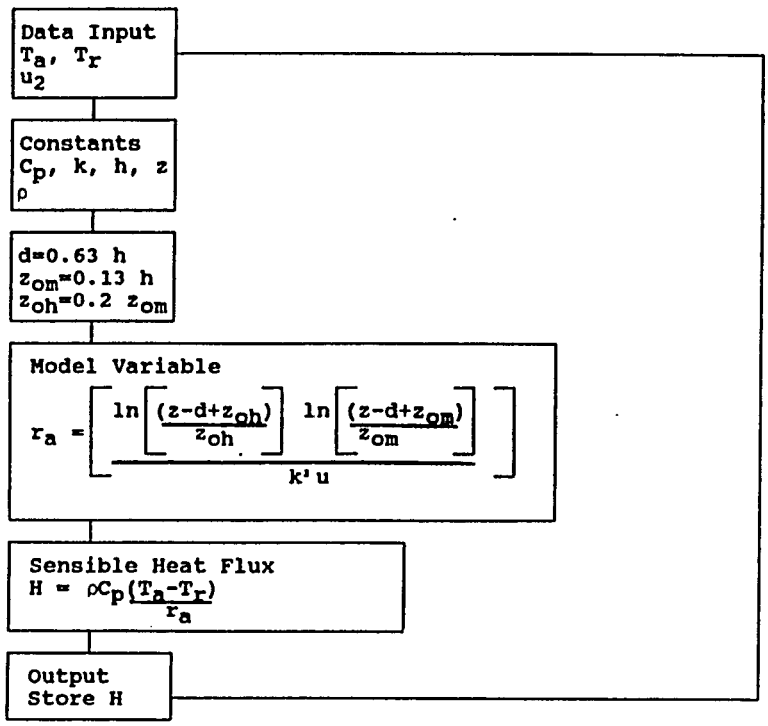

Figure 13. Flow chart for Campbell aerodynamic resistance model computations.

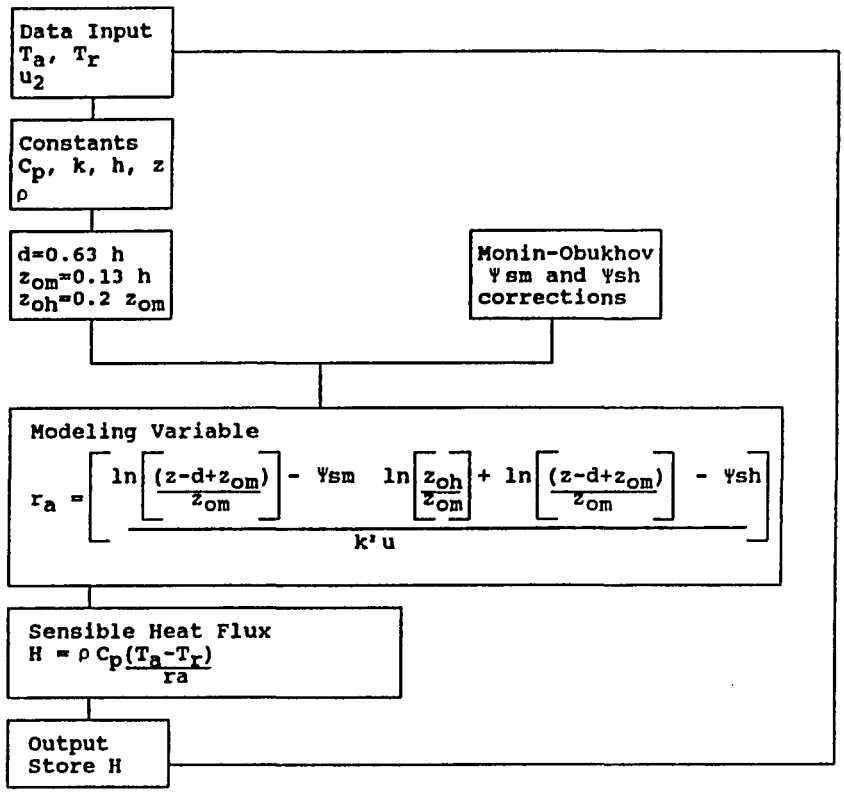

Figure 14. Flow chart for Kustas aerodynamic resistance model computations.

to 5.15, computed as in Figure 12) are entered into the Kustas model.

3. The air temperature, surface temperatures, wind speed and plant height data are entered into the model.
4. The aerodynamic resistance is computed.
5. The sensible heat flux is calculated and stored.

Finally, sensible heat flux estimated by the Monin-Obukhov model and the two aerodynamic resistance models was compared with the Bowen ratio sensible heat flux. The comparison extended over 137 days at the irrigated winter wheat site at MAC. The comparisons are discussed in the next chapter.

6. COMPARISONS OF MODEL PREDICTIONS WITH BOWEN RATIO RESULTS

Turbulent transfer and aerodynamic resistance theory were used to estimate H from three different models that are potentially useful for remote-sensing applications. The models used wind speed, air temperature, and remotely sensed canopy temperatures. The data were acquired simultaneously with Bowen ratio measurements of H for 137 days over winter wheat. Results from the turbulent transfer model developed by Monin-Obukhov (1954) are designated as HMO, those from the aerodynamic resistance model results of Campbell (1977) as HCm, and those from the model of Kustas et al. (1989) as HKu. Modeled H-estimates were compared with the Bowen ratio truth-set to determine the applicability of each approach for evaluating the surface energy balance.

The three models were not adjusted or "calibrated" to fit the climate or environment of the unique test site in order to evaluate how well they predict H under a wide range of environmental conditions. The surface conditions at the test site include both transpiring and senesced wheat. The atmospheric stability during daytime at the experimental site was quite stable during the growing season (transpiration) and unstable after senescence. The diabatic condition of the atmosphere is defined by z/L, where L is the Monin-Obukhov length (Chapter 5). The ratio $z/L > 0$ is stable, $z/L \approx 0$ is neutral, and $z/L < 0$ is unstable.

The three major sections of this chapter deal with analysis of: (1) diurnal comparisons of 12-min estimates throughout two selected days, (2) seasonal comparisons of 30-min and 24-hour mean estimates over the entire measurement period, and (3) an examination of model variability with respect to the Bowen ratio results.

Analysis of Two Example Days

Sensible heat H was computed for all three models from meteorological and remotely sensed data at 12-min intervals for each of the 137 days of measurement. Two 24-hour periods, days 87 and 146, illustrate the results obtained from this large volume of data. These days represent the surface and climatological conditions associated with transpiring and senesced wheat, respectively. The data taken on these two days were examined for diurnal trends and evaluated by regression analysis with the Bowen ratio data.

Diurnal Trends

The surface energy balance of both transpiring and senesced wheat is affected by a wide range of surface conditions and atmospheric processes over a 24-h period. The physiological status of wheat controls the partitioning of available energy into latent and sensible heat, and this partitioning affects the atmosphere in and above the canopy.

Diabatic condition above growing and transpiring wheat during the daytime in semiarid climates is typically stable (day 87). In contrast, unstable atmospheric conditions develop during the daytime above non-transpiring wheat (day 146). The environments associated with these two markedly different stages are ideal for demonstrating the diurnal behavior of the three models with respect to Bowen ratio measurements.

Figures 15A and 15B show, for the two sample days, diurnal sensible heat fluxes measured by the BREB system and estimated by the HMO turbulent transfer model and by the HCm and HKu aerodynamic resistance models. The data is plotted at the midpoint of the 12-min (0.2-hour) intervals.

Day 87

The wheat was growing and transpiring on day 87 (Figure 15), and the diabatic atmospheric condition was stable ($z/L > 0$) throughout this 24-hour period. With regard to the measured sensible heat flux (HBr), the Bowen ratio in the early morning— from 0000 to 0724— approached -1.0, and the Bowen ratio filter developed from Ohmura's (1982) rejection criteria set HBr to 0 (Chapter 2, page 34). HBr began to rise about 0748 as ß shifted from -1. HBr rose sharply at midday, reaching a peak of 450 W/m^2 at 1312, and remaining around 300 W/m^2 until available energy dropped in the late afternoon. HBr fluxes then steadily declined down to zero in the evening.

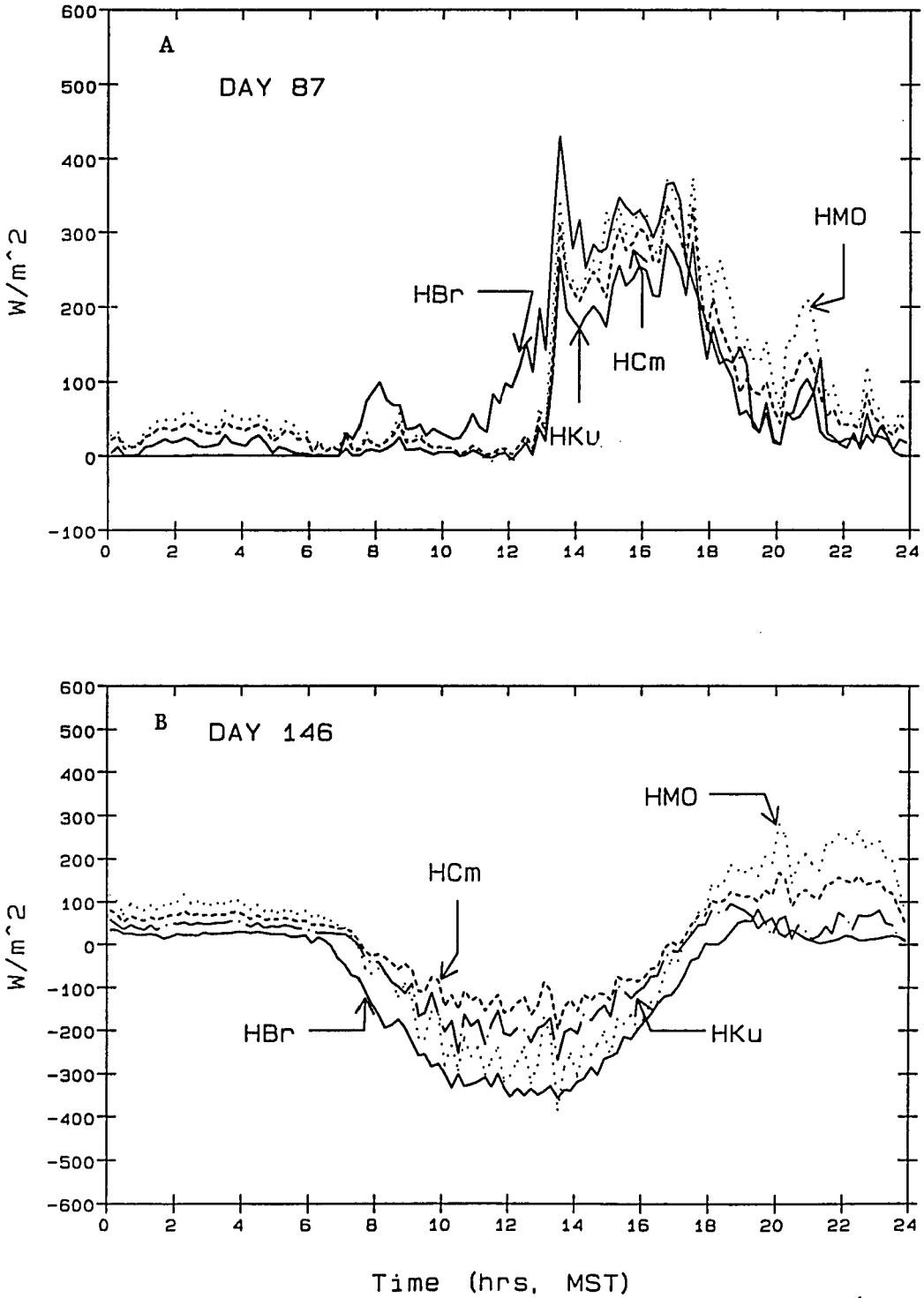

Figure 15. Diurnal 12-minute sensible heat fluxes measured (Bowen ratio), and Modeled (Campbell, Kustas, and Monin-Obukhov)
A. Transpiring wheat on day 87. B. Senesced wheat on day 146.

The H-values from all three models remained low (typically less than 50 W/m^2) in the morning and then climbed rapidly to around 300 W/m^2 in the early afternoon and remained there until early evening. In general, the three models underestimated the absolute value of HBr during the daytime, and overestimated HBr at night. The HMO daytime estimates were closer to the HBr data than either HCm or HKu modeled values.

Day 146

The atmosphere on day 146 was stable during the night periods ($z/L > 0$), and unstable during the daytime ($z/L < 0$). The HBr values were generally small, consistent and slightly positive at night, and negative during the daytime, reaching a peak of -350 W/m^2 at 1336 hours.

The three models predicted larger (more positive) H-fluxes than HBr during the stable, early morning period, and smaller (less negative) fluxes throughout the unstable daytime period. Oscillations in the model predictions were larger then those observed in the Bowen ratio measurements. The contrast between the performances of the turbulent transfer and aerodynamic resistance models is greater for day 146 (daytime instability, Figure 15). During the daytime period of large sensible energy losses, the Monin-Obukhov 2-level stability corrected model gave best agreement with HBr, while the two aerodynamic resistance models underestimated convection. In the stable conditions of the evening, all three models overpredicted the positive fluxes that were

measured by the Bowen ratio, while the HMO estimates showed the greatest overestimation.

The comparison between the Bowen ratio H–values and the predicted estimates from the three models over the daytime period can be quantified with standard statistical methods.

Regression Relationships for 12-Minute Data

The 12-min daylight (0736 to 1736 hour) H–values from the Bowen ratio and the three models were analyzed with RS/1 statistical programs. Bowen ratio data were linearly regressed against the three models for days 87 and 146 with the statistical form H_{model}=a HBr + b and slopes, intercepts and associated standard errors, r^2–values, and regression standard errors were calculated. With this statistical form, the regression coefficients from the three models can be compared with one another with respect to the Bowen ratio. Model performance was also expressed as the difference between the daily totals of HBr and the model predictions for each day, with smaller differences between HBr and model totals indicating a better fit. The statistical analyses for the three models are presented in Table 4.

Table 4. Regression of Campbell, Kustas, and Monin-Obukhov model predictions vs. Bowen ratio measurements.

Comparison	Slope W/m^2	Intcp. W/m^2	r^2	SE W/m^2	Totals Difference MJ/m^2	MJ/m^2
Day 87						
HBr					8.29	
HBr vs HCm	0.91±0.04	-38.6±04	0.91	37.5	6.57	1.72
HBr vs HKu	0.78±0.03	-39.5±18	0.91	31.9	5.27	3.02
HBr vs HMO	1.01±0.04	-43.6±10	0.91	42.1	8.73	-0.44
Day 146						
HBr					-10.51	
HBr vs HCm	0.57±0.02	53.7±05	0.92	19.9	0.17	-10.68
HBr vs HKu	0.72±0.02	44.9±06	0.93	23.5	-2.59	-7.92
HBr vs HMO	1.01±0.04	66.7±10	0.91	37.8	-6.22	-4.29

Consider first the growing, transpiring wheat crop on day 87. The HMO slope is closest to 1.0, but HMO also has the largest intercept and standard error. The HMO daily sum also deviates least from HBr. The difference between the summed HBr and HMO is one-fourth the size of the HBr and HCm difference and one-seventh the size of the HBr and HKu difference. However, the standard error for the HKu model was substantially lower than for the other two models.

Now consider the comparisons over the dry canopy on day 146. HMO was again the best predictor of HBr, with a slope close to unity and the smallest difference between daily sums. However, HMO variability was again substantially higher than that of HCm and HKu. The diurnal plot of observed and predicted values in Figure 15 and the regression analysis in Table 4 show that while the HMO modeled mean values are closer to HBr then either the HCm or HKu modeled values, the variability in the HMO values

reduces its usefulness.

On both days, all three models had high r^2-values, indicating that they were able to predict changes in the magnitude of H equally well. However, the standard errors and intercepts were relatively large, indicating high variability in the predictions. The pattern seen on these two selected days is repeated for all three models for most of the days analyzed. The HCm and HKu models tends to overestimate the HBr-values during stable periods, and underestimate HBr-values during unstable periods. In contrast, the HMO model predicts H-values close to those of the Bowen ratio during daytime periods, but tends to overestimate during nighttime periods when the energy exchange is low.

Analysis of Seasonal Data

The variability of high-temporal-resolution sensible heat flux values over a diurnal period is related to the rapidly changing environmental conditions. Comparisons between the Bowen ratio and modeled H-values are effected by these changes. Averaging the 12-min H-values into a single daily mean over the 24-hour diurnal period will reduce the short-term, high-frequency variability on H. The daily averages were analyzed over 137 days to evaluate how differing surfaces (growing vs senesced) and climatic conditions affect the Campbell, Kustas, and Monin-Obukhov models' ability to predict sensible heat flux.

The high-temporal-resolution data can also be pooled for the entire season into one population and the measured values regressed against the modeled estimates to remove the dependency between time and the H-flux size from the analysis. When the time domain is removed, the variability associated with the day-to-day changes in the environment—such as weather front movements and advection—are reduced, and the observed data and the modeled estimates are related by magnitude. The pooled population data are used to compare the performance of the three models with Bowen ratio sensible heat flux values over a wide range of conditions in a semiarid region. For the pooled, high temporal analysis, the 12-min Bowen ratio and modeled data were averaged into 30-min mean values to reduce the size of the pooled data set for management and computational ease.

Seasonal Trends

Changes in the wheat physiology and the climate at Maricopa were used to analyze the performance of the three models over the 137-day measurement period. Daily means from the HCm, HKu, and HMO models were evaluated with HBr daily means acquired over the growing and senesced wheat and during periods of frontal change and advection. Seasonal trends and unique events help in determining if the models are deficient under specific conditions.

Daily averages of the measured and modeled data

The daily means of the measured and modeled values show how changes in the wheat surface and climate affected the sensible heat flux over the winter wheat season. The daily 24-hour average H-values for the Bowen ratio and the three models were plotted for the entire season in Figure 16. In Figure 16A, the HCm, HKu, and HMO model estimates can be compared with HBr measurements for the period from day 15 to 151. The same four variables are plotted in Figure 16B on an expanded scale from day 110 to 151 to show with greater clarity the affect of the change from transpiring to senesced wheat.

In general, the plots show that all models were in reasonable agreement with the HBr measurements during the growing (stable) period. For the green transpiring wheat, the three models tracked HBr fairly well. However, when the wheat senesced and dried, near the end of the measurements, the Monin-Obukhov model was more effective in predicting HBr than the Campbell or Kustas models. The 24-hr means from all three models tended to be larger then HBr for stable conditions during the growing season and for unstable conditions after senescence. The HCm and HKu estimates were substantially larger than HBr during unstable periods after senescence.

The average daily HBr flux over the growing wheat tended to increase as the season progressed up to senescence. The 24-hour means varied

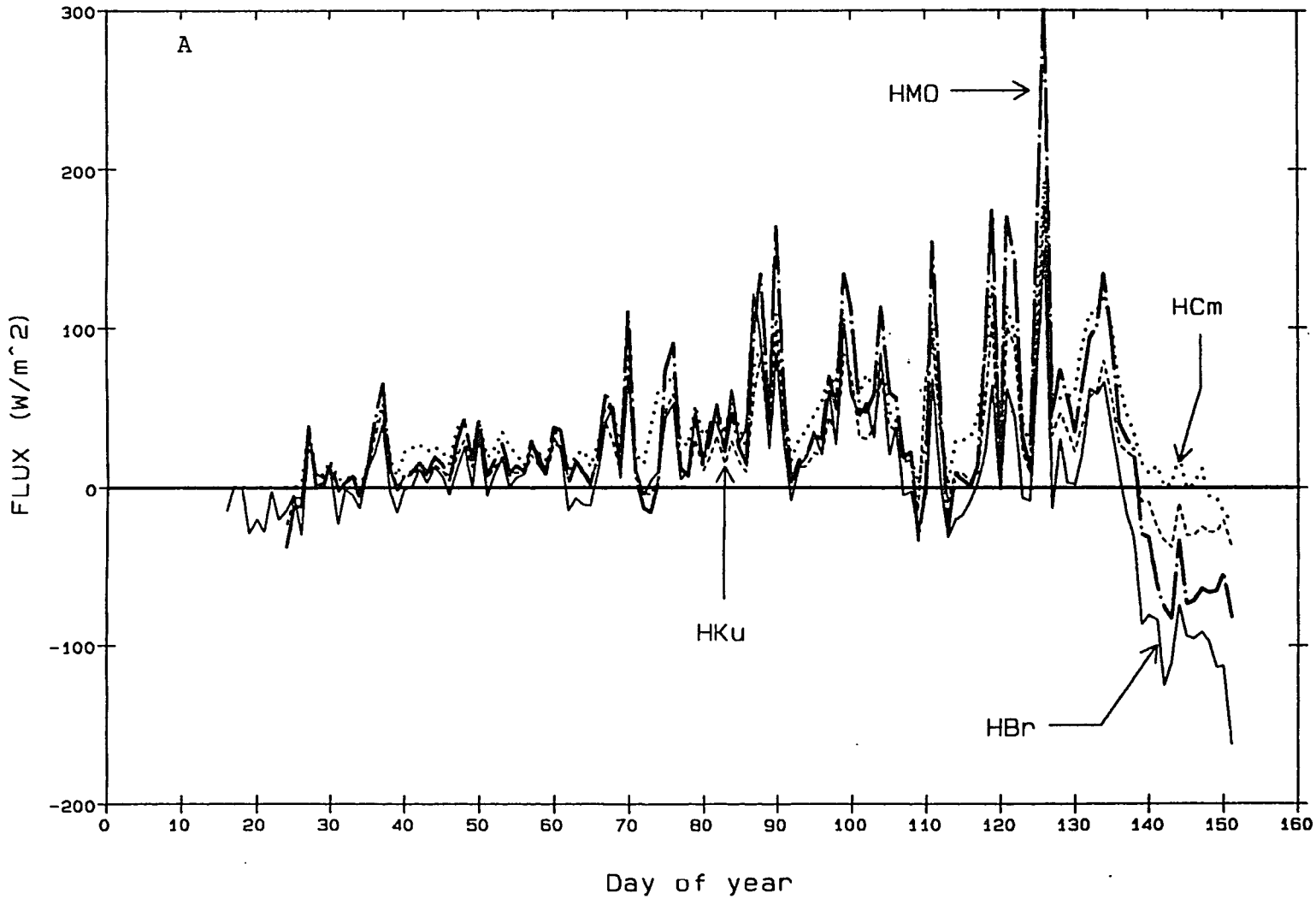

Figure 16. Mean 24-hour sensible heat fluxes from the Bowen ratio (HBr) and Campbell (HCm), Kustas (HKu), and Monin-Obukhov (HMO) models
A. For the season.

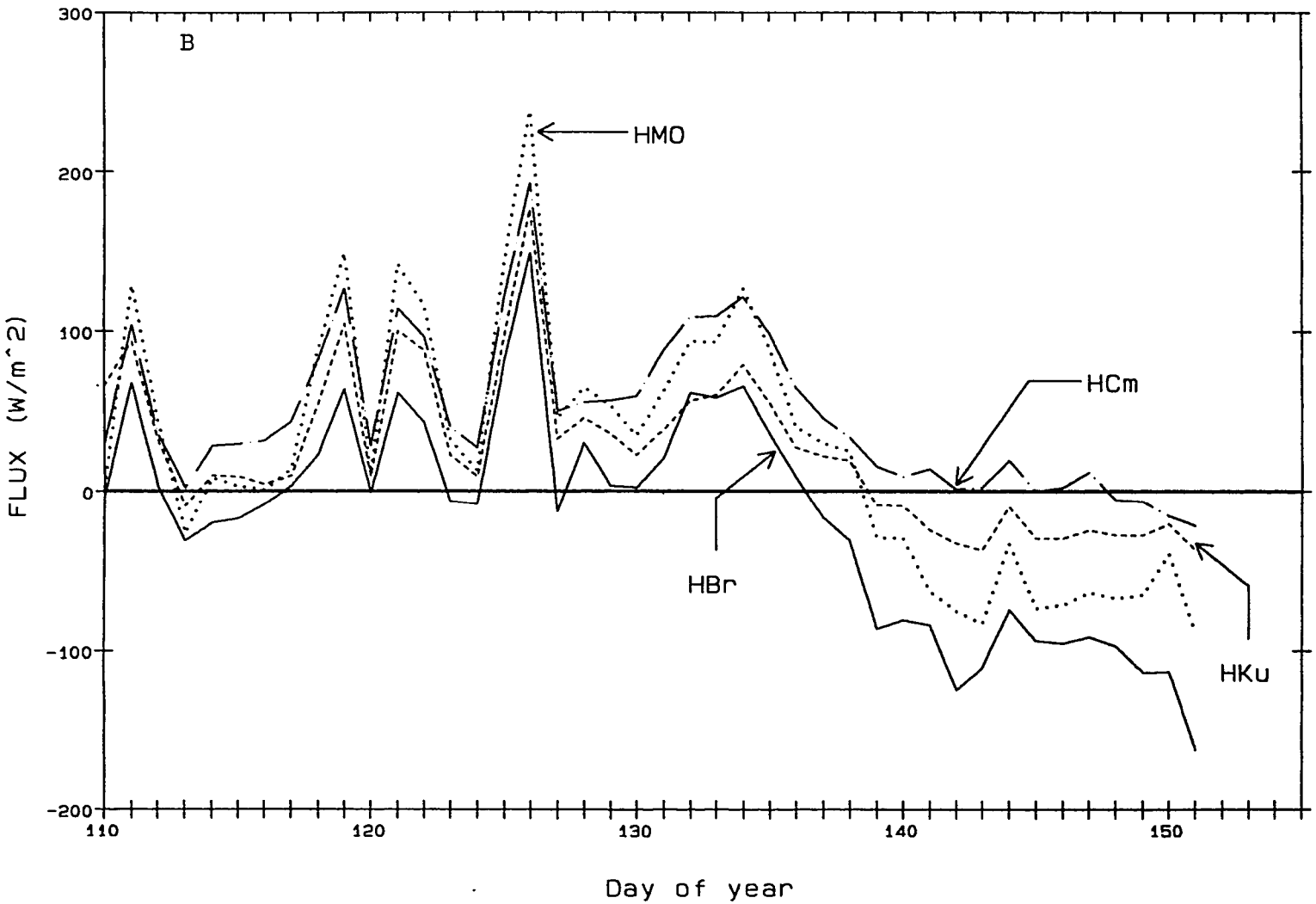

Figure 16. Mean 24-hour sensible heat fluxes from the Bowen ratio (HBr) and Campbell (HCm), Kustas (HKu), and Monin-Obukhov (HMO) models. B. For period of senescence.

considerably from day to day, and on occasion switched polarity, such as the change from day 126 (+149 W/m^2) to day 127 (-13 W/m^2). The variability between days was associated with climatic factors such as high wind and air mass changes. The fluctuations in H observed with the Bowen ratio were consistently predicted by the models.

A close inspection of 24-hour means of wind, air temperature and surface temperature plotted in Figure 17 indicates the importance of weather patterns on diurnal variability of H. On day 126, for example wind averaged 4.8 m/s and air temperature 19.6°C. On day 127, daily means were 2.5 m/s for wind and 13.3°C for air temperature. The high wind and warm air on day 126 contributed to a large and positive H-flux. With the cooler, less windy conditions on day 127 sensible heat flux HBr dropped substantially, and even became negative.

Similar observations about H-flux, wind speed, and air temperature on other days show that the large changes in daily averages of HBr are associated with movement of weather systems through southern Arizona. Overestimation by the models under these conditions indicates their insensitivity to wind which often increases substantially with frontal movement.

Analysis with the inclusion of error bars

Bowen ratio and eddy-correlation means for the daylight hours of

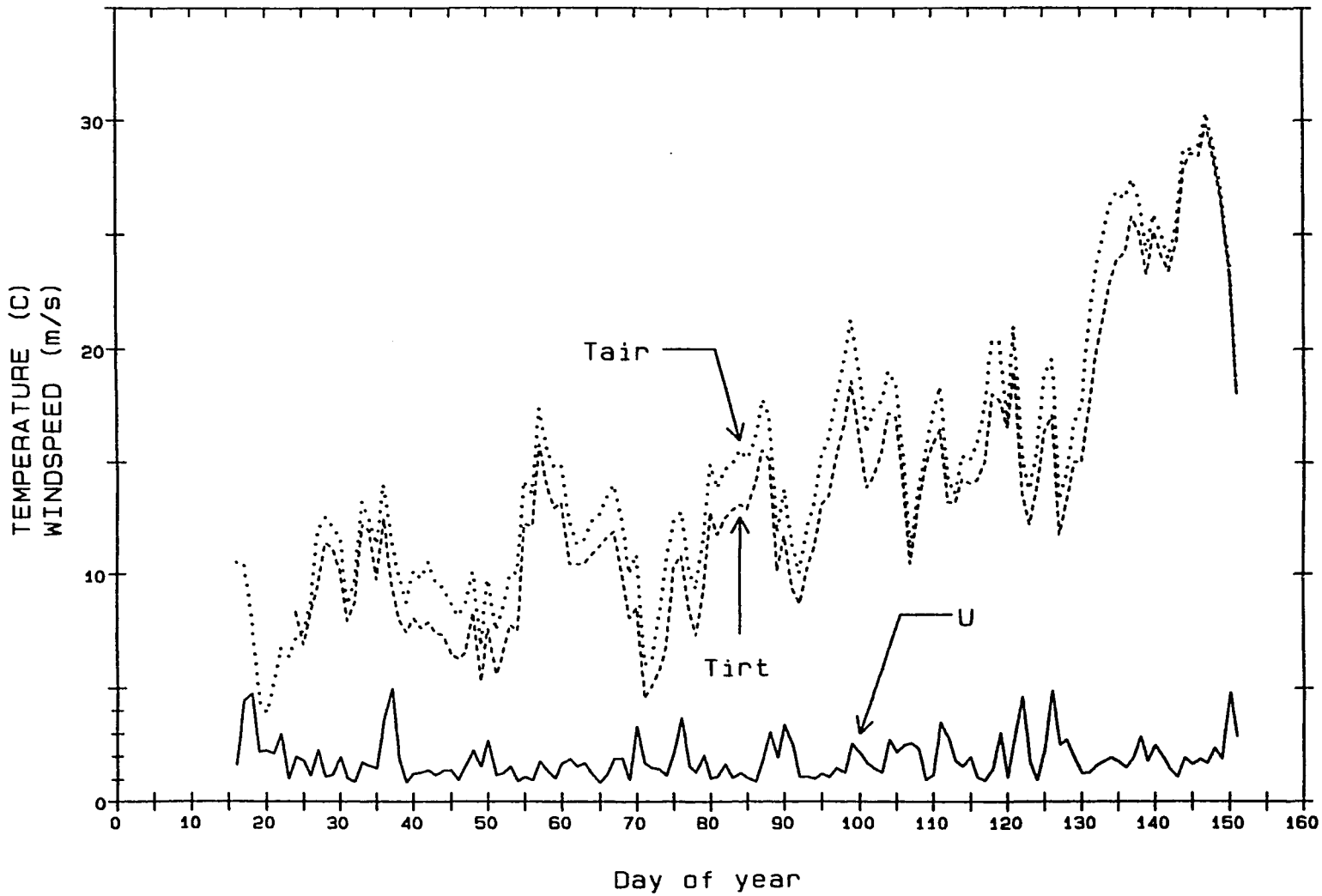

Figure 17. Average 24-hour air and canopy temperature and wind speed measurements over the winter wheat for the 1988 season.

days 135 to 151 are plotted in Figure 18. The error bars in the plot represent one standard error at 68% confidence, developed earlier from the regression of the daylight values of Bowen ratio and eddy-correlation sensible heat fluxes, as described in Chapter 4. The error bars are assumed to cover the range of "true" sensible heat flux within the confidence limits. The daylight means of the HCm-, HKu-, and HMO-models are also plotted in Figure 18. The daylight means were averaged from 0730 to 1730 hours. The modeled fluxes should fall within the two error bars. If they fall outside the error bars, then the model has failed to predict a reasonable estimate of H.

The HMO predictions (diamonds) are within the error bars on 10 of the 13 unstable days from day 137 to 151 when the H-flux was large and negative. The HCm predictions (triangles) were outside the error bars for all 13 of these days, and the HKu predictions are within the confidence limits only on day 137. When the atmosphere was stable and fluxes positive, H-values were smaller and results from the three models were closer together. Unfortunately, the eddy correlation data used with the HBr estimates to generate the error bars in Figure 18 were available for only two days with stable conditions, so the comparisons under these conditions are inconclusive. However, this analysis suggests to me that HMO is superior to the resistance models for unstable periods.

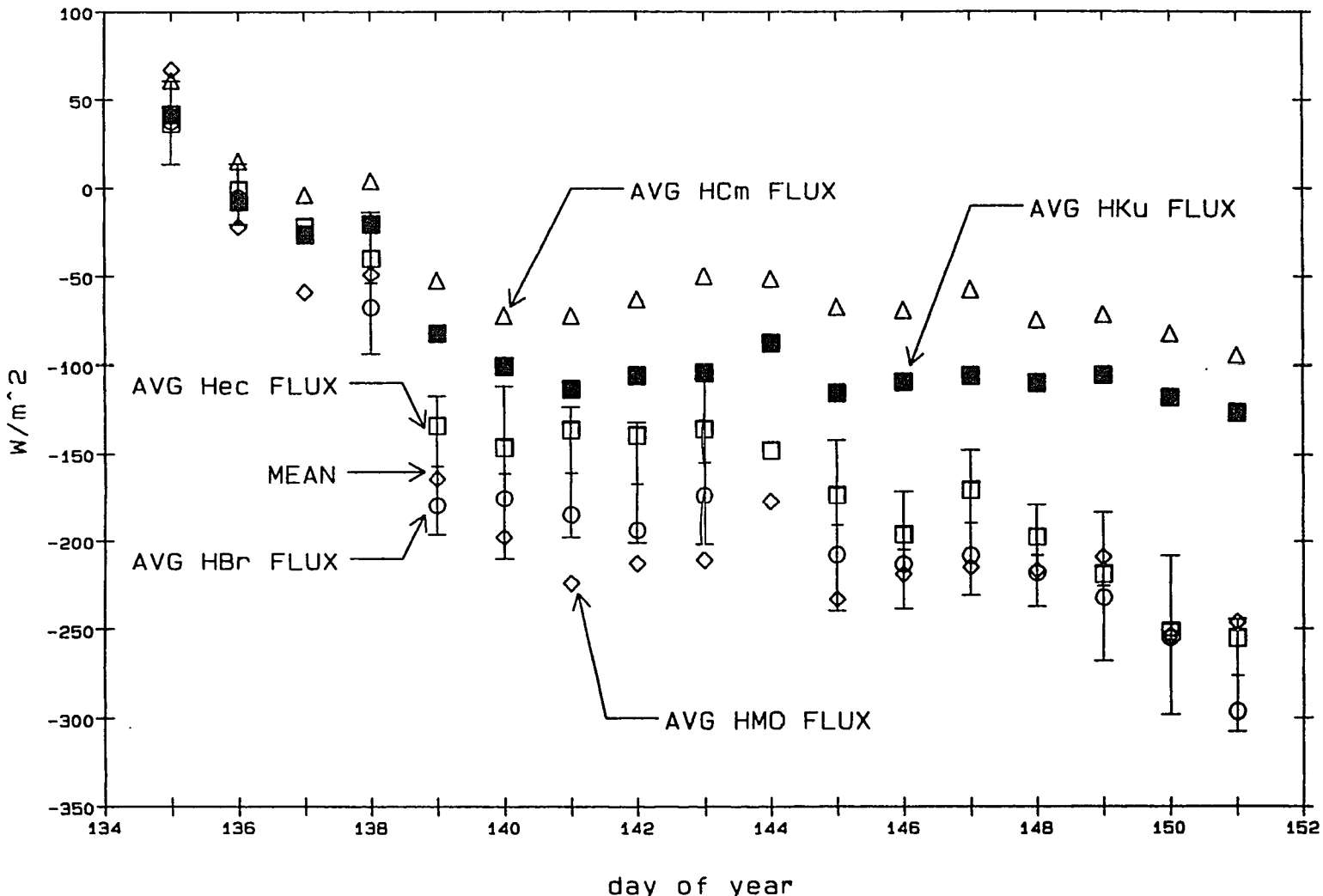

Figure 18. Comparison of measured error bars and modeled sensible heat fluxes for days 135 to 151.

Descriptive statistics of pooled population

Large-scale characteristics of the measured data can be used to determine if the models are operating within reasonable limits over the season. The dynamic range and means of the models should be similar to those of the measured values if the models are properly predicting the events observed over the 137-day measurement period. The pooled population of measured and modeled H-fluxes (30-min means, daylight values) are described in Table 5 with basic descriptive statistics: the maximum, minimum, range, and mean. Maximum and minimum Bowen ratio H-values were relatively symmetrical, from 442 to -470 W/m^2 with a mean of -1.6 W/m^2. Negative values correspond to unstable atmospheric conditions typical of mature wheat; in contrast, positive fluxes correspond to stable conditions when the wheat is transpiring. The range is the summation of absolute values of the maximum and minimum fluxes.

Table 5. Descriptive statistics of measured (HBr) and modeled (HCm, HKu, and HMO) sensible heat flux for daylight hours over the entire 1988 measurement period.

Data	n	Max W/m^2	Min W/m^2	Range W/m^2	Mean W/m^2
HBr	2510	442	-470	912	-1.6
HCm	2510	337	-250	587	18.0
HKu	2510	332	-258	590	6.4
HMO	2510	558	-510	1068	0.8

The range and mean of the HMO predictions are closer to those of HBr than either the HCm or HKu predictions. The Monin-Obukhov model overestimated the HBr maximum, range, and mean, while the Campbell and

Kustas models substantially underestimated the maximums and the ranges, and overestimated the means. The HCm and HKu ranges were only about 64% of the HBr range, with much of the error occurring in estimates of the minimum (negative) values associated with the senesced wheat. The poor performance of the Campbell and Kustas models in the unstable conditions associated with the senesced wheat is clearly evident. When the descriptive statistics of HBr are compared with the modeled estimates for the 137 day measurement period, the Monin-Obukhov model appears to produce better estimates than either the Campbell or Kustas models.

Regression Relationships

The performance of the three models relative to seasonal changes in the surface and climate were evaluated with a statistical analysis of the pooled population of 30-min, daylight values. The statistical analysis used linear regression to determine which model(s) adequately predicted Bowen ratio H-values over pooled populations consisting of (1) the transpiring wheat (days 16 to 136), (2) the senesced wheat (days 137 to 151), and (3) the combined populations of transpiring and senesced wheat (days 16 to 151).

The pooled population data set consisted of the 30-min values from the daylight hours (0630 to 1730) for each day. These were tabulated in a single table containing 2510 rows and 4 columns representing HBr and

estimates from the three models. Restriction of the population to daylight values is important for this analysis. If nighttime data were included in the analysis, about half of the population would be around 0 W/m^2 since night and early morning fluxes are usually quite small. Divergence of the Bowen ratio and modeled fluxes would be difficult to evaluate because the regression coefficients would be heavily biased by the large population of small night and early morning fluxes relative to the larger daylight values. Thus, each of the three model data sets was restricted to daylight hour values only. The daylight file was then subdivided into two smaller data sets to examine the effects of growth and senescence on the modeled fluxes. Shorter, time-dependent phenomena associated with moving weather fronts, advection, and the diurnal cycle are organized in the pooled data by flux size rather than by time. In this way the variability associated with these events is minimized in the pooled analysis.

The regression analysis has some inherent limitations as a result of serial autocorrelation associated with high-resolution energy-balance data measured frequently at a point. Serial autocorrelation reduces the regression "power" by constraining the accuracy of the confidence limits for a specified probability such as 95%. But, within the framework of the comparisons presented in this study, the standard errors are correct relative to each other. Unfortunately, there are no ways to correct the effects of autocorrelation on the confidence limits without employing

nonparametric methods that fit the temporal distribution of the fluxes to the "model." The nonparametric techniques minimize the deviations between the fitted function and the data so that the effects of time are removed. However, "model" fit depends solely on individual data distributions, and better fitting distributions would reduce model errors. Furthermore, the "models" cannot be used with any other data set, reducing the analysis to opinion rather than objective information. In contrast to the confidence limits, the slopes, intercepts, and r^2-values are less subjective indicators of relationships between HBr (the truth-set) and the three models because these regression terms are not affected by serial autocorrelation.

RS/1 statistical routines were used to regress Bowen ratio measurements against the three models from the transpiring, senesced, and combined populations. Linear regression coefficients that were computed and tabulated included slopes, intercepts (Intcp.) and their associated standard errors, correlation coefficient (r^2), regression line standard error (SE), and population size (n).

Regression relationships for transpiring wheat

Data for the days when the wheat was transpiring (days 16 to 136) were pooled into a separate data set consisting of 2163 30-min mean values of HBR, HCm, HKu, and HMO data (Table 6). The canopy of transpiring wheat allowed the three models to be evaluated under a stable

atmospheric regime.

Table 6. Regression analysis of measured (HBr) and modeled (HCm, HKu, and HMO) sensible heat flux for transpiring winter wheat.

Model	Slope	Intcp. W/m^2	r^2	SE W/m^2	n
HCm	0.75±0.01	7.0±0.8	0.71	33	2163
HKu	0.71±0.01	-1.0±0.7	0.74	30	2163
HMO	1.24±0.02	-8.9±1.2	0.73	52	2163

The data presented in Table 6 show that the Campbell, Kustas, and Monin-Obukhov models predicted HBr for the transpiring (stable atmosphere) canopy with similar degrees of uncertainty. The slopes for all three models were approximately ±25% of unity, the intercepts were about ±8 W/m^2 and the three r^2–values were within about 2% of their mean. One difference between the aerodynamic resistance models and the turbulent transfer model was the size of the standard error, which was substantially less for HCm and HKu than for HMO. Another feature was that the aerodynamic models underestimated the HBr by about 25%, whereas the two–level stability corrected turbulent transfer model overestimated HBr by 24%. Furthermore, the one–level stability corrected Kustas model produced results that were only slightly better than those of the Campbell model, which was not stability corrected.

Regression relationships for senesced wheat

The data from senesced wheat (days 137 to 151) were pooled into a data set consisting of 347 30-min mean values of the measured and modeled

fluxes in order to evaluate how well the models estimated sensible heat flux under unstable conditions (Table 7).

Table 7. Regression analysis of measured (HBr) and modeled (HCm, HKu, and HMO) sensible heat flux for senesced winter wheat.

Model	Slope	Intcp. W/m^2	r^2	SE W/m^2	n
HCm	0.50±0.01	18.5±2.9	0.82	30	347
HKu	0.60±0.01	15.7±3.2	0.85	33	347
HMO	1.18±0.03	21.2±6.3	0.85	65	347

The results in Table 7 of the linear regression analysis for the senesced (dry) wheat share some similarities with those for the transpiring wheat shown in Table 6, but they also show some marked differences. The regression slopes of the estimates versus HBr measurements are relatively low for the Campbell and Kustas aerodynamic resistance models, 50% and 40% of unity, respectively, while the slope for the Monin-Obukhov turbulent transfer estimates was 18% above unity. The regression intercepts and r^2-values were higher during the senesced period than during the growing period. The regression standard error for HMO vs HBr was considerably larger than for HCm and HKu in both transpiring and senesced conditions. An important similarity between the results for the transpiring and senesced wheat is that the aerodynamic resistance models underestimate the absolute value of the Bowen ratio measurements and the turbulent transfer model overestimates the absolute value of the Bowen ratio measurements. Overall, the Monin-Obukhov model predicted HBr better than either the Campbell or Kustas models, but the

regression standard error was substantially larger.

Regression relationships for transpiring and senesced wheat

The measured and modeled H-values for transpiring and senesced wheat (days 16 to 151) were combined into a final set of daylight data consisting of 2510 30-min mean values of the HBr, HCm, HKu, and HMO fluxes (Table 8). This data set was used to evaluate performance of the models over the entire season, regardless of plant water status. The combined data set for each model regression is plotted in Figures 19A,B,C; these figures contain the data points, the regression lines, the 1:1 line, and confidence bands calculated at 95% probability level.

Table 8. Regression analysis of measured (HBr) and modeled (HCm, HKu, and HMO) sensible heat flux for all daylight measurements.

Model	Slope	Intcp. W/m^2	r^2	SE W/m^2	n
HCm	0.57±0.01	15.0±1.4	0.77	35	2518
HKu	0.61±0.01	4.0±1.3	0.83	32	2518
HMO	1.14±0.02	-3.4±2.2	0.84	55	2518

The analysis again suggests that the Monin-Obukhov model has the best fit to the Bowen ratio data, but with a large standard error of regression. Caution should be taken in interpreting the HMO results, however. The large negative values of HMO during senescence (unstable conditions) forces the regression line towards unity. Altering the data population size of either transpiring or senesced wheat could affect the regression coefficients. The slope, intercept and r^2 of the HMO to HBr

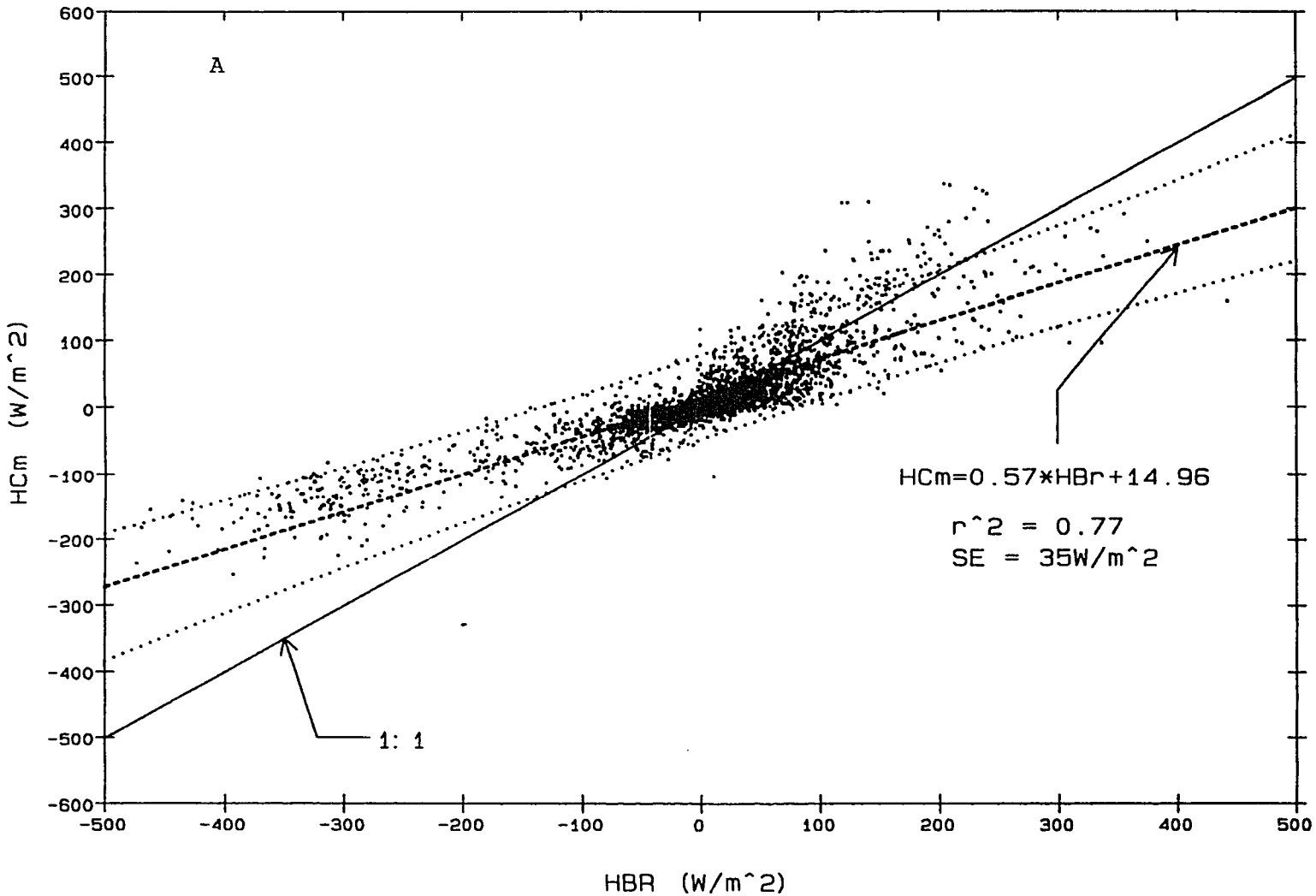

Figure 19. Regression of pooled 30-minute daylight data between A. Campbell model vs. Bowen ratio values.

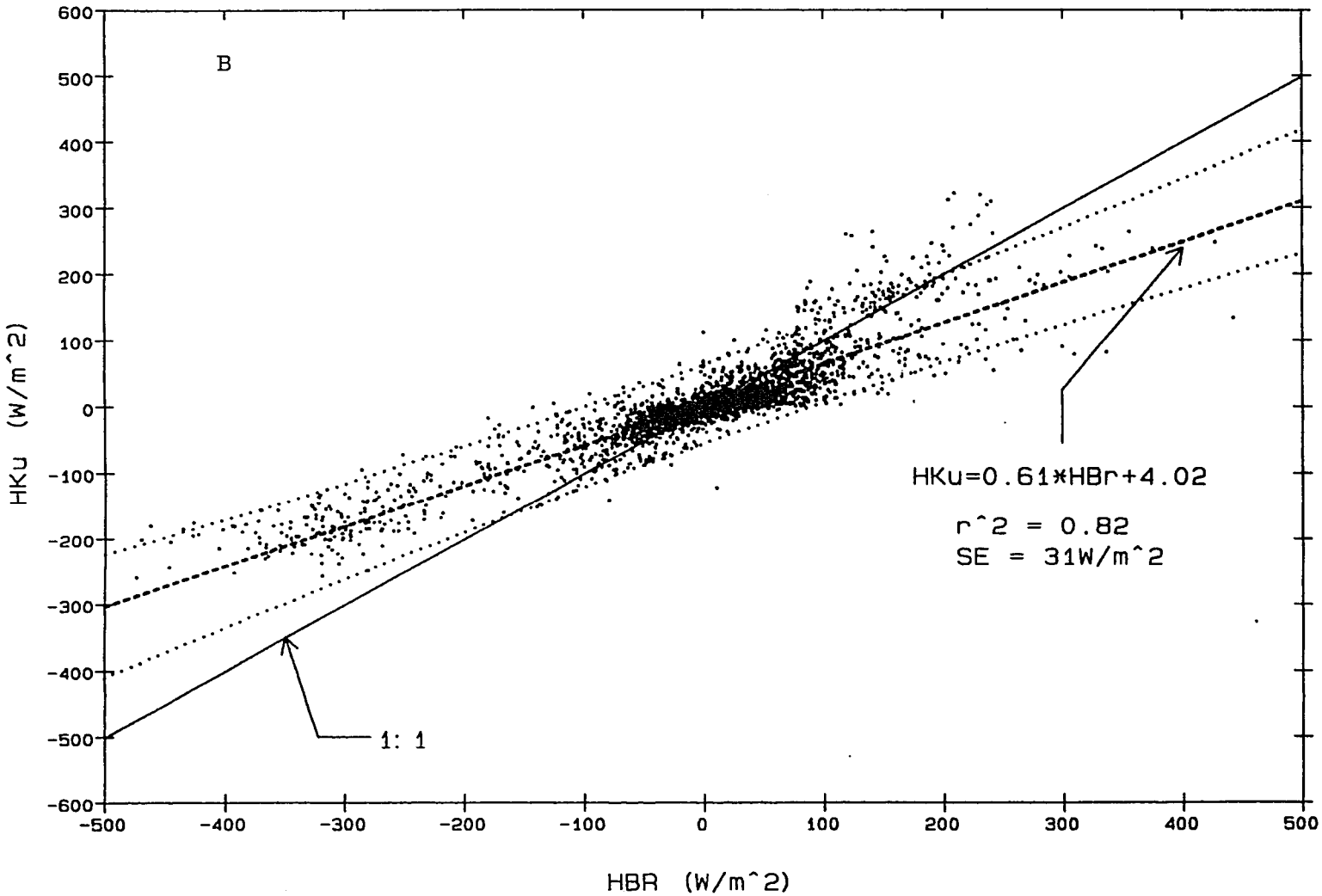

Figure 19. Regression of pooled 30-minute daylight data between B. Kustas model vs. Bowen ratio values.

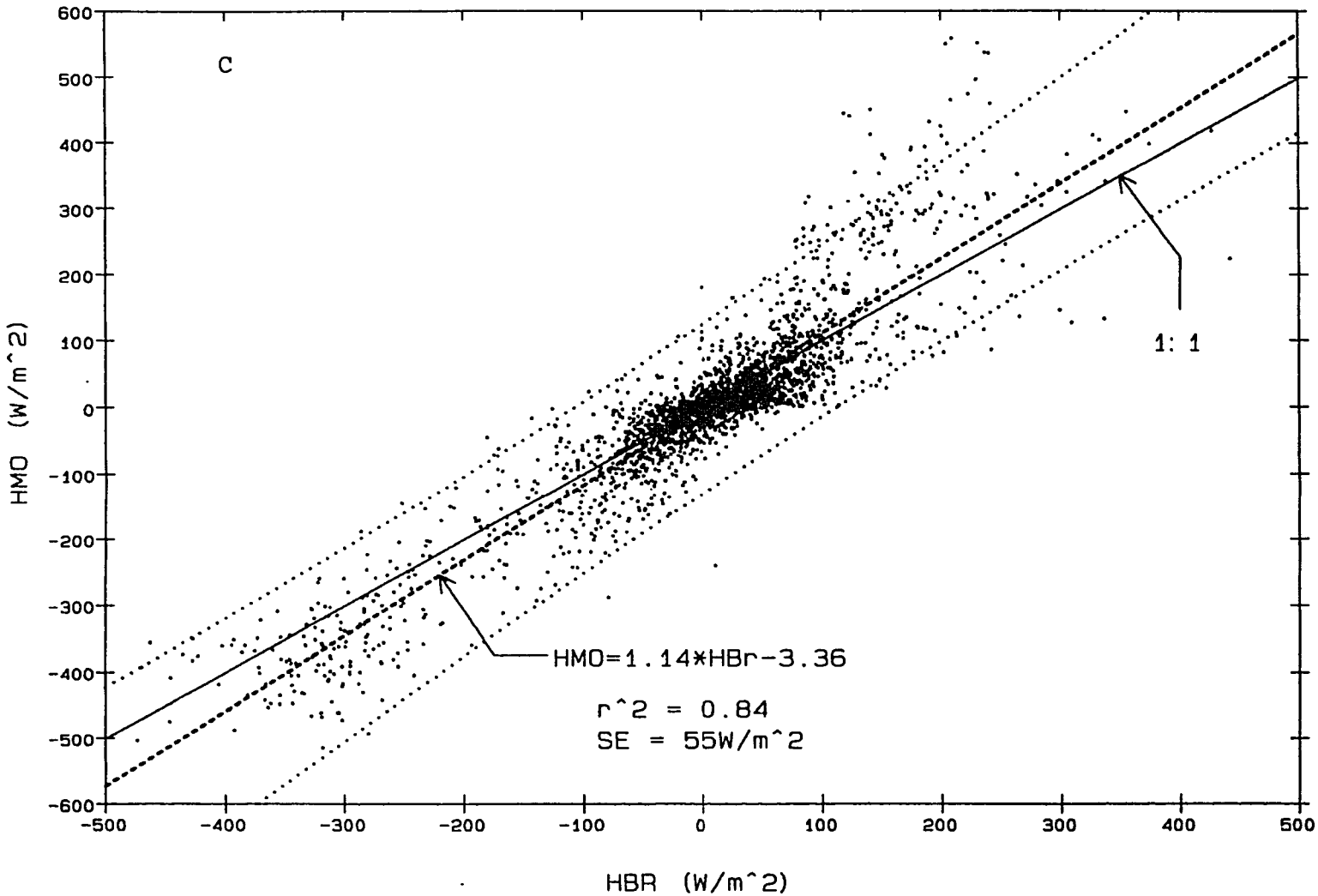

Figure 19. Regression of pooled 30-minute daylight data between C. Monin-Obukhov model vs. Bowen ratio values.

regression line were the closest to ideal, where ideal would be slope and r^2 both equal to 1 and the intercept and standard error both equal to 0. However, the divergence of data about the regression line (standard error) is almost 50% greater for HMO vs HBr than for HCm or HKu vs. HBr. The slopes of the HCm and HKu regressions were lower than unity by 43% and 39%, respectively, and the HCm regression had a somewhat lower r^2 than either the HKu or HMO regressions.

The regression plots show the relationship between the Bowen ratio data and the model estimates. The results of the analysis for the Campbell (Figure 19A) and Kustas (Figure 19B) plots show that both models underestimated the absolute value of HBr during both stable and unstable periods. The Monin-Obukhov plot (Figure 19C) shows that this model distributed the estimates about the 1:1 line about as well as the Campbell and Kustas models during stable periods, but performed better then the other models during the unstable periods. While Monin-Obukhov regression slopes appear better then those of the Campbell or Kustas models, the variability in the HMO data is substantially larger.

Discussion of regression analysis results

The two-level stability corrected, Monin-Obukhov turbulent transfer model appears to have performed better than either the single-level, stability corrected, Kustas resistance model or the non-stability corrected Campbell resistance model. However, the regression model HMO

= 1.14 HBr - 3.4 overestimated the absolute values of HBr under both stable and unstable conditions. Furthermore, under stable conditions (positive HBr values), the HMO predictions generated unusual fluctuations and showed higher variability than the other models. Of the two aerodynamic resistance models, the Kustas model had higher r^2-values, and slope closer to unity than did the Campbell model. The differences between the 1:1 line and the regression slopes for HCm and HKu are very large because these models underestimated the absolute values of HBr under both stable and unstable conditions. The simple Campbell model was the least satisfactory of the three, as its slopes and r^2-values were the smallest, and it had the largest regression intercepts. Both resistance models consistently underestimated absolute values of HBr measurements in the unstable conditions that prevailed at the end of the season when the wheat was dry.

If an empirical correction factor were to be introduced into the Campbell or Kustas models to rotate the regression slopes towards the 1:1 line, then the results would likely be better than those of the two-level stability corrected Monin-Obukhov model. This was not done, since the purpose of this experiment was to evaluate the generality of the models, not to develop a site-specific correction factor. However, the following analysis of the differences between models suggests that a revision is needed in the formulation of the Monin-Obukhov model used up to this point. The implications of a reformulation of the model are discussed

in the following section and in the Conclusions.

Examination of Model Variability

For model evaluations at diurnal, daily, and seasonal time scales, the Monin-Obukhov model consistently exhibited much larger variability than either the Campbell or Kustas aerodynamic resistance models.

Three possible causes for the discrepancy between the HCm, HKu and HMO estimates were examined. These were: (1) effects of aeroelasticity (the change in wheat height as the plants bend under high wind speeds), (2) the validity of the assumption that the aerodynamic temperatures are equivalent to IRT-measured temperatures, and (3) the effect of different stability correction formulations upon the model predictions.

The Effects of Aeroelastic Corrections to Models

In theory, maturing wheat plants are aeroelastic; that is, wind speeds greater than the stalk flexing resistance bend the wheat, until the wind speed decreases below the threshold and the plants return to their original height. When the plants bend, the height of the canopy also decreases, as will the displacement height and roughness length. Since the crop geometry in the models depends on canopy height, the aeroelastic properties of the wheat should be considered.

The Monin-Obukhov model (Tables 4 to 8) tended to overestimate H with respect to the Bowen ratio measurements. An inspection of the regression of Monin-Obukhov estimates with Bowen ratio measurements (Figure 19C) shows an unusual grouping of data points corresponding to high positive HMO values (600 W/m^2) and lower positive HBr values (200 W/m^2). These points were also associated with wind speeds in excess of 4 m/s, and very small Monin-Obukhov lengths of $z/L < 0.001$. This combination of wind and near-neutral stability is not common at Maricopa. The conditions identified in Figure 19C were associated with cool fronts moving through the Maricopa area, with high winds and cooler air temperatures. Normally, the sensible heat flux is small when temperature gradients are small, as in near-neutral conditions. However, in this case, the sensible heat fluxes were large, and the Monin-Obukhov model did not handle them well.

If these high HMO-to-HBr points were removed from the data set, the variability and overestimation of the Monin-Obukhov model would be reduced, resulting in a better fit with Bowen ratio measurements. However, deleting these data requires some rationale other than improving the statistical fit.

Finnigan (1979) studied the aeroelastic properties of wheat, but his research was designed to model the wheat as a mechanical spring rather than to produce functions of wind speed versus canopy height. Munro and

Oke (1973) made micrometeorological observations of wheat with aerodynamic profile instruments; their analysis included the aeroelastic effects of wind speed on wheat height. They developed a linear relationship to predicts d and z_o as functions of wind speed. Although measurement uncertainty renders their regression model only marginally significant and they questioned the model's validity, it did show that d and z_0 decrease as wind speed increases. Monro and Oke's measurement uncertainties might have been lower had they studied growing crops instead of dry, stiff senesced wheat. However, their relationship for wind to wheat height suggests that winds between 4 and 6 m/s will decrease d and z_0 by approximately 25%.

A correction tested here was based upon a simplification of the results of the Munro and Oke (1973) paper. Whenever wind speed > 4 m/s and $0 > z/L < 0.001$, the plant height was reduced by 25%, and d and z_o were recalculated for a smaller canopy height. This correction was applied to daylight data for the Campbell, Kustas, and Monin-Obukhov models for the 135 days that data were collected. The correction operated infrequently—on about 25 days, mostly in the middle of the season—and a total of about 200 data points were adjusted. The subset of adjusted points is illustrated in Figure 20A, with respect to the Bowen ratio measurements.

After the corrections were made, the aeroelastic-adjusted Campbell,

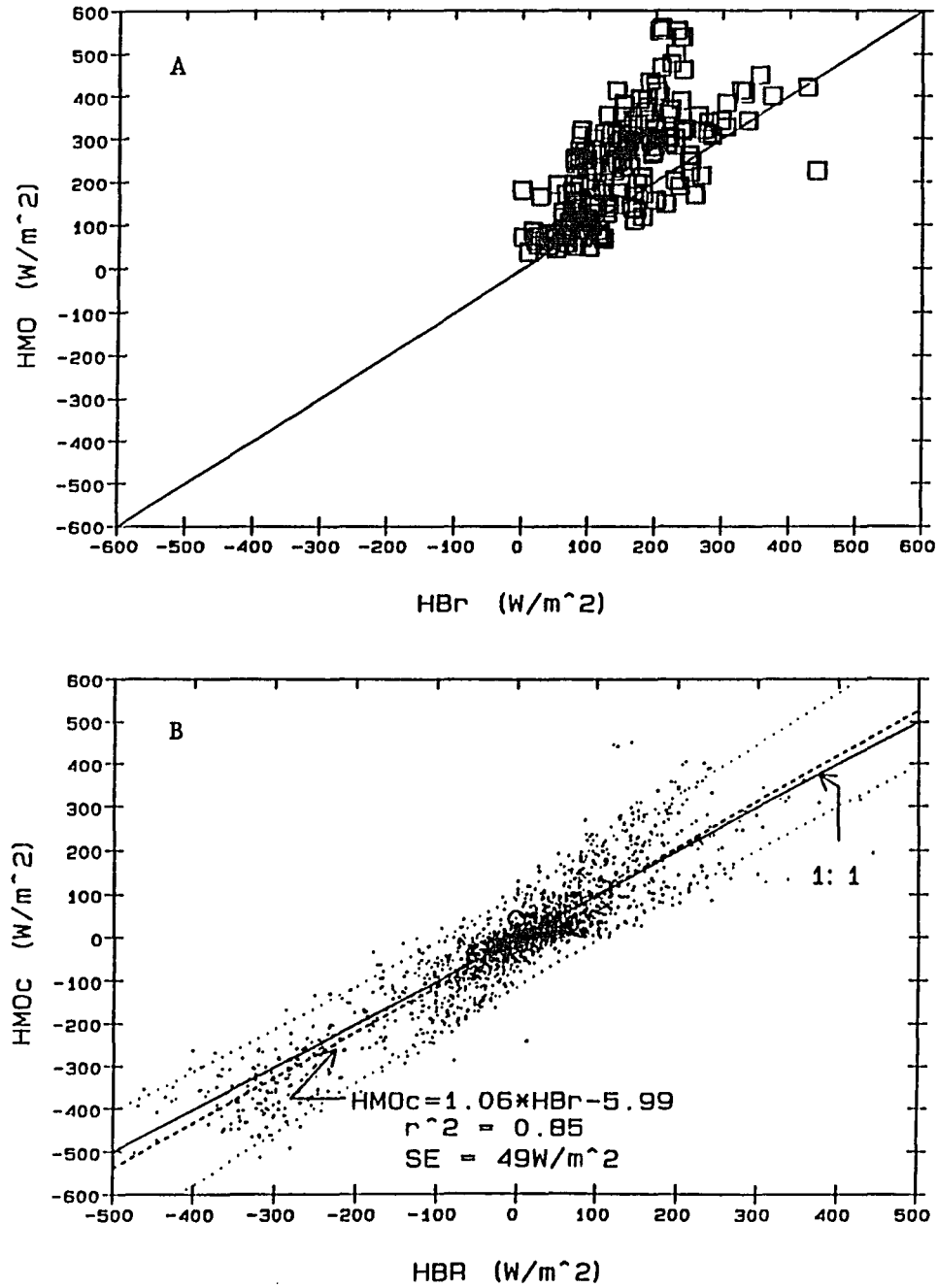

Figure 20. Modifications of Monin-Obukhov sensible heat flux for aeroelasticity

A. Points adjusted for aeroelasticity.

B. Comparison between Bowen ratio measurements and Monin-Obukhov adjusted for aeroelasticity.

Kustas, and Monin-Obukhov estimates were regressed against the Bowen ratio measurements to determine if the correction improved the results. The regression analysis was performed on the 135-day data set, consisting of 2518 30-min observations and the HMO vs HBr comparisons are plotted in Figure 20B. Linear regression coefficients, such as slopes, intercepts and associated standard errors, r^2-values, and regression line standard errors are displayed in Table 9.

Table 9. Regression analysis of measured (HBr) and modeled (HCm, HKu, and HMO) sensible heat flux adjusted for aeroelastic effects on all measurements.

Model	Slope	Intcp. W/m^2	r^2	SE W/m^2	n
HCm	0.57±0.01	14.8±1.4	0.77	35	2518
HKu	0.61±0.01	3.9±1.2	0.83	32	2518
HMO	1.06±0.02	-6.0±2.0	0.85	49	2518

The analysis shows that the adjustment substantially improved the slope, intercept, and standard error of the Monin-Obukhov model but did not improve the Campbell or Kustas models. The overestimation of the HMO vs HBr slope was reduced by 8% and the standard error by 12%, although this remained substantially higher than for the other models.

Considering that this correction did not adjust the data for stable or unstable conditions when the wind speed was greater than 4 m/s, caution should be used in judging its usefulness. While the improvements to the Monin-Obukhov model are clear, the empirical nature of the

correction is questionable, and alternative explanations for the HMO variability should be considered.

Equality of Aerodynamic Temperature and IRT Temperature

One of the major assumptions made for the turbulent transfer and aerodynamic resistance models is that the IRT measures the canopy temperature at the exchange height. This temperature is called the aerodynamic temperature. Such an assumption facilitated the use of remotely sensed temperatures in these models because temperature profile data would not be available. Several investigators evaluated differences between the IRT-measured canopy temperature and the theoretical aerodynamic temperature extrapolated from the log-linear temperature profile data. An evaluation of the differences between IRT and aerodynamic temperatures was also made with data collected at MAC.

Both the Monin-Obukhov and aerodynamic resistance models were derived with the aid of the log-linear profile of wind speed. This profile is valid for regions several meters above the canopy (Monteith 1973). Using similarity theory, I fitted temperature profiles with a log-linear relationship, similar to that used for profiles. Monteith (1973) estimates the "aerodynamic" temperature (T_0) by linear extrapolation of the log-linear temperature profile down to the level of the exchange height ($z_0 + d$) where $u=0$.

The correspondence between the T_0 and the surface temperature T_r is worthy of examination. Little work has been done to determine the precise vertical location of canopy temperatures observed by the IRT. Bonn (1977) reported that IRT measurements of a grass canopy (h = 0.45 m) agreed with measurements from thermocouples located at 0.6 m, confirming that sources for thermal radiation within the canopy were near the exchange height.

Huband and Monteith (1986a) concluded that aerodynamic and IRT temperatures were different in a winter wheat field. Their regression equating T_0 to IRT temperatures[2] is $T_r = 0.98\ T_0 + 0.6$, with a SE = ±1..5°C and $r^2 = 0.95$. Since the slope is close to 1, the intercept is small, and the uncertainty is ±1.5°C, so the observed differences between T_r and T_0 are probably due to instrumentation uncertainty. Choudhury et al. (1986) compared T_0 and T_r temperatures from winter wheat grown in a precision lysimeter at Phoenix, Arizona, and found no differences between T_0 and the T_r under near-neutral conditions (H = 0 ±50 W/m^2). However, the T_r was higher than T_0 under stable conditions and lower than T_0 under unstable conditions. Since the differences were small, they concluded that little would be gained from using T_0 instead of the T_r values in their models. Stewart et al. (1989) reported that differences between T_o and T_r temperatures at a grassland site in Kansas increased from 0°C

[2]The emissivity and view angles used by Huband and Monteith were 0.96 and 55°, respectively. These values were also used in the Maricopa experiment.

to about 2°C as canopy temperatures rose from 19.5°C to 32.4°C. These difference are substantial, but the canopy, on a "heavily grazed plateau", was probably incomplete. An incomplete canopy will increase the variability in temperature measurement and above the grass (and soil) as well as affect the location of the displacement height and roughness length. The 2°C difference between the T_r and T_0 temperatures in this environment could also result from instrument or measurement error.

Smith et al. (1989) evaluated an aerodynamic resistance model with lysimeter data in Australia. They also compared differences between T_o and T_r (DT) by subtracting lysimeter LE from modeled LE as follows: $DT = r_a[LE-LE(IRT)]/\rho C_p$. They found that DT was negligible for neutral and near-neutral conditions ($H = 0 \pm 50$ W/m^2). Deviations that did occur were under stable conditions, with differences ranging up to 4°C. These differences are not surprising because Smith et al. (1989) assumed that all measurement uncertainties and instrument errors were insignificant. This assumption is questionable considering the lysimeter variability reported by Brownridge (1985).

I compared T_0 and T_r to determine the validity of the assumption that they are similar. The aerodynamic temperature is usually estimated from an atmospheric temperature profile measured over the canopy by regression of the adjusted height [log(z - d)] and temperature relationship into the canopy at the z_0–intercept (Monteith 1973). This approach is valid only

for neutral diabatic conditions, which do not occur often during the day. Therefore, I used an analytical solution derived from Monin-Obukhov theory by Panofsky and Dutton (1984). This solution is corrected for diabatic conditions and does not require extensive temperature profile data. Their equation for the "Monin-Obukhov scalar temperature" T_*, the temperature analog to U_* is

$$T_* = \frac{TU_*}{kgL} = \frac{k(T-T_o)}{[\ln(z-d)/z_o]+\Psi sh_2} , \qquad (6.1)$$

and thus

$$T_o = \frac{-\{T_*[\ln(z-d)/z_o]+\Psi sh_2\}+T}{k} , \qquad (6.2)$$

where

T_* is the Monin-Obukhov scalar temperature [K/m],
k is Von Karman's constant,
T is the air temperature [K],
T_o is the aerodynamic temperature [K],
z is the height of the temperature sensor [m],
d is the displacement height [m],
z_o is the roughness length [m],
Ψsh_2 is the upper level diabatic stability correction for heat,
U_* is the friction velocity [m/s],
g is the acceleration due to gravity [m/s^2], and
L is the Monin-Obukhov Length [m].

Values of T_o were calculated with the 12-min dry-bulb air temperatures according to equations (6.1) and (6.2); the values of U_*, L and stability corrections were taken from the Monin-Obukhov model, and d and z_o were set at 0.63 and 0.13 times canopy height, respectively (Huband and Monteith 1986a, Matthias et al. 1990). The value of T_o was computed from day 125 to day 145, 10 days before and 10 days after the

wheat had matured, thus ensuring that the comparisons were made under a wide range of environmental conditions. The value of T_r was subtracted from the value of T_o and plotted against air temperature for the 20 days reported in Figure 21. The absolute value of the T_r - T_o deviations reaches about -13°C. However, 85% of the 2400 points plotted in Figure 21 are within 3°C of 0°C and 44% are within 0.5°C, suggesting that the two temperatures are in reasonable agreement most of the time. In Figure 22, T_r and T_o are plotted against time for days 132 and 144. These plots show that T_r and T_o are similar through much of a diurnal cycle, even though the two days shown contain some of the largest deviations that occurred. The deviations appear most pronounced for stable atmospheric conditions ($z/L > 0$), such as those found after 1700 on day 132, and for highly unstable conditions ($z/L < 0$) such as those found around 1200 on day 142.

Most of the deviations between T_r and T_o shown in Figures 21 and 22 are within the experimental error of the temperature sensors. From my observations and those of others, I conclude that the aerodynamic and IRT canopy temperatures for closed, uniform canopies are roughly equivalent. The deviations reported by other researchers can probably be attributed to instrument and measurement uncertainties. However, some conditions (high wind speed) promote large deviations between T_r and T_o, and they could be responsible for some of the divergence between the measured and modeled fluxes. Under high wind speed conditions, the assumption that

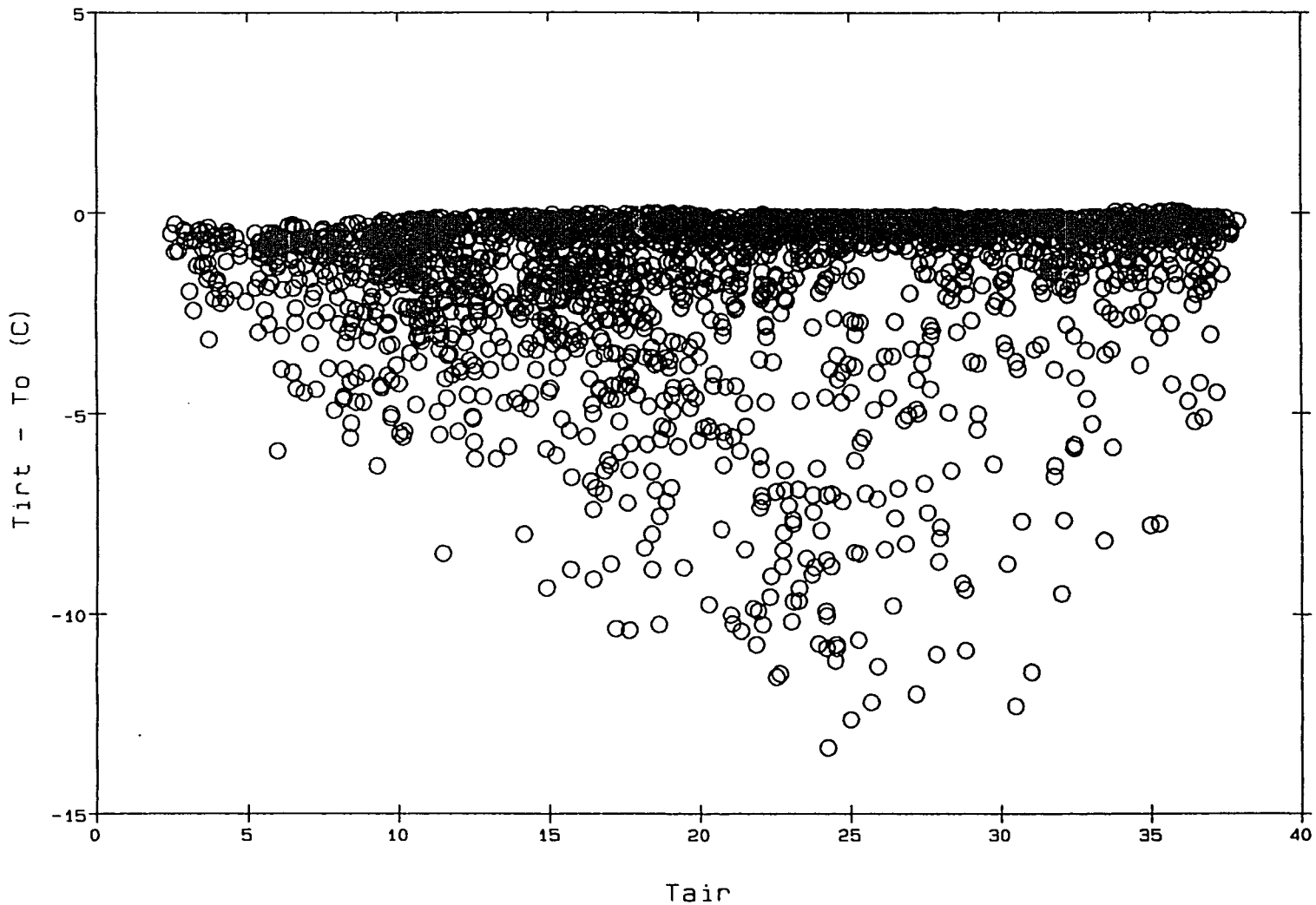

Figure 21. Distribution of T_r-T_o with respect to air temperature data.

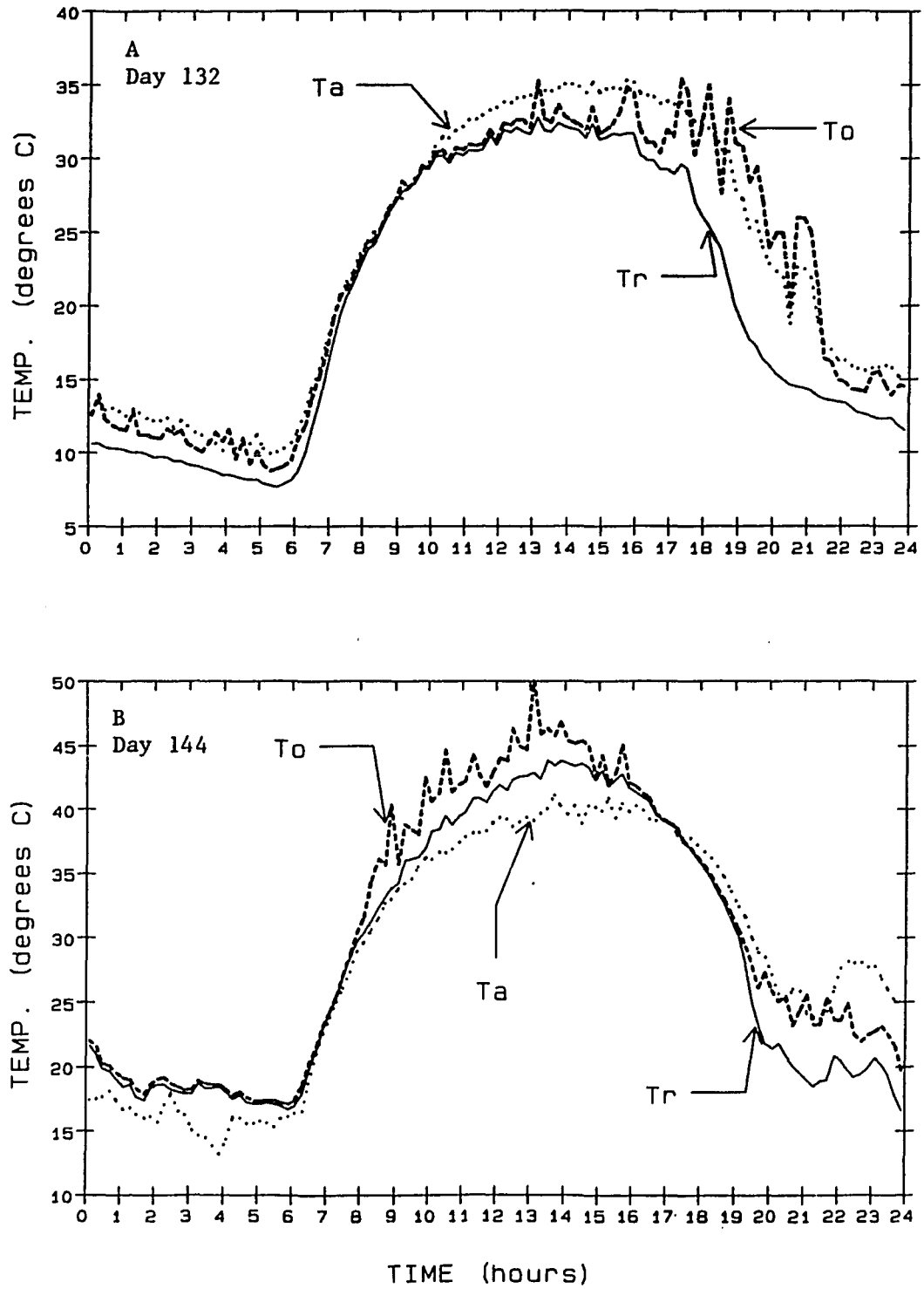

Figure 22. Comparison of diurnal IRT and aerodynamic temperatures
A. Day 132.
B. Day 144.

d and z_o are fixed may not be valid and might be the cause for the deviations that has been observed between T_r and T_o.

The variability seen in the Monin-Obukhov model might be a product of the difference between T_o and T_r. Applying T_o [equations (6.1) and (6.2)] instead of T_r to the models might produce better estimates of H. However, T_o cannot be measured by a thermal sensor, such as an IRT, a fact that reduces the feasibility of this approach for remote-sensing applications.

Model Formulation Differences

The Campbell, Kustas, and Monin-Obukhov models are derived from turbulent transfer theory (Campbell 1977, Kustas et al. 1989, and Brutsaert 1982). There are two differences in the formulation of these models. The primary difference is in their application of diabatic stability corrections, and the second difference is in their respective definition of surface geometry. The models were examined to determine how the different formulations contribute to the differences observed between the modeled H-values.

The Campbell model does not use stability corrections, whereas the Kustas and Monin-Obukhov models use Paulson's (1970) Ψ-function stability corrections. Stability corrections for momentum and heat (Ψsm and Ψsh,

respectively) in the Monin-Obukhov model are evaluated at two levels in the atmosphere. The upper- and lower-level stability corrections are calculated from two wind and air temperature measurement heights made above the canopy. In this dissertation, the upper-level stability correction is computed at the measurement heights for wind and air temperature, while the lower-level Ψ-functions were evaluated at the level of the displacement height within the canopy. This is assumed to be the exchange heights for momentum and heat, respectively, where $T_0 = T_r$ and $u = 0$. In contrast, the Kustas model uses a single set of Ψsm- and Ψsh-functions, evaluated at the measurement heights for wind and air temperature above the canopy with the assumption that $\Psi = 0$ at the exchange height where $u = 0$. Further, the surface geometry used for exchange height in the Monin-Obukhov model in this dissertation is $z - d$ leading to a slope term in the logarithmic wind profile (equation 5.4) of $\ln[(z - d)/z_o]$. The Campbell and Kustas models use a slightly different but equivalent term of $\ln[(z - d + z_o)/z_o]$.

The Campbell model was not corrected for stability and so it was not expected to perform as well as the two stability corrected models. However, the differences in H-values between the Kustas and Monin-Obukhov stability corrected models were unexpected, since these two models are essentially equivalent. The regression analyses for the HKu and HMO data in Tables 4 to 8 indicate that the differences between one-level and two-level stability correction formulations applied in this dissertation

can be substantial. The number of stability corrections and the differing surface geometries were examined to determine their effect on the Kustas and Monin-Obukhov sensible heat flux estimates.

The Monin-Obukhov model was first modified to calculate the sensible heat flux in the same manner as the Kustas model, using a single stability correction evaluated at the upper level only, while assuming the lower-level stability correction is zero. These initial calculations retained the geometry formulation of $\ln[(z-d)/z_o]$. The Monin-Obukhov one-level model was then rerun using the crop geometry formulation of the Kustas model (i.e., $\ln[(z-d+z_{om})/z_{om}]$). The two modified Monin-Obukhov models were applied to the earlier examples of stable (day 87) and unstable (day 146) conditions. The sensible heat estimates from the revised Monin-Obukhov model are designated HMO' for revision 1 and HMO" for revision 2. Since the Kustas model uses the upper-level stability correction from the Monin-Obukhov model, the Kustas model was rerun with the new stability corrections computed from the HMO' and HMO" analysis. These new Kustas estimates are designated as HKu' and HKu", corresponding to HMO' and HMO", respectively.

Table 10. Examples of sensible heat flux estimated from original and modified HMO and HKu models. All values are in W/m^2, averaged over 0.2 hours.

	Day 87			Day 146		
	1350	1410	1430	1350	1410	1430
HMO	305	284	310	-395	-408	-328
HKu	183	171	186	-194	-205	-163
HMO'	198	184	202	-189	-209	-166
HKu'	190	177	194	-170	-188	-148
HMO"	192	179	196	-184	-203	-161
HKu"	189	176	192	-173	-191	-151

Sample midday H-values from the new models on days 87 and 146 are tabulated in Table 10. The original estimates of HMO and HKu differ widely on the two days. With revision 1, however, the differences in HMO' and HKu' estimates are about 4 percent in the stable conditions on day 87, and about 10 percent in the unstable conditions of day 146. With revision 2, the differences between HMO" and HKu" were about 2 percent on day 87 and 6 percent on day 146. The data in Table 10 shows that the major difference between the original and modified models are due to the number of stability corrections used in the formulation. In contrast, surface geometry appears to play a minor role in generating the differences observed between the original estimates from HMO and HKu.

The HMO" and HKu" estimates and the HBr measurements were examined by regression analysis (slope, intercept, and associated ±1 SEs, r^2, and SE of the regression line, where HBr is the independent variable) in Table 11 for all the daylight values on days 87 and 146. The HMO" vs.

HKu" regression coefficients for days 87 and 146 were not statistically different, confirming that HMO" is equivalent to HKu". Further, the HBr vs. HKu" regression coefficients in Table 11 for days 87 and 146 are quite similar to the analysis shown earlier in Table 4, indicating that the recomputation of the stability correction in revision 2 had little effect on the Kustas model. In contrast, the HBr vs. HMO" regression coefficients in Table 11 differ markedly from those of the original regression between HBr vs. HMO in Table 4.

Table 11. Regression analysis of HMO", HKu" and HBr sensible heat fluxes for days 87 and 146. Data are daylight, 12-minute means.

Comparison	Slope W/m^2	Intcp. W/m^2	r^2	SE W/m^2
Day 87				
HMO" vs HKu"	1.03±0.03	-0.23±.5	0.99	00
HBr vs HKu"	0.71±0.03	-34.6±6	0.91	29
HBr vs HMO"	0.73±0.03	-35.6±7	0.91	30
Day 146				
HMO" vs HKu"	1.01±0.01	4.5±.2	0.99	1
HBr vs HKu"	0.70±0.02	45.9±5	0.94	22
HBr vs HMO"	0.71±0.02	42.3±6	0.93	23

The slope was 1.01 in the original HBr vs. HMO regression analysis for days 87 and 146; it dropped to 0.73 and 0.71 for the same days in the new analysis, about the same as the Kustas model. The standard error dropped by 50 percent between the original and the new regressions, reaching a lower value similar to that of the Kustas model.

From the analyses of HMO', HMO", HKu', and HKu", two conclusions can be drawn regarding the application of the Monin-Obukhov model in this

dissertation. First, I conclude that the contribution of surface geometry to the differences between the H-values generated by the original Kustas and Monin-Obukhov models is small. Second, since the differences between the HKu" and HMO" models are small, I conclude that the primary factor in the substantial differences observed earlier between HKu and HMO estimates is in fact due to the different formulation of Ψ-functions in the two models. This is further supported by good agreement in the regression analysis presented in Table 11.

I believe that the high variability observed in the Monin-Obukhov model formulated with 2 levels is due to the behavior of the lower-level Ψ-functions computed at the height of the exchange surface at z-d. In this model, d, z_{om}, and z_{oh} are assumed constant, but any deviations in the exchange height will contribute to the variability of HMO. It now appears that the lower-level correction in the Monin-Obukhov model should be set to zero in the application made here, since the lower level of measurements is at the height where the wind speed equals zero. With this formulation, the Monin-Obukhov and Kustas estimates should be equal.

Since a single-level stability corrected Monin-Obukhov model is equivalent to the Kustas model, then the final comparisons should be between the Campbell and Kustas models. Recall that the major difference between the Campbell and Kustas models is that the Campbell model is not stability corrected, whereas the Kustas model is. The comparison between

the Campbell and Kustas models is then an evaluation of the effectiveness of stability corrections upon remotely sensed sensible heat flux estimates. The quality of the Campbell and Kustas sensible heat flux estimates were determined from the regression analysis of transpiring, senesced, and the combined growing and senesced data presented in Tables 6,7, and 8.

Inspection of the transpiring period regression data in Table 6 shows that the HCm vs HBr and HKu vs HBr slopes and SE's are not significantly different (±2 standard errors, at 95% confidence), but the intercepts and r^2 are different. This indicates that the two models estimate the Bowen ratio measurements with the same degree of precision, but the Kustas model generates a better overall prediction (higher r^2, lower intercept and SE) than the Campbell model under stable conditions. During the senesced period (Table 7), the HCm vs HBr and HKu vs HBr regression slopes and r^2 are significantly different at 95% confidence, but the intercepts and SE's are not significantly different. This shows that the Kustas model is a better predictor of Bowen ratio sensible heat flux than the Campbell model under unstable conditions, but the variability of the two models are about the same. Finally, the combined transpiring and senesced regression analysis (Table 8) shows that the HCm vs HBr and HKu vs HBr slopes and SE's are not significantly different at 95% confidence, whereas the intercepts and r^2's are significantly different. I conclude from this information that the Kustas model gives

better predictions (lower variability) of Bowen ratio sensible heat flux under most diabatic conditions than the Campbell model.

Since the Kustas model out-performed the Campbell model under the three different test outlined above, I conclude that the stability corrections applied to the Kustas model significantly improves the prediction of Bowen ratio sensible heat flux estimates over non-stability corrected models.

7. CONCLUSION

The research described in this dissertation concerns measurements from traditional energy-balance systems and remote-sensing instruments. Bowen ratio energy balance and infrared thermometer measurements were made over winter wheat at 12-min intervals for 137 days during 1988. The measurements began on day 15 (January 15), about 15 days after emergence and continued until day 152, just before harvest. The BREB system measured surface fluxes of net radiation, soil heat, sensible heat, and latent energy as well as air temperature and vapor concentration. The remote-sensing IRT measured the surface temperature of the wheat. The BREB system measurements were used as the "truth-set" to evaluate models that predict the sensible heat flux from remotely sensed canopy temperatures and meteorological data.

Evapotranspiration equivalent depths (ET) were calculated from the daily totals of LE, and a water use budget was estimated. The daily ET values were affected by crop development and by energy supply. They ranged from 1.3 mm/day early in the season to 11.9 mm/day when the fully grown wheat was transpiring at a maximum. For the growing season over days 1 to 137. I conclude that the winter wheat ET totaled approximately 659 mm while irrigation and precipitation totaled 1098 mm, leaving about 439 mm for drainage.

Bowen ratio sensible heat fluxes were validated with eddy-correlation measurements over winter wheat that matured from a transpiring to a fully senesced canopy between days 134 and 151. The evaluation experiments showed that the Bowen ratio sensible heat fluxes tracked with the eddy-correlation estimates, regardless of diabatic atmospheric conditions, variable cloudiness, or soil-plant moisture status. The difference between the mean daily sensible heat flux density measured by the two systems is about ± 40 W/m^2. Much of this difference may be associated with errors in the measurement of available energy, primarily in the net radiation. I conclude that both approaches can give good measurements of sensible heat flux if properly applied.

Three models were used to estimate sensible heat flux from measurements of air temperature, surface temperature and wind speed. The Monin-Obukhov (1954) turbulent transfer model, the Campbell aerodynamic resistance model (Campbell 1977) and the reformulation of the Monin-Obukhov model into a resistance model (Kustas et al. 1989) were evaluated against sensible heat flux estimates from the Bowen ratio.

The Monin-Obukhov model was originally designed to use air temperature and wind speed measurements acquired above the surface. In my application of Monin-Obukhov theory, I used remotely sensed surface temperatures and assumptions about wind speed within the canopy to model the sensible heat flux from a winter wheat surface. Since the Kustas

model and my model use Monin-Obukhov theory, they should have generated similar results. However, the two models produced different sensible heat flux estimates under both stable and unstable conditions.

The most notable difference between the Kustas formulation of Monin-Obukhov and the one that I used was in the number of stability correction levels. I formulated the Monin-Obukhov model with a two-level stability correction for momentum and heat with the upper level at the height of air temperature and wind measurements, and with the second (lower) level placed in the canopy at the height of the exchange surface where wind speed $u = 0$. The Kustas model used only a single-level stability correction above the canopy for momentum and heat, with the second level corrections assumed to equal zero where $u = 0$. From the analysis presented in Chapter 6, I conclude that the divergence of sensible heat flux estimates between the Monin-Obukhov and Kustas models is due to my formulation of the Monin-Obukhov model with a second, lower level stability correction at the exchange height in the canopy where $u = 0$. This conclusion is supported by additional analysis shown in Tables 10 and 11 of Chapter 6 that indicate that the Kustas and Monin-Obukhov models generate equivalent sensible heat fluxes when the application and number of stability corrections are the same. Considering the variability exhibited by the two-level Monin-Obukhov modeled sensible heat fluxes, I conclude that the single-level stability corrected model is more appropriate for remote sensing applications in semi-arid

environments, such as those found at Maricopa.

For stable conditions when the wheat was growing and transpiring, all three models appeared to have worked well. However, when all the regression coefficents are taken into account (slope, intercept, r^2, and SE), I conclude that the Kustas model worked better than the Campbell or Monin-Obukhov models in predicting Bowen ratio sensible heat flux. Under unstable conditions found over senesced wheat, the two-level Monin-Obukhov model appears to predict Bowen ratio sensible heat fluxes better than the Campbell or Kustas models, with the understanding that the Monin-Obukhov variability is higher than the Campbell or Kustas estimates. However, if some form of calibration is used, then the Kustas model would be the best predictor (smallest SE, highest r^2) of Bowen ratio sensible heat flux.

The statistical comparisons between the Bowen ratio measured sensible heat fluxes and the three modeled estimates showed that the Campbell non-stability corrected model was not as good as the Kustas and Monin-Obukhov turbulent transfer models for estimating fluxes in semi-arid regions. Overall, the single-level stability corrected turbulent transfer model (Kustas et al. 1989) predicted fluxes closest to the Bowen ratio sensible heat flux measurements then either the Campbell or two-level stability corrected Monin-Obukhov models in the experiments performed at Maricopa.

In order to apply the Monin-Obukhov model with remotely sensed surface temperatures, several data requirements must be met. Air temperature, wind speed, and roughness lengths must be measured or estimated from surface based instrumentation. With the present remote sensing technology, it is not yet possible to measure these other variables from a remote sensing system. This means that this approach is only useful as a method to augment surface measurements, and can not be used as a surface independent technique for estimating fluxes. Considering the sensitivity of the single-level stability corrected Monin-Obukhov model to changes in temperature and surface geometry, if remote sensing data is to be used for area estimates of sensible and latent heat fluxes careful consideration must be given to the degree of uncertainty acceptable to the user before these types of models are applied. I conclude that if spatial measurements of sensible heat flux are required, then the single-level Monin-Obukhov turbulent transfer model is the best method available for utilizing remotely sensed surface temperature data to support surface measurements.

DEFINITION OF SYMBOLS

C_p specific heat of air [J/kgK],
d displacement height [m],
e atmospheric vapor pressure [mb],
g gravitational acceleration [9.8 m/s^2]
G soil heat flux [W/m^2],
H sensible heat flux [W/m^2],
k Von Karman's constant, = 0.41 [dimensionless],
K_e eddy diffusivity for water vapor [m/s],
K_h eddy diffusivity for heat [m/s],
L latent heat of vaporization [J/kg],
L Monin-Obukhov length [m],
LE latent energy [W/m^2],
P_o ambient atmospheric pressure [mb],
P sea level atmospheric pressure [1013 mb],
Q net radiation [W/m^2],
Ta air temperature [K],
T_o aerodynamic temperature [K],
T_r radiative temperature [K],
T_* Monin-Obukhov scalar temperature [K/m],
T' temperature variance [K^2],
u wind speed [m/s],
U_* friction velocity [m/s],
W' wind speed variance [$(m/s)^2$],
z measurement height [m],
z_o generalized roughness length [m],
z_h roughness length for heat [m],
z_m roughness length for momentum [m],
ß Bowen ratio [dimensionless],
ϵ ratio of the molecular weight of water to air [dimensionless],
θ potential temperature [K],
ζ Monin-Obukhov parameter [dimensionless],
ρ density of air, [1.01 g/m^3],
Ψ_{sh} stability correction for heat [m],
Ψ_{sm} stability correction for momentum [m],
γ psychrometric constant [mb/K].

REFERENCES

Blad, B.L., and N.J. Rosenberg, 1974: Lysimetric calibration of the Bowen ratio energy balance method for evapotranspiration estimation in the central great plains. J. Appl. Meteor., 13,227-236.

Bonn, F.J., 1977: Ground truth measurement for thermal infrared remote Sensing. Photo. Eng. Rem. Sen., 43,1001-1007.

Bowen, I.S., 1926: The ratio of heat losses by conduction and evaporation from any water surface. Phys. Rev., 27,779-787.

Brown, P.W., 1988: User's Guide to the Arizona Meteorological Network. Arizona Cooperative Extension, Phoenix, 50 p.

Brownridge, A.M., 1985: Comparisons of Lysimetric and Bowen Ratio Estimates of Evapotranspiration. M.S. thesis, School of Renewable Natural Resources, University of Arizona 93 p.

Brutsaert, W.H., 1982: Evaporation into the Atmosphere, Theory, History, and Applications. Reidel, 299 p.

Businger, J.A., Wyngaard, J.C., Izumi, Y., and E.F. Bradley, 1971: Flux profile relationships in the atmospheric surface layer. J. Atmos. Sci., 28,181-189.

Carlson, T.N., Todd, J.K., Benjamin, S.G., and J.N. Cooper, 1981: Satellite estimation of the surface energy balance, moisture availability and thermal inertia. J. Appl. Meteor., 20,67-87.

Campbell, G.S., 1977: An Introduction to Environmental Biophysics. Springer-Verlag, 159 p.

Campbell, G.S., and M.H. Unsworth, 1979: An inexpensive sonic anemometer for eddy correlation. J. Appl. Meteor., 18,1072-1077.

Choudhury, B.J., Reginato, R.J., and S.B. Idso, 1986: An analysis of infrared temperature observations over wheat and calculation of latent heat flux. Agric. Forest Meteor., 37,75-88.

Cowan, I.R., 1968: Mass, heat and momentum exchange between strands of plants and their atmospheric environment. Quart. J. Roy. Meteor. Soc., 94,318-332.

Denmead, O.T., and E.F. Bradley, 1985: Flux gradient relationships in a forest canopy. In: Hutchinson, B.A., and B.B. Hicks (Eds.), The Forest-Atmosphere Interaction, pp. 421-442. Reidel, 584 p.

Denmead, O.T., and I.C. McIlroy, 1970: Measurements of non-potential evaporation from wheat. Agric. Meteor., 7,285-302.

Dyer, A.J., 1967: The turbulent transport of heat and water vapor in an unstable atmosphere. Quart. J. Roy. Meteor. Soc., 93,501-508.

Dyer, A.J. and B.B. Hicks, 1970: Flux-gradient relationships in the constant flux layer. Quart. J. Roy. Meteor. Soc., 96,715-721.

Finnigan, J.J., 1979: Turbulence in waving wheat, structure and momentum transfer. Bound.-Layer Meteor., 16,213-236.

Fritschen, L.J., 1965: Miniature net radiometer improvements. J. Appl. Meteor., 4,528-532.

Fuchs, M., and C.B. Tanner, 1970: Error analysis of Bowen ratios measured by differential psychrometry. Agric. Meteor., 7,329-334.

Gay, L.W., 1986: Evaluation of Surface Radiation and Energy Balance Stations on the Konza Prairie. Part B: AZET System Procedures and Data. NASA report from Grant #NAG 5-521, College of Forest Resources, University of Washington, Seattle WA 98195.

Gay, L.W., 1988: A portable Bowen ratio system for ET measurements. Proc. Nat. Conf. Irrig. Drain. pp 625-632. ASCE, New York, NY.

Gay, L.W., and R.J. Greenberg, 1985: The AZET battery-powered Bowen ratio system. Proc. 17th Conf. Agric. Forest Meteor., Scottsdale, AZ. Amer. Meteor. Soc., p. 181.

Hatfield, J.L., 1985: Wheat canopy resistance determined by energy balance Techniques. Agro. J., 77,279-283.

Holbo, R.H., 1973: Energy Exchange Studies at the Earth's Surface II. Energy Budget of a Pumice Desert. Oregon State University, Corvallis. Technical Report No. 73-II, 142 p.

Huband, N.D.S., and J.L. Monteith, 1986a: Radiative surface temperature and energy balance of a wheat canopy I. Bound.-Layer Meteor., 36,1-17.

Huband, N.D.S., and J.L. Monteith, 1986b: Radiative surface temperature and energy balance of a wheat canopy II. Bound.-Layer Meteor., 36,107-116.

Jackson, R.D., Reginato, R.J., and S.B. Idso, 1977: Wheat canopy temperature, a practical tool for evaluating water requirements. Water Resour. Res., 13,651-656.

Jackson, R.D., Moran S.M., Gay, L.W., and L.H. Raymond, 1987: Evaluating evaporation from field crops using airborne radiometery and ground-based meteorological data. Irrig. Sci., 8,81-90.

Kustas, W.P., Choudhury, B.J., Moran, R.J., Reginato, R.D., Jackson, R.D., Gay, L.W., and H.L. Weaver, 1989: Determination of sensible heat flux over sparse canopy using thermal infrared data. Agric. Forest Meteor., 44,197-216.

Mahrt, L., and M. Ek, 1984: The influence of atmospheric stability on potential evaporation. J. Climate Appl. Meteor. 23,222-237.

Matthias, A.D., Kustas, W.P., Gay, L.W., Cooper, D.I., Alves, L.M., and P.J. Pinter Jr. 1990: Aerodynamic parameters for a sparsely-roughened surface of small cotton plants and ridged soil. Remote Sens. of Environ. (accepted, 5/90).

Massman, W.J., Fox, D.G., Zeller, K.F., and D. Lukens 1990: Verifying eddy correlation measurements of dry deposition: A study of the energy balance components of the Pawnee grasslands. Res. Paper RM-288, Fort Collins CO., USDA Forest Service, 14 p.

McNeil, D.D., and W.J. Shuttleworth, 1975: Comparative measurements of the energy fluxes over a pine forest. Bound.-Layer Meteor., 9,297-313.

Monin, A.S. and A.M. Obukhov, 1954: Basic laws of turbulent mixing in the ground layer of the atmosphere. Tr. Geofiz. Instit. Akad. Nauk, S.S.S.R. 24,163-187.

Monin, A.S., and A.M. Yaglom, 1971: Statistical Fluid Mechanics: Mechanics of Turbulence. Vol. 1, MIT Press, 769pp.

Monteith, J.L., 1964: In "The State and Movement of Water in Living Organisms"; Symp. Soc. Exp. Biol., Cambridge Univ. Press., 19,205-234.

Monteith, J.L., 1973: Principles of Environmental Physics. Edward Arnold, 241 pp.

Munro, D.S., and T.R. Oke, 1973: Estimating wind profile parameters for tall dense crops. Agric. Meteor., 11,223-228.

Murray, F.W., 1967: On the computation of saturation vapor pressure. J. Appl. Meteor., 6,203-204.

Ohmura, A., 1982: Objective criteria for rejecting data for Bowen ratio calculations. J. Appl. Meteor., 21,595-598.

Osmolski, Z., 1985: Estimating Potential Evaporation From Climatological Data in an Arid Environment. PH.D. dissertation, School of Renewable Natural Resources, University of Arizona, 132 p.

Osmolski, Z., and L.W. Gay, 1983: Comparison of Bowen ratio estimates from two sets of sensors. Proc. 16th Conf. Agric. Forest Meteor., Scottsdale, AZ. Amer. Meteor. Soc., p. 77-78.

Panofsky, H.A., 1963: Determination of stress from wind and temperature measurements. Quart. J. Roy. Meteor. Soc., 89,85-93.

Panofsky, H.A., and J.A. Dutton, 1984: Atmospheric Turbulence, Models and Methods for Engineering Applications. John Wiley, New York. 397 p.

Paulson, C.A., 1970: The mathematical representation of wind speed and temperature profiles in the unstable atmospheric surface layer. J. Appl. Meteor., 9,857-861.

Philip, J.R., 1987: A physical bound on the Bowen ratio. J. Climate Appl. Meteor., 26,1043-1045.

Prandtl, L., 1932: Meteorologische anwendungen der stromungslehre. Beitr. Phys. Fr Atmos., 19,188-202.

Price, J.C., 1980: The potential of remotely sensed thermal infrared data to infer surface soil moisture and evaporation. Water Resour. Res., 16,787-795.

Sargent, D.H., and C.B. Tanner, 1967: A simple psychrometric apparatus for Bowen ratio determinations. J. Appl. Meteor., 6,179-185.

Seguin, B., and B. Itier, 1983: Using midday surface temperature to estimate daily evaporation from satellite thermal IR data. Inter. J. Remote Sens., 4,371-383.

Sellers, P.J., Hall, F.G., Asrar, G., Strebel, D.E. and R.E. Murphy, 1988: The First ISLSCP Field Experiment (FIFE). Bull. Amer. Meteor. Soc., 69,22-27.

Sellers, W.D., and R.H. Hill, 1974: Arizona Climate 1931-1972. University of Arizona Press, Tucson, 616 p.

Shuttleworth, W.J., Gash, J.H.C., Lloyd, C.R., Moore, C.J., Roberts, J., Filho, A.M., Fisch, G., Filho, V.P.S., Ribeiro, M.N.G., Molion, L.C.B., Sá, L.D.A., Nobre, J.C.A., Cabral, O.M., Patel, S.R., and J.C. Morales, 1984: Eddy correlation measurements of energy partition for Amazonian forest. Quart. J. R. Meteor. Soc., 110,1143-1162.

Sinclair, T.R., Allen, L.H. Jr., and E.R. Lemon, 1974: An analysis of errors in the calculation of energy flux densities above vegetation by a Bowen-ratio profile method. Bound.-Layer Meteor., 8,129-139.

Smith, R.C.G., Barrs, H.D., and W.S. Meyer, 1989: Evaporation from irrigated wheat estimated using radiative surface temperature: an operational approach. Agric and Forest Meteor., 48,331-344.

Spittlehouse, D.L., and T.A. Black., 1979: Determination of forest evapotranspiration using Bowen ratio and eddy correlation measurements. J. Appl. Meteor., 18,647-653.

Spittlehouse, D.L., and T.A. Black, 1980: Evaluation of the Bowen ratio/energy balance method for determining forest evapotranspiration. Atmos.-Ocean, 18,98-116.

Swinbank, W.C., 1951: The measurement of vertical transfer of heat and water vapor by eddies in the lower atmosphere. J. Meteor., 8,135-145.

Stewart J.B., Shuttleworth, W.J., Blyth, K., and C.R. Lloyd, 1989: FIFE: A comparison between aerodynamic surface temperature and radiometric surface temperature over sparse prairie grass. Proc. 19th Conf. Agric., Forest Meteor. Amer. Meteor. Soc., Boston, p. 144-146.

Tanner, C.B., 1960: Evaporation of water from plants and soil. In: T.T. Kozlowski (Ed), Water Deficits and Plant Growth, pp. 74-106. Vol. I. Academic Press.

Thom, A.S., and H.R. Oliver, 1977: On Penman's equation for estimating regional evaporation. Quart. J. Roy. Meteor. Soc., 103,345-357.

Wallace, J.B., Lloyd, C.R., Roberts, J., and W.J. Shuttleworth, 1984: A comparison of methods for estimating aerodynamic resistance of Heather (Calluna vulgaris (L.) Hull) in the field. Agric. Forest Meteor., 32,289-305.